CANADIAN THESES ON MICROFICHE

I.S.B.N.

THESES CANADIENNES SUR MICROFICHE

National Library of Canada
Collections Development Branch

Canadian Theses on
Microfiche Service

Ottawa, Canada
K1A 0N4

Bibliothèque nationale du Canada
Direction du développement des collections

Service des thèses canadiennes
sur microfiche

NOTICE

The quality of this microfiche is heavily dependent upon the quality of the original thesis submitted for microfilming. Every effort has been made to ensure the highest quality of reproduction possible.

If pages are missing, contact the university which granted the degree.

Some pages may have indistinct print especially if the original pages were typed with a poor typewriter ribbon or if the university sent us a poor photocopy.

Previously copyrighted materials (journal articles, published tests, etc.) are not filmed.

Reproduction in full or in part of this film is governed by the Canadian Copyright Act, R.S.C. 1970, c. C-30. Please read the authorization forms which accompany this thesis.

AVIS

La qualité de cette microfiche dépend grandement de la qualité de la thèse soumise au microfilmage. Nous avons tout fait pour assurer une qualité supérieure de reproduction.

S'il manque des pages, veuillez communiquer avec l'université qui a conféré le grade.

La qualité d'impression de certaines pages peut laisser à désirer, surtout si les pages originales ont été dactylographiées à l'aide d'un ruban usé ou si l'université nous a fait parvenir une photocopie de mauvaise qualité.

Les documents qui font déjà l'objet d'un droit d'auteur (articles de revue, examens publiés, etc.) ne sont pas microfilmés.

La reproduction, même partielle, de ce microfilm est soumise à la Loi canadienne sur le droit d'auteur, SRC 1970, c. C-30. Veuillez prendre connaissance des formules d'autorisation qui accompagnent cette thèse.

THIS DISSERTATION
HAS BEEN MICROFILMED
EXACTLY AS RECEIVED

LA THÈSE A ÉTÉ
MICROFILMÉE TELLE QUE
NOUS L'AVONS REÇUE

NL-339 (r. 82/08)

Canada

PETROLOGY AND GEOCHEMISTRY OF SOME ULTRAMAFIC ROCKS OF THE THOMPSON NICKEL BELT AND THE CUTHBERT LAKE DIKES OF THE PIKWITONEI REGION, NORTHERN MANITOBA

by

A. Doğan PAKTUNÇ

A thesis
presented to the University of Ottawa
in partial fulfillment of the
requirements for the degree of
Doctor of Philosophy
in
Department of Geology

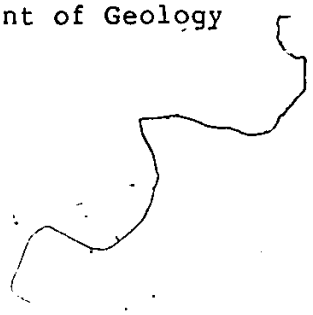

OTTAWA, Ontario, 1983

UNIVERSITÉ D'OTTAWA
UNIVERSITY OF OTTAWA

The University of Ottawa requires the signatures of all persons using or photocopying this thesis. Please sign below, and give address and date.

ABSTRACT

The Thompson Nickel Belt is a tectonic mobile belt that lies in a northeasterly direction on the boundary between the Churchill and Superior Provinces in north-central Manitoba. Abundant sill-like bodies of serpentinized ultramafic rocks, associated with nickel sulfide deposits, are found on the western side of the Thompson Nickel Belt near the Moak-Setting Lakes cataclastic fault zone. The ultramafic rocks range in composition from dunite to orthopyroxenite. All feature variable alteration. Common mineral assemblages are : Ol+Opx+Tr+Sp; Opx+Tr+Sp+Phl (in order of decreasing modal amount). Ultramafic rocks in the Thompson Mine were found to be partly altered prior to being progressively metamorphosed under upper amphibolite facies conditions. The maximum temperature reached during metamorphism is estimated to have been 700°C. Rocks were deformed during metamorphism and were subsequently recrystallized, which resulted in the formation of equigranular mosaics of olivine neoblasts. As a result of a retrogressive metamorphism, following prograde metamorphism, rocks were serpentinized to various degrees. This second stage of serpentinization is believed to be responsible for the pervasive serpentinization that affected the majority of ultramafic rocks in the belt.

These complex events, however, do not seem to have affected the chemistry of some of the bodies, especially those that were slightly altered or unaltered during the retrogressive metamorphism. Chemical variation across the bodies is suggestive of in-situ differentiation that is controlled mainly by olivine and orthopyroxene. Thus it is suggested that relative abundances of some elements, incompatible for olivine and orthopyroxene, should represent original liquid composition; this liquid being komatiitic.

Both ultramafic and mafic rocks are petrogenetically linked. It is believed that a high degree of partial melting of mantle material and subsequent low-pressure crystal fractionation are responsible for the spectrum of compositions from ultramafic to mafic.

Parallel to the Thompson Nickel Belt, northeasterly trending Cuthbert Lake dikes of ultramafic to mafic compositions cut the Pikwitonei gneisses which constitute the northwestern edge of the Superior Province in north-central Manitoba. The major Cuthbert Lake dike is approximately 60 meters in width and can be traced approximately 160 km along its length.

These dikes are laterally differentiated; that is, the modal amount of olivine shows an increase whereas plagioclase decreases toward the dike center. This feature is probably due to flowage differentiation. Moreover, Mg/(Mg+Fe)

ratios of olivines and of the bulk rock increase from the dike margins inward.

Bulk chemistry of the dike rocks is controlled mainly by olivine. The crystallization sequence, at 1 atm pressure, is: Ol, Cpx, Opx, Pla. At higher pressures orthopyroxene crystallized before clinopyroxene since the orthopyroxene stability field expands at the expense of clinopyroxene (and plagioclase). Equilibration of orthopyroxene and clinopyroxene was reached at 1150°C.

The liquid composition of major dikes is regarded as komatiitic. Minor dikes were formed from more evolved basaltic liquids. These differing liquid compositions probably resulted from fractional crystallization processes that took place in a subcrustal magma chamber.

ACKNOWLEDGEMENTS

The study has been supervised by Dr. G. A. Armbrust during the years of 1980-1982 and by Dr. C. R. Pride during the final year.

Scholarships from the Mineral Research and Exploration Institute of Turkey (Maden Tetkik ve Arama Enstitusu) for the years of 1979-1982 and from the Ontario Ministry of Colleges and Universities for the years of 1982-1983 are greatly acknowledged. INCO Metals Ltd. Manitoba Division supported field work.

The author is greatly indebted to Dr. W. V. Peredery for suggesting the topic, for his generous help in the field and for a discussion half-way through the project. From time to time, discussions with Drs., A. Baer, R. Kretz, O. R. Eckstrand, and M. Duke were very helpful.

CONTENTS

LIST OF FIGURES

LIST OF TABLES

Chapter I

INTRODUCTION

1.0.1 Previous Study

The Thompson Nickel Belt, containing important nickel sulfide deposits, lies on the boundary between the Churchill and Superior Provinces; therefore, the belt is structurally and economically important. For these reasons, the belt has been mapped in detail and various geological aspects have been studied.

A brief regional geology accompanied by a compilation map is given in Coats et al. (1972). Wilson & Brisbin (1961) considered the belt as a remnant root of an island-arc or alpine mountain belt. According to Bell (1971), the belt could be 1) an autochthonous slice from the Flin Flon sub-province, 2) a horst of Archean basement underlying the Churchill Province, or 3) an Archean allochthon related to the Pikwitonei-Superior continental block. Peredery (person. comm., 1980) interprets the belt as a long graben-like structure, favouring the third possibility of Bell (1971).

Previous studies concerning the ultramafic and mafic rocks are summarized as follows: Coats (1966) studied the

petrography, chemistry and serpentinization of the ultramafic rocks of the belt, concentrating mainly on a body in the Setting Lake area. He interpreted the rocks to be typical of alpine-type peridotites that were emplaced as a crystal mush along faults originating from the mantle. Bliss (1972) studied the ultramafic rocks covered by Paleozoic sediments near the southern part of the belt. According to him, the bodies may have crystallized in-situ, based on the absence of relict deformational textures commonly accompanying the solid intrusion of such bodies. Stephenson (1974), from a study of rocks around the Ospwagan Lake area, considered the ultramafics to be genetically related to picrites and basalts. DeSaboia (1978) studied Pipe 2 and West Manasan ultramafic bodies and interpreted them to be derived from a tholeiitic magma by gravity differentiation and flow differentiation respectively. According to Peredery (1979), ultramafic rocks of the belt were formed from ultrabasic magma by in-situ fractional crystallization that also produced metapicritic rocks.

The Cuthbert Lake dikes cut the Pikwitonei granulites which constitute the northwest part of the Superior Province, adjacent to the Thompson Nickel Belt. The Pikwitonei region has been considered as a separate province (Bell 1971, Cranstone & Turek 1976), and conversely as part of the Superior Province (Weber & Scoates 1978).

There are several studies on the Cuthbert and/or Molson dikes: 1) petrology of the Cuthbert Lake dike (McDonald,1960), 2) chemistry and paleomagnetism of dikes near Molson, Cross and Playgreen Lakes (Ermanovics & Fahrig, 1975), and 3) petrology and chemistry of dikes around Witchai, Pikwitonei, Landing, Cuthbert, Cross and Gods Lakes (Scoates & Macek, 1978).

1.0.2 Purpose of the Study

Objectives of this study of the Thompson ultramafic rocks are to investigate 1) the effects of metamorphism on the mineralogy, chemistry, and texture of the rocks, 2) the igneous petrogenesis of the rocks, 3) the genetic link with the mafic rocks in terms of partial melting vs. fractional crystallization processes. The purpose for the study of the Cuthbert Lake dike is to determine 1) the geological conditions before, during and following emplacement, 2) whether they can be the feeders to the spatially associated Thompson ultramafic rocks.

1.0.3 Methods of Study

Field work and sample collection were carried out during the summer of 1980. The majority of ultramafic rocks were collected from the Thompson Mine; included are cores from two diamond-drill holes and specimens from different levels

of the mine. Other samples were taken from the Mystery Lake deposit, Birchtree mine, and Pipe 2 mine. Mafic rocks were collected from the Ospwagan Lake and Mystery Lake areas in addition to those from the Thompson mine. Cuthbert Lake dike samples were collected from a diamond-drill hole that represents a cross section of the dike.

Approximately 150 thin and polished thin sections, supported by X-ray diffraction analyses, were used in petrological investigations. The chemistry of 226 mineral grains was determined by electron microprobe. Major and trace elements from 95 rock samples were determined using X-ray fluorescence.

Chapter II

GENERAL GEOLOGY

The Thompson Nickel Belt, lying in a northeasterly direction, separates the Churchill and Superior Provinces of the Canadian Shield in northern Manitoba (Figure 1). The belt coincides with a gravity low (Wilson & Brisbin 1961). The Moak-Setting Lakes cataclastic fault zone, a steeply dipping zone of variable width (0.9 to 1.5 km), defines the northwestern boundary with the Churchill Province. The southeastern boundary with the Pikwitonei region is partly a cataclastic fault zone and partly a metamorphic transition zone (Cranstone & Turek 1976).

This belt has been extended southward to the Canada-U.S.A border underneath the Paleozoic sediments using gravity data (Wilson & Brisbin 1961). A continuation of the structure extends northeasterly along the Fox River Belt, Hudson Bay and through the Cape Smith-Wakeham Bay Belt in Ungava peninsula (Wilson & Brisbin 1961; Baragar & Scoates 1981).

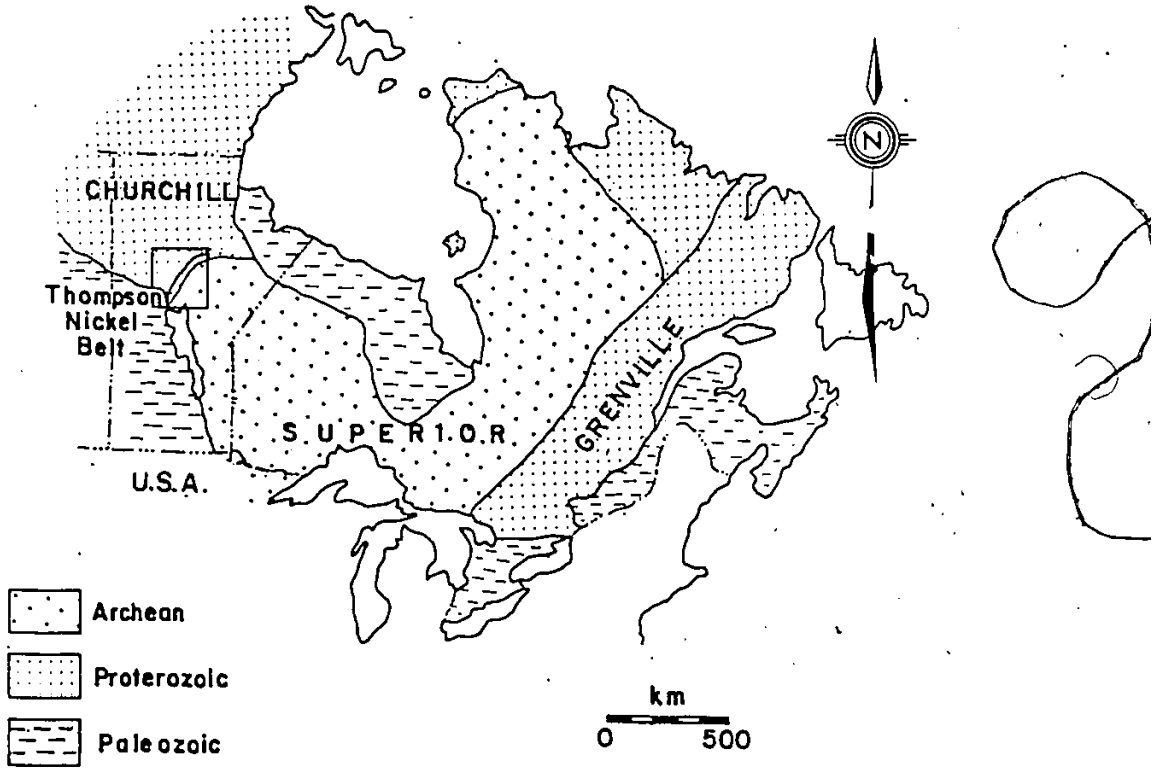

Figure 1: Regional setting and location of the study area.

2.1 THE THOMPSON NICKEL BELT

The Thompson Nickel Belt is underlain predominantly by migmatitic gneisses which comprise paragneiss, orthogneiss and porphyroblastic gneiss. These gneissic basement rocks contain mainly amphibolite facies mineral assemblages. However, granulite facies mineral assemblages are also common in the belt and are interpreted by Weber & Scoates (1978), Peredery (1979), and Russell (1981) as relict Archean granulites that survived the Hudsonian orogeny.

These Archean rocks include layered basic to ultrabasic rocks as well as gneisses (Peredery 1979), mafic to ultramafic banded gneisses and enderbitic gneisses (Russell 1981). They are interpreted as remobilized (Cranstone & Turek 1976), retrogressed (Weber & Scoates 1978; Russell 1981) equivalents of the Pikwitonei basement rocks. Rb/Sr age determinations (Cranstone & Turek, 1976) on the basement gneisses reflect Hudsonian overprint (1.7 Ga) and an older event (2.8 Ga). The Hudsonian metamorphic event at about 1.7 Ga (Bell, 1971) is recorded by K-Ar age determinations as well.

Near the western margin of the belt, these basement rocks are overlain by thin (150-1500 meters) Aphebian supracrustal rocks (Peredery 1982) which include metasedimentary and metavolcanic assemblages (Figure 2). These supracrustal rocks contain abundant subvolcanic mafic and ultramafic intrusions, and economic nickel sulfide deposits.

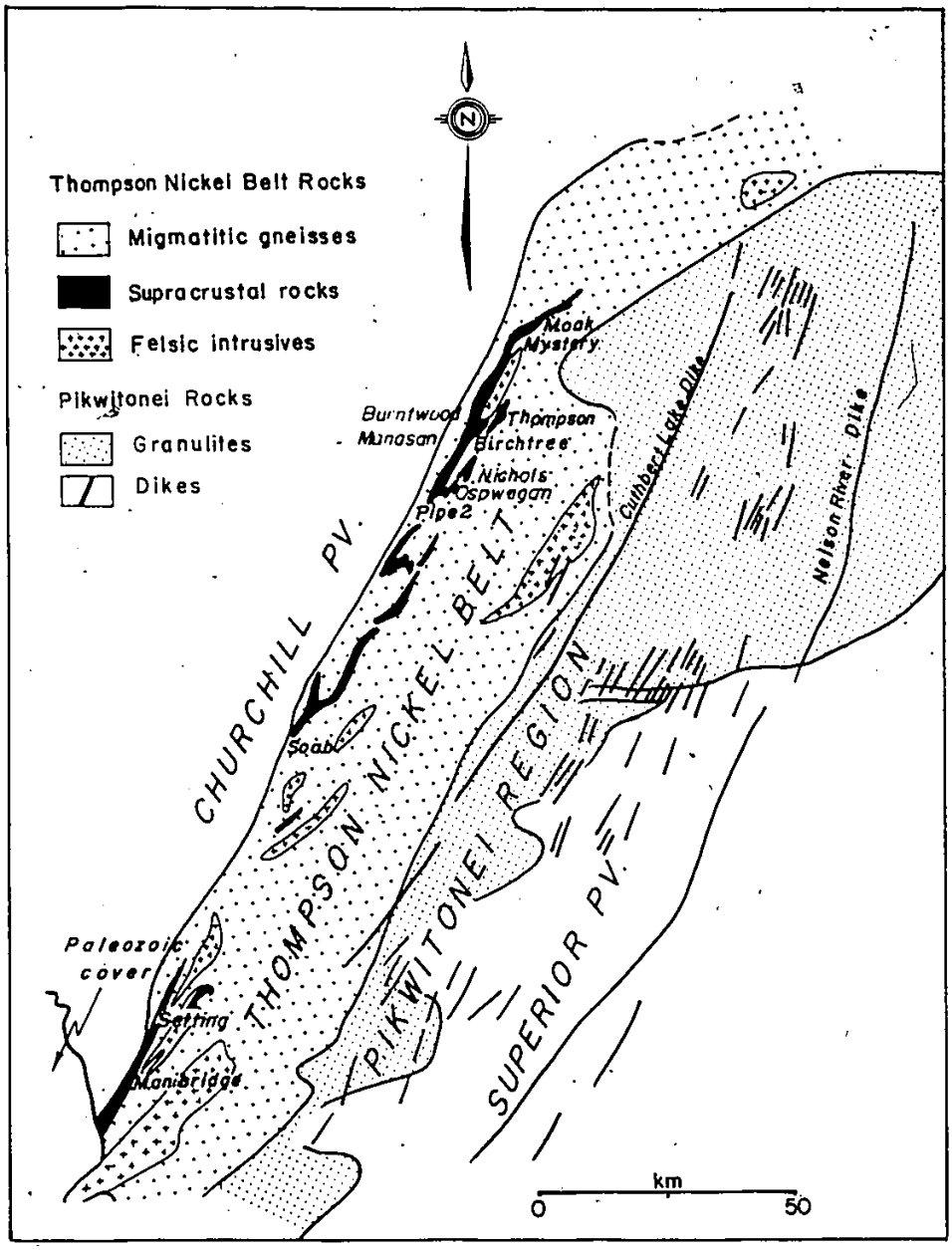

Figure 2: Geological map of the Thompson Nickel Belt and Pikwitonei region (simplified from the Geological Map of Manitoba, Manitoba Mineral Resources Division, 1979).

The metasedimentary assemblages include siliceous, calcareous, pelitic and ferruginous rocks (Peredery 1979). They show a range of metamorphic grade from middle amphibolite to upper amphibolite facies and carry effects of retrogressive metamorphism. Peredery (1982) has distinguished two metasedimentary assemblages: the Thompson sequence and the Pipe sequence. The Thompson sequence that includes the units around the Thompson mine is separated from the Pipe sequence by a fault zone. The Pipe sequence extends from the Pipe mine in the south to Moak Lake in the north. Both sequences start with siliceous rocks at the bottom which overlie gneisses. These siliceous rocks are first overlain by calcareous assemblages and followed by iron formation and quartzites on top. The Thompson sequence has minerals such as sillimanite and garnet in pelitic rocks; grunerite, garnet, clinopyroxene and orthopyroxene in iron formation; olivine and diopside in calcareous rocks, indicating upper amphibolite-granulite facies metamorphism. However, mineral assemblages of the Pipe sequence correspond to middle amphibolite facies metamorphism. These are staurolite and garnet in pelites; grunerite and garnet in iron formation; diopside and microcline in skarn. According to Brooks & Theyer (1982), the Pipe sequence metasediments have a maximum age of 2.1 Ga based on the Sr evolution diagram.

The majority of the metavolcanic rocks are found around Ospwagan and Mystery Lakes. These include basaltic, picri-

tic and ultramafic rocks. Metabasalts are the most common variety which consist of pillowed and massive flows and minor fragmental rocks (Peredery 1979). They are generally fine grained and have strongly foliated fabrics. The pillows are generally highly deformed and elongated, this feature being well documented in the variolitic varieties in which the varioles are stretched along the regional foliation. Minor fragmental rocks associated with metabasalts contain closely packed elongated fragments of amphibolites and gneisses. Magnesian metabasalts are characterized by quench texture long, needle-like mafic crystals forming parallel, radiating and sheaf-like patterns similar to spinifex texture (Figure 3). Ultramafic flows, in the form of pillowed lavas are found south of Lower Ospwagan Lake (Peredery 1979). They are composed of fine grained amphibole and minor colourless chlorite.

Abundant mafic and ultramafic sill-like bodies are found in the gneisses and metasedimentary rocks. Whether they are sills, flows or dikes is not certain since original textures and contacts with country rocks are largely obliterated by metamorphism and tectonism. The mafic varieties, mainly amphibolites, are generally massive and/or foliated. In the massive variety, textures such as 'diabasic texture' are found whereas no relict texture is present in the foliated variety. According to Stephenson (1974), sill-like bodies of amphibolites occurring within the gneisses represent metamorphosed igneous rocks.

Figure 3: Quench texture in magnesian basalts at Mystery Lake.

A large majority of the ultramafic rocks occurs close to the northwestern side of the belt. They are generally lensoid or tabular in shape and vary in width from several meters to several hundreds of meters. The most common ultramafic rock types are serpentinite and serpentinized peridotites. A descriptive field term 'ultramafic amphibolites' is used by Peredery (1979) to describe a variety of ultramafic rocks that ranges in composition from picrite to pyroxenite. They are particularly associated with serpentinites in the Thompson mine area. According to Zurbrigg

(1963) these rocks may have developed from serpentinized peridotite through progressive metamorphism. According to Peredery (1979), however, they represent differentiates of an ultrabasic magma because they have mineralogical banding suggestive of primary layering and because contacts with the serpentinites are gradational.

Nickel sulfide deposits occur for a length of 130 km or more along the belt from Wabowden to Moak Lake. The majority of them are associated with ultramafic rocks. Their mode of occurrence is: 1) as disseminated sulfides with partly preserved net-texture (Figure 4) in ultramafic rocks, 2) as veins and matrix in brecciated serpentinite, 3) as massive sulfide bodies adjacent to ultramafic bodies, 4) as discrete massive bodies with abundant wall-rock fragments (Figure 5) within metasediments, 5) as stringers parallel to the foliation of country rock. The dominant sulfide minerals are pyrrhotite, pentlandite, and some pyrite and chalcopyrite (Figure 6). Pb isotope dating of the sulfides has recorded events of four distinct ages (Cummings et al 1982), among which the oldest age, 2320±30 Ma, is interpreted as the time of emplacement of the nickel sulfide deposits and their ultramafic hosts.

Migmatitic gneisses and supracrustal rocks of the belt were intruded by hornblende-quartz monzonite and porphyritic or porphyroblastic granodiorite. K-Ar age determinations of

Figure 4: Interstitial sulfides in peridotite. Grey interstitial material is chlorite.

these intrusions gave Hudsonian ages and they are, therefore, either syntectonic with or pretectonic to the Hudsonian orogeny according to Cranstone & Turek (1976). Also, older acidic intrusions, called orthogneisses by Peredery (1979), exist in the belt in addition to these younger intrusions. These acidic intrusions are extensively cut by a network of pegmatite veinlets.

Northwesterly trending nearly vertical diabase dikes, part of the Mackenzie dike swarm, cross cut most of the rocks in the belt and the Moak-Setting Lakes cataclastic

Figure 5: Massive nickel sulfide with abundant wall rock fragments.

fault zone, postdating the Hudsonian orogeny. The rocks are fresh and unmetamorphosed.

COLOURED PICTURES
Images en couleur

Figure 6: Massive nickel sulfide. Pyrrhotite, dark yellow; pentlandite, light yellow; chalcopyrite, gold yellow. Grey and black patches are wall rock fragments. Diameter of the core is 7 cm.

2.2 PIKWITONEI REGION

The Pikwitonei region is underlain predominantly by granulite facies gneisses and minor amounts of amphibolite facies rocks. Bell (1971) considered these rocks which formed during a pre-Kenoran metamorphic event, as a basement to the Superior greenstone belts. Cranstone & Turek (1976), following this hypothesis, consider the Pikwitonei region as the oldest geological unit in the area which is unconformably overlain on the southeastern margin by rocks of the Su-

perior Province. Weber & Scoates (1978) argued against this hypothesis because the unconformity at Cross Lake which had been used by Bell (1971) and Cranstone & Turek (1976) as the main support for their hypothesis, may represent an unconformity within the supracrustal succession and not the base of the greenstone belt.

The Pikwitonei region rocks are cut by a northeasterly trending dike swarm, parallel to the Thompson Nickel Belt (Figure 2). The dikes range in composition from mafic to ultramafic. The Cuthbert Lake dike, trending from Cuthbert Lake to Begg Lake is mostly ultramafic in composition and is considered as a part of the Molson dike swarm by Scoates & Macek (1978). Mafic dikes are more common than the ultramafic ones. Although mafic dikes with similar trend occur in the Superior Province as far as 92°00 W, the majority of the dikes occur to the west side of the Nelson River. There are no known N-NE striking dikes in the Thompson Nickel Belt according to Bell (1971). However, taking into account the complex deformation and metamorphism in the belt, their absence is not surprising. Rare amphibolite dikes (Rance 1966) and metamorphosed and deformed dikes on the eastern side of the belt (Cranstone & Turek 1976; Peredery, pers. commun. 1982) are present. The northern extension of the dikes is bounded by the Split Lake fault. They are absent from the Churchill Province.

Chapter III

ULTRAMAFIC-MAFIC ROCKS OF THE THOMPSON NICKEL BELT

3.1 PETROLOGY AND GEOCHEMISTRY

Special attention was given in this study to an ultramafic body (T-3) at the 4000 level of the Thompson mine, since it is unusually fresh. Mineralogical and petrographical description of the rocks seen along the body resemble those of the other ultramafic rocks from other localities in the belt, some of which are relatively fresh and others which are highly altered; therefore, their descriptions are not given separately.

3.1.1 Mineralogy and Petrography

The ultramafic body at the 4000 level of the Thompson mine, as seen along two diamond-drill holes (Figure 7), is 130 meters thick, probably lensoid in shape and enclosed in a garnet-sillimanite-biotite schist.

The body is composed of dunitic, peridotitic, olivine-orthopyroxenitic, orthopyroxenitic, and amphibolitic rocks. Using the scheme of Evans (1977), the rocks can be named tremolite peridotite and tremolite pyroxenite (Figure 8).

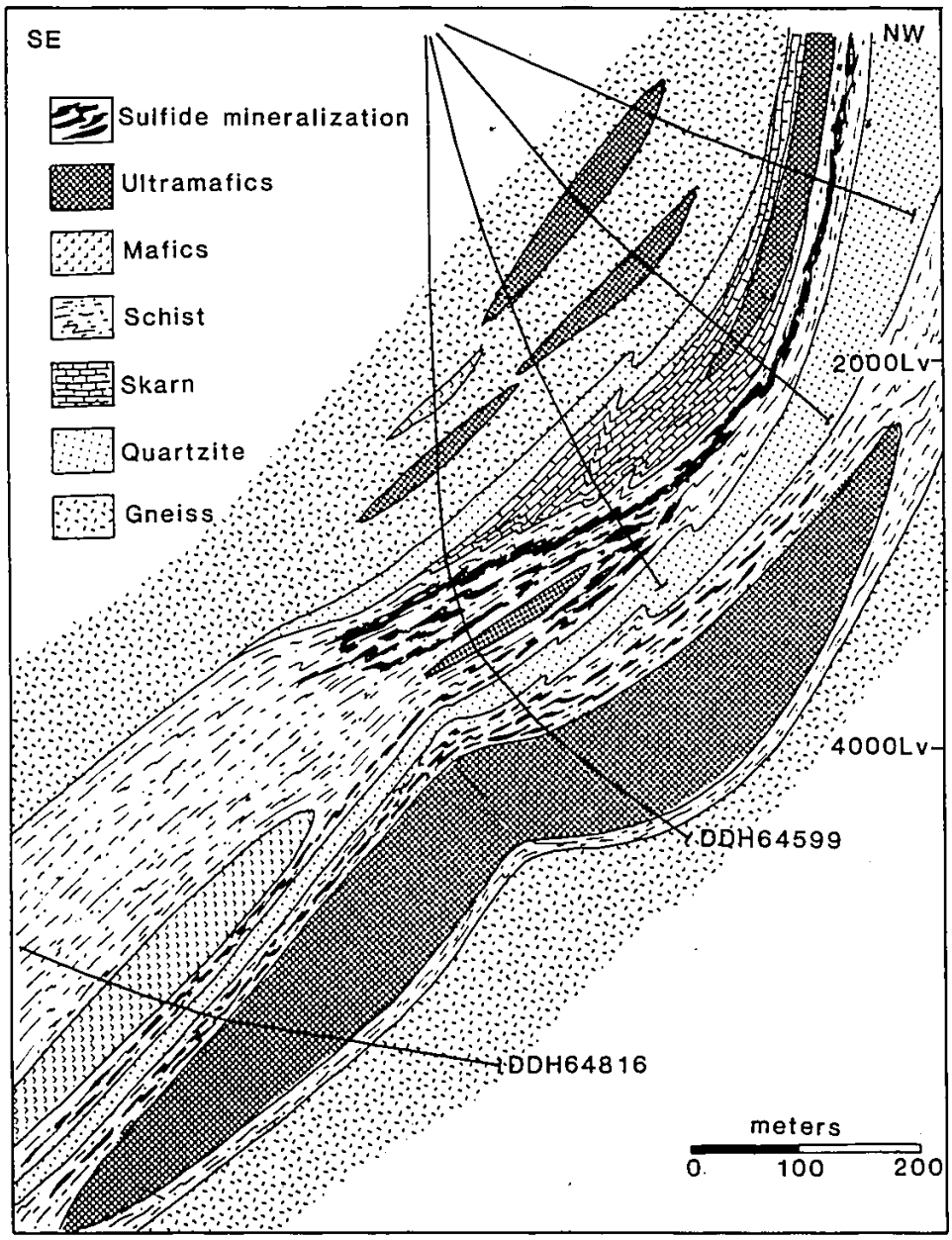

Figure 7: 3600 N vertical section of the Thompson mine (T-3)

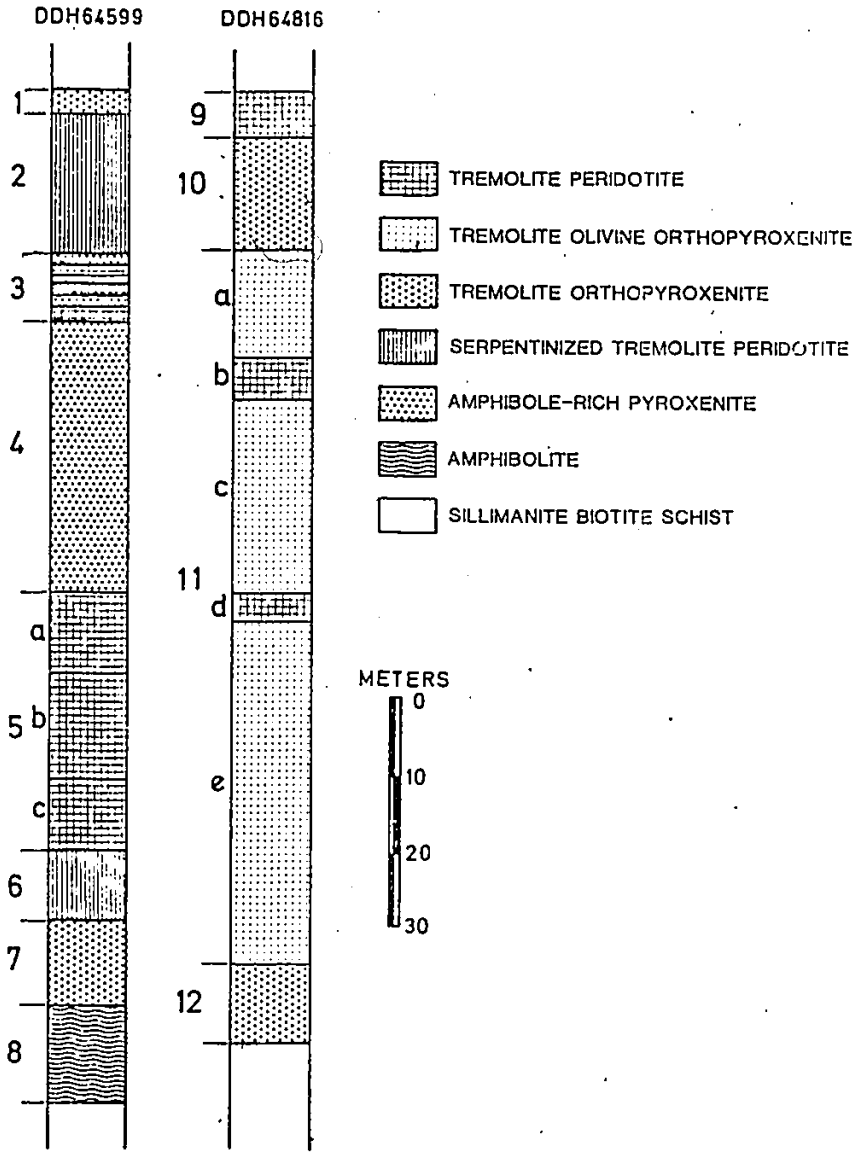

Figure 8: Ultramafic body as observed through two diamond-drill holes Samples were obtained from each of the zones as indicated in Table 7 (Appendix B).

The unit which is named 'amphibole-rich pyroxenite' in

Figure 8 is mineralogically similar to ultramafic amphibolite of Peredery (1979). The main sulfide mineralization is found in the enclosing schist in the form of massive, brecciated and stringer ore. Minor disseminations of sulfides are present in the ultramafic body, close to its contact with mineralized schist. As observed in cores from diamond-drill hole 64599, tremolite peridotite and its serpentinized equivalents amount to one half of the body, whereas the tremolite pyroxenite makes up more than one third (Figure 8). Tremolite-olivine pyroxenite is the main rock type seen along the diamond-drill hole 64816.

3.1.1.1 Tremolite peridotite

Olivine crystals in the peridotitic zones are of two types: megacrystic (2-4 mm) olivine and fine grained (less than 1mm) olivine. Megacrystic olivines are usually black, due to fine opaque dusty material disseminated and/or concentrated along irregular fractures in olivine (Figure 9). This material, possibly a magnetite, may be the product of high temperature oxidation of olivine (Haggerty & Baker 1967; Champness 1970; Putnis 1979). Alternately it may be magnetite formed during previous serpentinization and included in metamorphic olivines during the progressive metamorphism (Arai 1975; Vance & Dungan 1977). A similar texture, black olivine megacrysts with dense tiny ilmenite granules occurring in the outermost zone of the Bergell au-

reole in the Melanco serpentinite, is described by Trommsdorff & Evans (1980). Fluid and fine solid inclusions are commonly associated with this dusty material. Pale brown to brownish yellow euhedral-subhedral solid inclusions are probably spinel. Some of the olivine megacrysts display undulatory extinction and kink banding (Figure 10).

Figure 9: Fine opaque dusty material disseminated and concentrated along irregular fractures in olivine. Fine grained opaque minerals distributed near the margin of the olivine are spinel.

Light-green coloured small olivine grains, on the other hand, do not contain opaque dusty material and are strain-

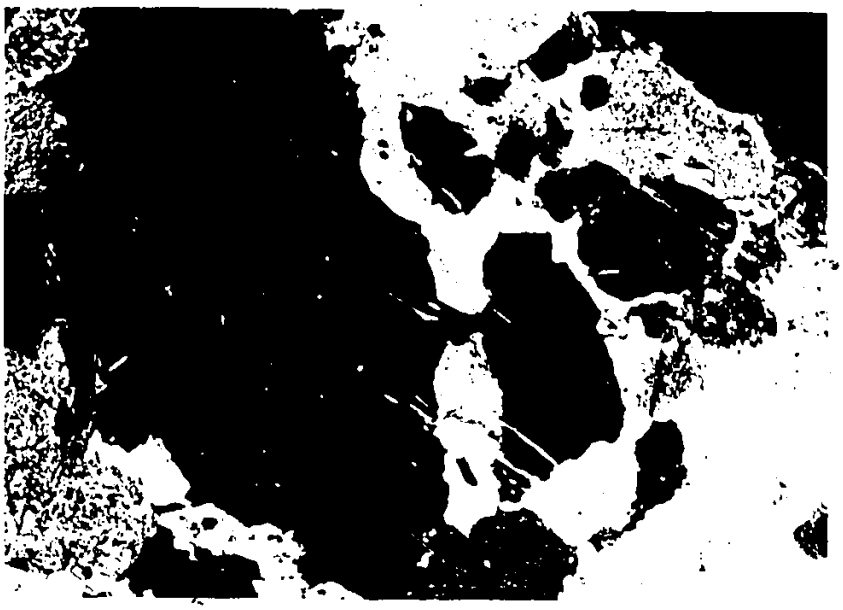

1mm

Figure 10: Kink-banding in an olivine megacryst (dark green crystal).
Parallel oriented crystals are amphibole and chlorite.

free. This variety forms an equigranular mosaic texture which is well developed in zone 5b (Figure 11). Among these olivine grains, 120° interfacial angles are commonly seen (Figure 12). Textural relations indicate that these fine grained olivines are formed from megacrystic olivines by re-crystallization processes. Recrystallization starts along grain boundaries and dislocations (Figures 10 and 13). This new generation olivine is called 'neoblast' following the terminology which Mercier & Nicolas (1975) used for deformed upper mantle peridotites.

COLOURED PICTURES
Images en couleur

Figure 11: Neoblastic olivines occuring together with megacrystic olivines from which they are derived. Megacrystic olivines are completely recrystallized into neoblasts forming mosaic texture on the right hand side of the photomicrograph.

Peridotite in zone 5a consists of loosely packed olivine megacrysts, neoblastic olivine mosaic and light green-gray orthopyroxene-amphibole matrix (Figure 11) giving the rock a 'spotted appearance'. Dunite in zone 5c, on the other hand, is composed of closely packed olivine megacrysts with a minimum interstitial area which is filled by orthopyroxene, amphibole, and aluminous chromite (Figure 14), displaying cumulus texture. These equigranular olivine megacrysts very often enclose tiny subhedral amphibole and chlorite inclusions forming parallel oriented flakes or bunches (Figure 10) which are somewhat similar to those constituting the ma-

COLOURED PICTURES
Images en couleur

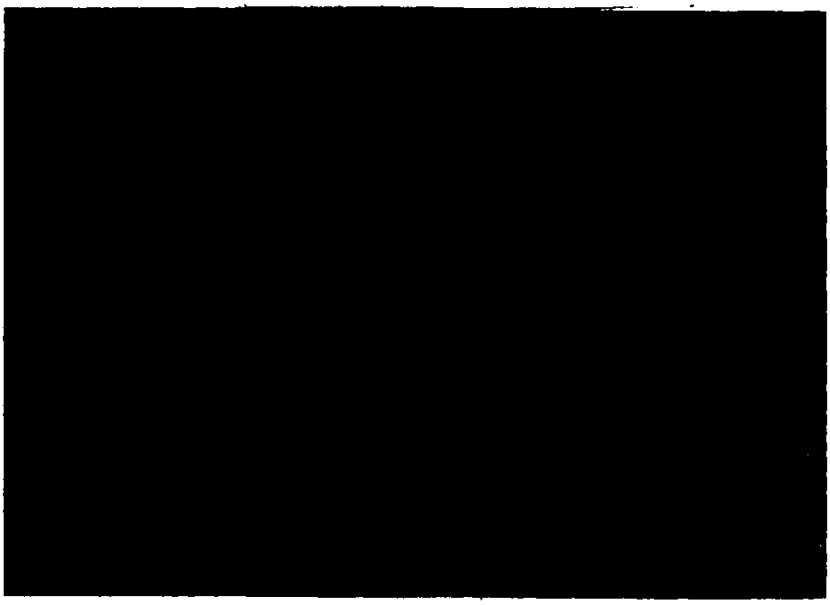

Figure 12: Fine grained neoblastic olivines occuring together with orthopyroxene megacrysts. Idioblastic flakes are chlorite.

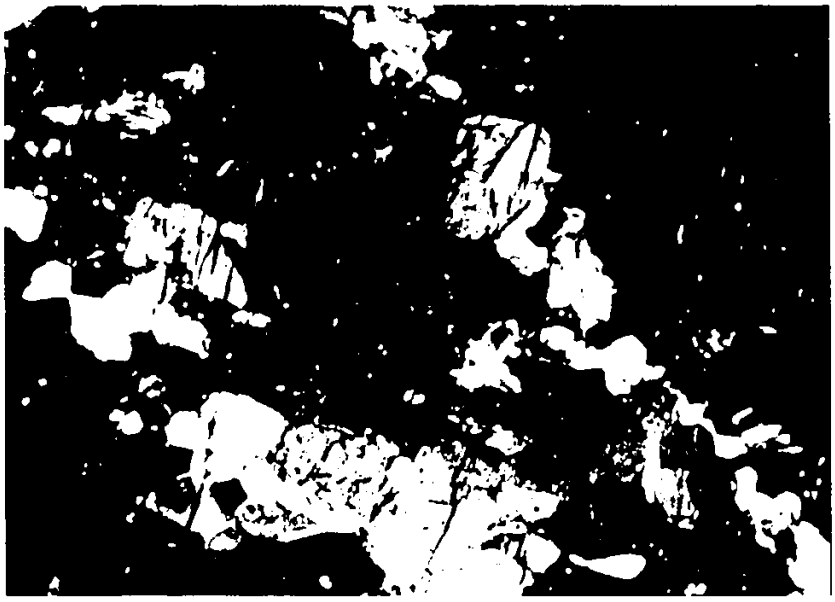

Figure 13: Large olivine megacryst containing two zones of olivine neoblasts, presumably developed along dislocation planes.

trix. Close to the serpentinized tremolite peridotite (zone 6), there are anhedral chlorite inclusions in megacrystic olivine. It seems that they develop along certain crystallographic directions of host olivine and usually enclose green-yellow spinel (Figure 15).

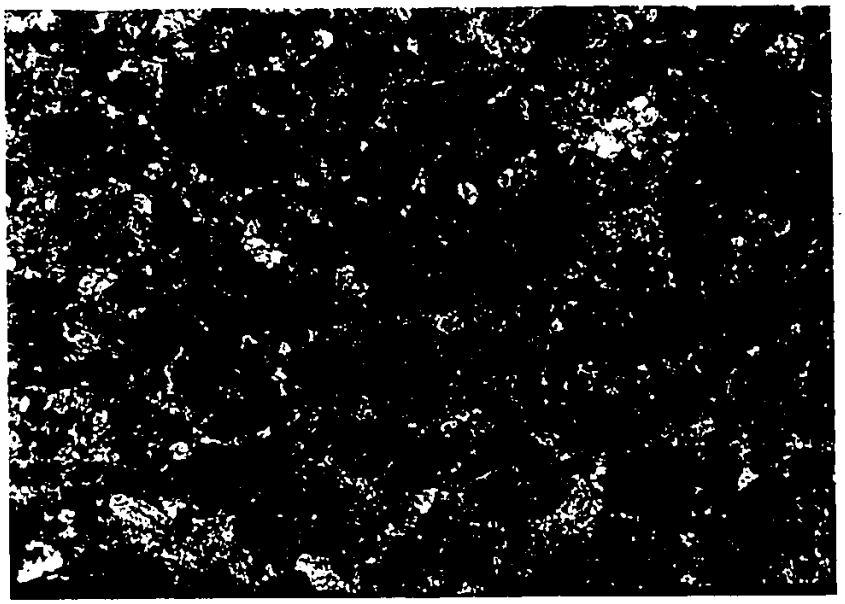

Figure 14: Closely packed olivine megacrysts forming cumulus texture.

Tremolite peridotites in zones 2 and 6 are serpentinized. The degree of serpentinization varies throughout the zones. Thin serpentine veins form planar veinlet systems probably parallel to the fabric of the body and to the foliation of the enclosing schist. They cut megacrystic and neoblastic olivines and tremolites. Magnetite occurs in stringers following serpentine veins and along the cleavages of chlorite. Minor carbonate is also present in thin serpentine veins.

COLOURED PICTURES
Images en couleur

Figure 15: Secondary chlorite developing along certain crystallographic direction of olivine megacryst, probably as a result of olivine and spinel reaction. Small relicts of spinel are enclosed by chlorite.

Orthopyroxene is medium grained. It is found interstitial to olivine megacrysts, enclosing xenomorphic islands of olivine showing communal extinction (Figure 16), and enclosing medium grained amphibole and chlorite.

Amphiboles are colourless tremolite and cummingtonite. They generally form small fibrous and prismatic crystals, coexisting with olivine neoblasts.

Two types of spinel are present. One is pale brownish yellow chromian-spinel which is commonly seen as fine disseminated grains in the olivine-orthopyroxenitic and orthopyroxenitic units. It is randomly disseminated throughout the

Figure 16: Orthopyroxene (at extinction) replacing olivine megacrysts.

peridotitic zones. In some places, however, it is preferentially concentrated along the grain boundaries of olivine megacrysts. It usually forms fine anhedral zoned grains, the cores of which are always darker than the rims. The other type of spinel is opaque aluminous chromite which is coarser than the former type. It occurs interstitial to the olivine megacrysts in zone 5b where the olivines are closely packed forming cumulus texture (Figure 17).

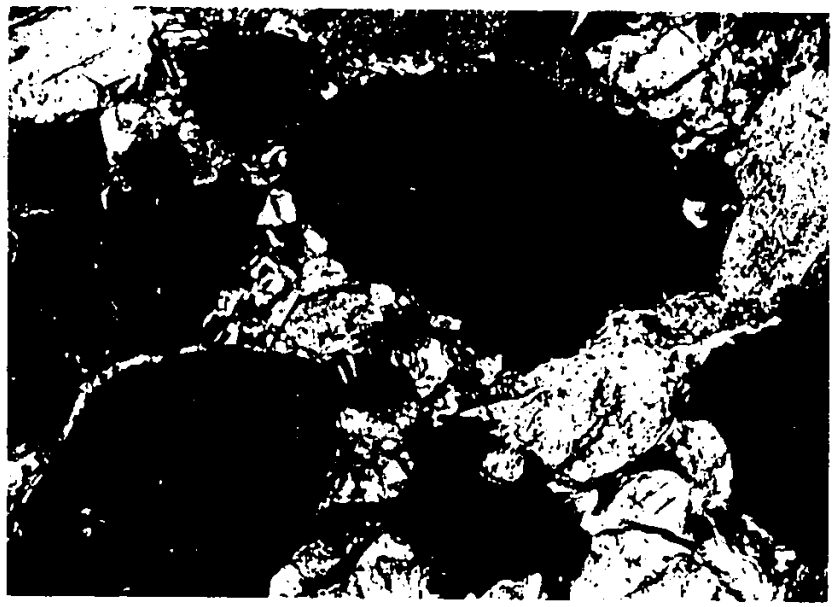

Figure 17: Euhedral-subhedral olivine megacrysts. Alchromite and minor orthopyroxene are interstitial to olivines.

3.1.1.2 Tremolite orthopyroxenite

Orthopyroxenes form coarse, slightly elongated equigranular grains, pale brownish in colour. Grain size ranges from 0.3 to 1 cm. Abundant fine grained amphibole, phlogopite and brown spinel disseminations are present in some of the orthopyroxene megacrysts. The interstices of the orthopyroxene megacrysts are occupied by fine grained light green amphibole and phlogopite which are similar to those enclosed in orthopyroxenes but coarser in grain size (Figure 18).

Thin lamellae[1] parallel to (100) of orthopyroxene (Figures 16 and 19), are observed in some grains. Strained crystals of orthopyroxene are common. The orthopyroxene megacrysts in zone 1 are elongated probably along the foliation plane of the enclosing schist. Tremolite is common. It is found as medium to coarse grained xenoblasts whereas anthophyllite forms randomly oriented, radiating prismatic blade-like crystals in a finer grained matrix. Phlogopite is seen as strained platy and fine grains. It is partly replaced by orthopyroxene in zone 1. In zone 12, on the margin of the body, phlogopites are recrystallized and pseudomorphed by green chlorite. Minor olivine is present as small inclusions in orthopyroxene, close to zone 3. Brown to greenish yellow spinel is very common as small subhedral to anhedral crystals, commonly zoned (with brownish core and yellow rim) disseminated grains, preferentially concentrated in the interstices of orthopyroxene megacrysts or in orthopyroxene close to its margins. Sulfides are present as disseminated anhedral grains.

3.1.1.3 Tremolite olivine orthopyroxenite

Texture is quite uniform in this unit. Olivine grain size is 4 mm and less and it forms xenomorphic grains which are usually enclosed in coarser (1-1.5 cm) orthopyroxenes.

---

[1] Lamellae have very low Ca content.

COLOURED PICTURES
Images en couleur

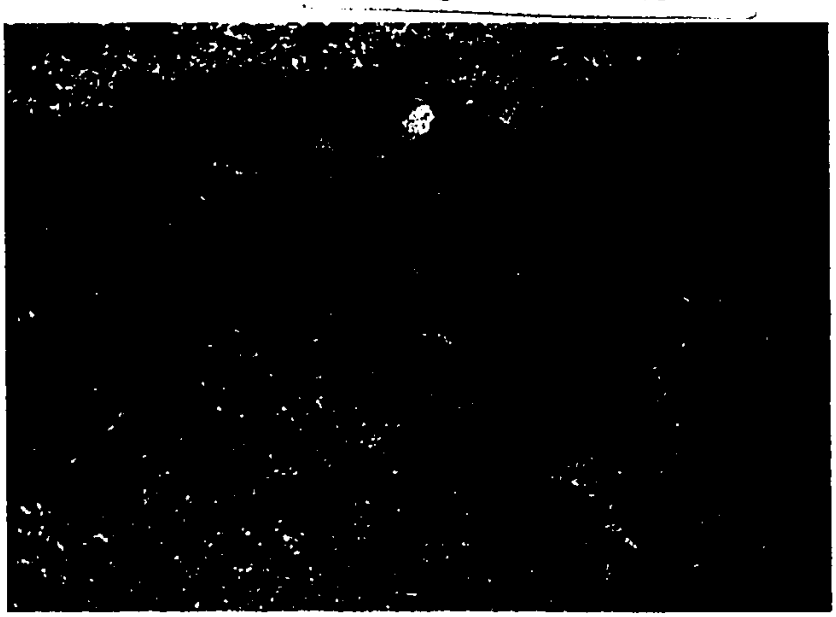

Figure 18: Elongate orthopyroxene megacrysts enclosing fine inclusions similar to those constituting matrix.

Some of these orthopyroxenes have triple junctions with 120° interfacial angles.

3.1.1.4 Amphibolite

The unit seen in zone 8 is composed of amphibole, phlogopite and minor plagioclase. Amphibole forms a medium grained (1 mm) granular texture with a weak fabric. Two amphiboles, magnesian cummingtonite and anthophyllite, are present. Medium grained phlogopite forms the groundmass for equigranular amphiboles. It shows foliation parallel to the margin of the body. Plagioclase, on the other hand, is fine to medium grained occurring in the interstices of phlogopite

0.6mm

Figure 19: Deformation lamellae in orthopyroxene.

and amphibole. This unit is cut by several thin (up to 1 cm) pegmatite veins.

3.1.2 Mineral Chemistry

Analytical procedure and the precision of the analyses obtained from replicate determinations are given in Appendix A, Table 1. Analyses of olivine, pyroxene, amphibole, and spinel are listed in Table 2. FeO and/or Fe are reported as total iron throughout the thesis except for spinel. Ferric and ferrous iron content of spinel were calculated assuming ideal spinel stochiometry.

3.1.2.1 Olivine

The composition of olivine in the dunitic zone 5b is uniform, ranging from Fo88 to Fo89. However, it is not uniform in zone 5a, and exhibits a rapid change from Fo89 to Fo85 towards zone 4. In zone 3, it is slightly more magnesian, being Fo89.5. The olivines from diamond-drill hole 64816 are more iron-rich showing a compositional range from Fo83 to Fo87. This compositional variation is controlled mainly by the bulk-rock composition (Figure 20). The NiO content of olivine ranges from the limit of detection to 0.40 (wt. %), increasing with the magnesian content (Figure 21). However, this relationship is not the same as that shown by magmatic olivines. The olivines with low nickel content fall outside the compositional range of olivines in cumulates and mantle peridotites. The MnO content ranges from 0.1 to 0.35 (wt. %) and shows negative correlation with forsterite content.

The compositional difference between megacrystic and neoblastic varieties is small, although the neoblastic olivines tend to be slightly enriched in Ni and Mn compared to the megacrystic olivines from which neoblastic olivines are formed (Figure 21). The individual grains of olivine megacrysts seem to be compositionally homogeneous.

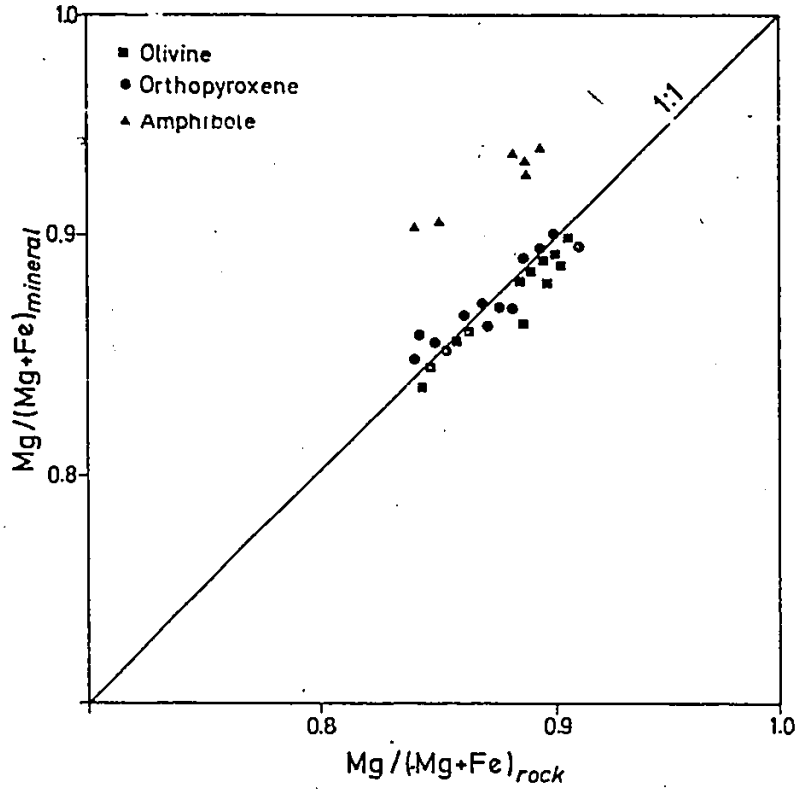

Figure 20: Relationship of bulk rock chemistry to the constituting minerals.

3.1.2.2 Orthopyroxene

The Mg/(Mg+Fe) atomic ratio (XMg) of the orthopyroxenes ranges from 0.84 to 0.91. It is 0.89 in zone 5b and decreases to 0.87 in zone 5a showing a similar pattern to XMg of olivines. In zone 4, this ratio is about 0.85 and shows an increase toward zone 3. It reaches a maximum value of 0.91 in zone 3, close to zone 4 and decreases toward zone

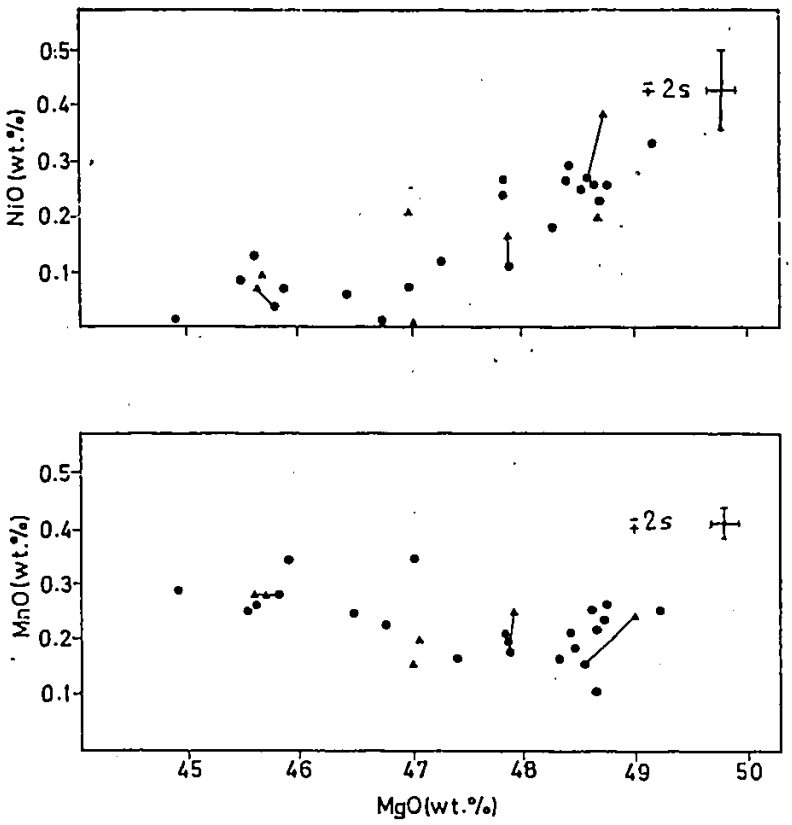

Figure 21: Plots of MgO vs. NiO and MnO in olivines. Tie-lines connect neoblastic olivine (triangle) to megacrystic ones (solid circle) from which they are derived.

2. The orthopyroxenes from zones 11 and 12 are more iron-rich, ranging from En85 to En87, similar to the coexisting olivines (Fo83-Fo87). XMg of both olivine and orthopyroxene is probably controlled by the bulk-rock chemistry (Figure 20).

The partition coefficient for the distribution of Mg and Fe between coexisting olivine and orthopyroxene

($Kd=(XMg/XFe)_{ol} \cdot (XFe/XMg)_{opx}$) is 0.985 (Figure 22). This is similar to the partition coefficient of regionally metamorphosed peridotites from the Alps (0.96; Trommsdorff & Evans 1974) and smaller than those of zone IV of the Tari-Misaka contact metamorphosed ultramafic complex (1.03; Arai 1975), Totalp serpentinites (1.05; Peters 1968) and metaperidotites of Paddy-Go-Easy Pass (1.10; Frost 1975). According to Medaris (1969), Mg and Fe partitioning between olivine and orthopyroxene is not sensitive to temperature over the range 700°C to 1300°C. However, recent thermodynamic formulations (Sack 1980) show that it is a potentially useful geothermometer.

CaO concentrations in orthopyroxene are very low (less than 0.21 wt. %), similar to orthopyroxenes from contact metamorphosed peridotites (Arai 1975) and from regionally metamorphosed peridotites (Evans & Trommsdorff 1974). Al_2O_3 content of orthopyroxenes is less than 1.75 (wt. %) and has been shown to be essentially a function of temperature (Dobretsov 1968; Fujii 1976; Mercier 1976) and of coexisting minerals. Its pressure dependence is restricted to temperatures above 1000°C according to the T-P phase diagram of Gasparik & Lindsley (1980). Low alumina and calcium contents are characteristics of orthopyroxenes in the amphibolite facies, though there is a gradual increase in these components as the higher temperature parts of the facies are reached (Evans 1977). Highly aluminous orthopyroxenes, on

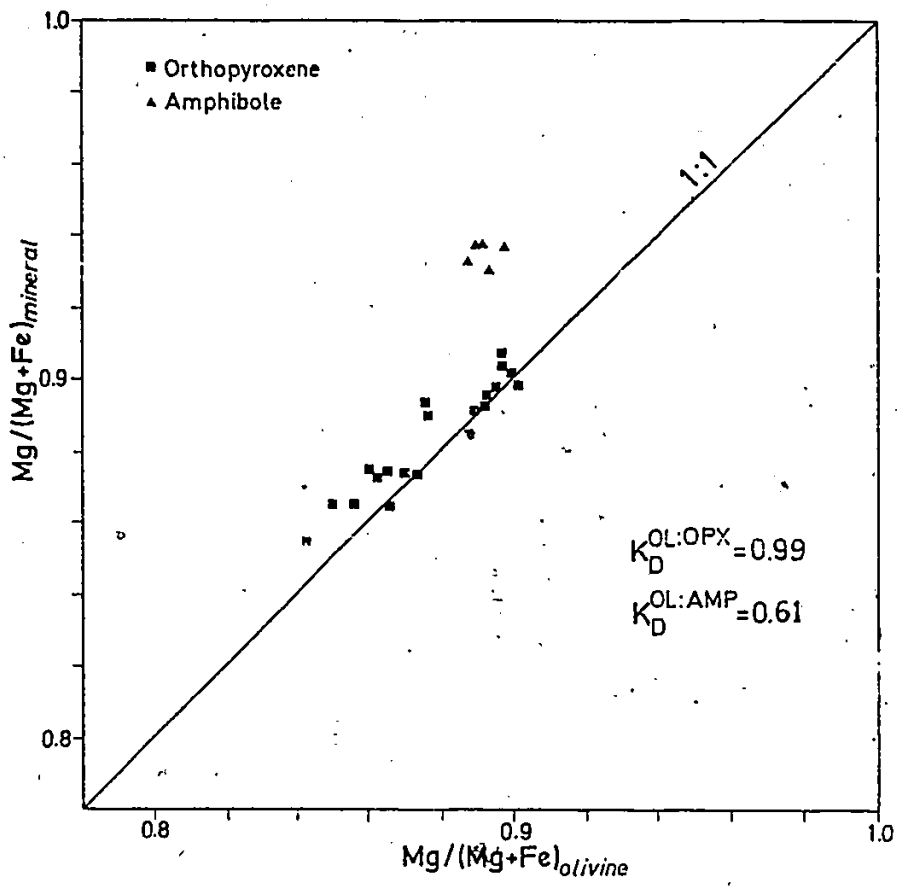

Figure 22: Partitioning of Mg and Fe between olivine and coexisting silicates

the other hand, are well known in alpine spinel peridotites of the granulite facies (Evans 1977).

3.1.2.3 Amphibole

Calcic amphibole analyses plot between tremolite and pargasite end member compositions forming a linear trend, on the Al^{IV} -(Na+K) diagram (Figure 23). This trend is in the

field of metamorphic amphiboles defined by Jamieson (1981). Al2O3 content ranges from 3.3 to 8.4 (wt. %), increasing with an increase in alkali content. The CaO content is relatively constant being about 12.5 (wt. %). Mg/(Mg+Fe) ratios of these calcic amphiboles range from 0.90 to 0.94 and are higher than those of coexisting olivine and orthopyroxene (Figure 22) and of the bulk rock (Figure 20).

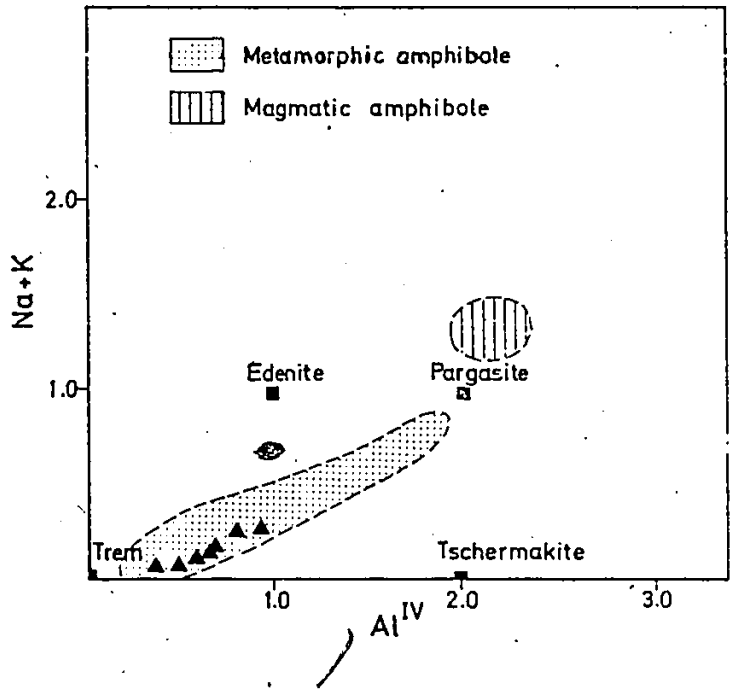

Figure 23: Plot of Al^{IV} vs. Na+K (number of atoms per 23 oxygen ions) of calcic amphiboles (triangles). Location of end member compositions are after Deer et al. (1966). Metamorphic and magmatic amphibole fields are after Jamieson (1981).

3.1.2.4 Spinel

In the peridotitic parts of the body, spinel ranges in composition from aluminous chromite to chromian spinel whereas in the pyroxenitic parts it is chromian spinel to Mg-Al-spinel. According to Evans (1977) these compositional ranges are confined close to the granulite and pyroxene hornfels facies transition. Evans also indicated that spinels are chromian magnetite in low grade serpentinites, ferritchromite in antigorite serpentinites and chromite in talc-olivine rocks.

$Cr/(Cr+Al+Fe^{+++})$ ratios (YCr) are between 0.60 and 0.75 in the dunitic part of zone 5b and range from 0.75 to 0.10 in the rest of zone 5. Some part of this wide range is confined to zoned grains and to grains in the same section. Rims of zoned spinels are enriched in Al and Mg relative to Cr and Fe^{++} (Figure 24). Similar paths from core to rim are reported by Evans & Frost (1975). This ratio is rather uniform in zone 4 ranging from 0.10 to 0.20.

The effect of temperature on YCr of spinel and the Mg-Fe^{++} partition between spinel and coexisting silicates, was first investigated by Irvine (1965), followed by Evans & Frost (1975), and Frost (1975). In general spinel becomes more Al- and Mg-rich relative to Cr and Fe^{++} similar to the path seen in Figure 24, as the grade of metamorphism increases.

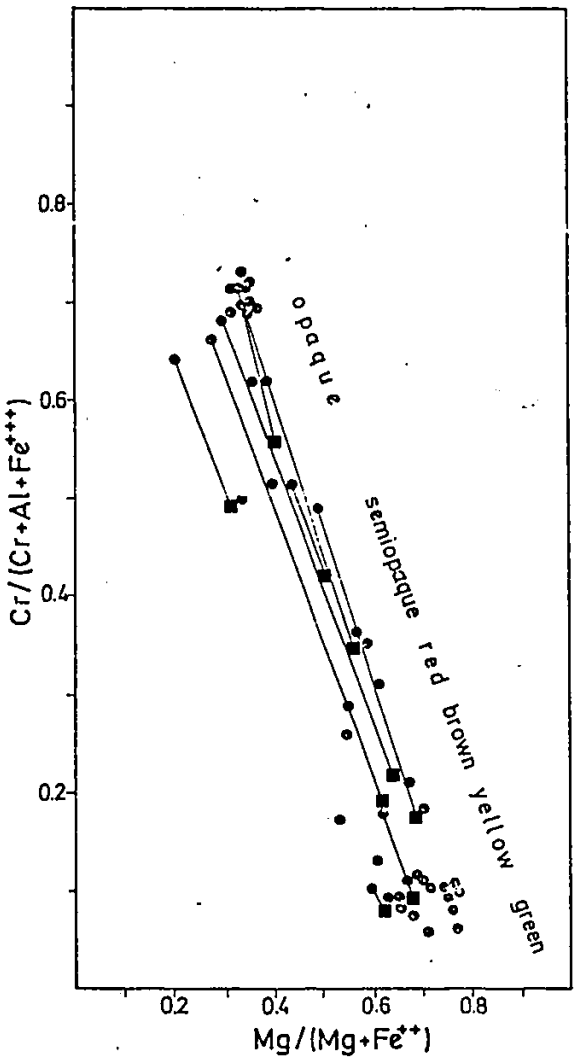

Figure 24: Plot of XMg vs. YCr in spinels. Core and rim (squares) compositions of zoned spinels are connected. Spinel changes from opaque to green colour as the temperature increases.

Minor elements such as Ti, V and Mn are enriched in Cr-rich varieties (Figure 25). No such correlation exists for Ni. TiO2 goes up to 0.30 (wt. %) whereas V2O3 reaches a maximum of 1.90 (wt. %).

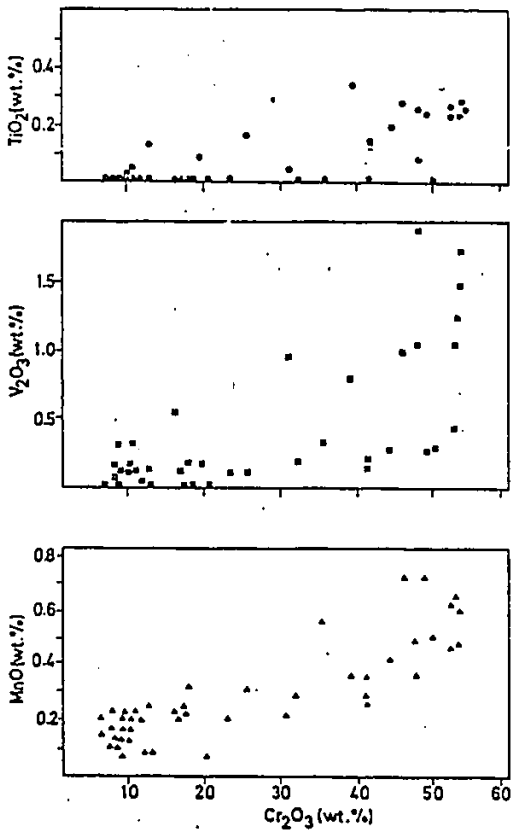

Figure 25: Plots of Cr2O3 vs. TiO2, V2O3 and MnO in spinels.

3.1.3 Geotemperature Estimates

3.1.3.1 Olivine-spinel geothermometer

Olivine-spinel geothermometer based on the partition of Mg and Fe^{++} between coexisting spinel and olivine has been applied to the Thompson olivine-spinel pairs. Two different calibrations of this geothermometry have been used. One of them is that of Roeder et al.(1979) which is basically the geothermometer of Jackson (1969) except that a different free energy value for $FeCr_2O_4$ has been used. The other is by Fabries (1979) which is based on the tentative graphical calibration of Evans & Frost (1975). The equation of Roeder et al (1979) is:

$$T(^{\circ}K) = \frac{3480YCr+1018YAl-1720YFe^{+++}+2400}{2.23YCr+2.56YAl-3.08YFe^{+++}-1.47+1.987\ln Kd}$$

and of Fabries (1979) is:

$$T(^{\circ}K) = \frac{4250YCr+1343}{1.825YCr+0.571+\ln Kd}$$

where;

$YCr=Cr/(Cr+Al+Fe^{+++})$

$YAl=Al/(Cr+Al+Fe^{+++})$

$YFe^{+++}=Fe^{+++}/(Cr+Al+Fe^{+++})$

$Kd=(XMg/XFe)_{ol} \times (XFe^{++}/XMg)_{sp}$

$XMg=Mg/(Mg+Fe^{++})$

$XFe=Fe^{++}/(Mg+Fe^{++})$

Temperatures obtained from these two calibrations are different. Those which are obtained from the equation of Roeder et al.(1979) vary from 400°C for the Cr-rich spinels to 1100°C for the Al-rich spinels. These temperatures are unreasonable for the mineral assemblages. The applicability of the Roeder et al.(1979) geothermometer has been challenged since their isotherms are inconsistent with recent reversed experimental data at low temperatures and with trends from metamorphic and igneous rocks (Engi & Evans 1980) and since the free energy values for the end member spinels are not known accurately (Fabries 1979).

In contrast to the isotherms of Roeder et al.(1979) (Figure 26), those of Fabries (1979) coincide with the regression line of the Thompson olivine-spinel pairs. They plot linearly with a correlation coefficient of 0.996 in the lnKd-YCr diagram (Figure 26). The regression line lies between the 600°C and 800°C isotherms and intersects the 700°C isotherm where YCr is 0.16. This may indicate that not all the samples have equilibrated under the same thermal conditions but some of them, with YCr<0.16, have reequilibrated during progressive metamorphism. As already mentioned, spinel changed its composition during progressive metamorphism; therefore, the regression line may represent the path of progressive metamorphism.

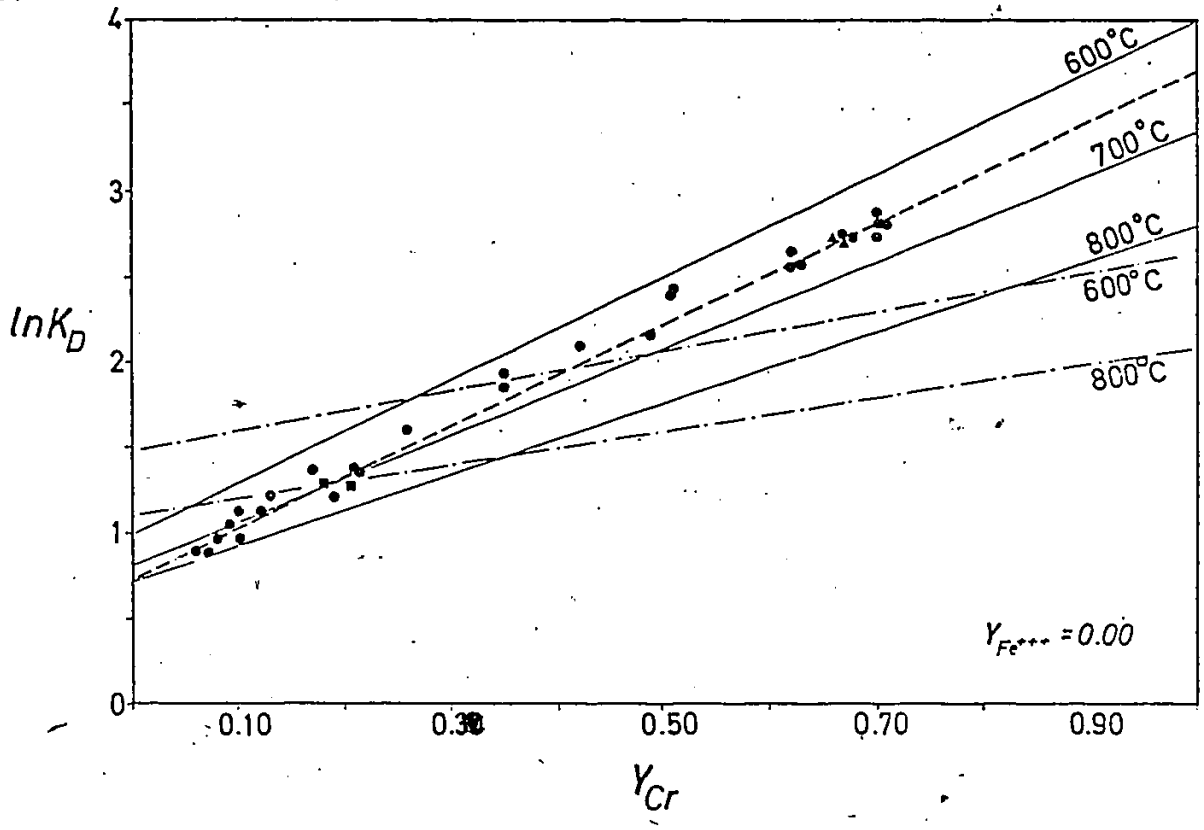

Figure 26: Plot of lnKd vs. YCr. Two spinel cores (triangles) and their rims (squares) are shown for comparison. Dashed line (2.97YCr-lnKd+0.755=0) is the regression line of plots with a correlation coefficient of 0.996. Solid lines are the isotherms calculated from the equation of Fabries (1979); dashed-dot lines are calculated using the equation of Roeder et al (1979).

The presence of zoned spinels indicates that complete equilibrium between olivine and spinel was not achieved at high grades. In the lnKd-YCr diagram, cores of two zoned spinel crystals plot near the 660°C isotherm. If we assume that the olivine is in equilibrium with spinel rims, it

plots very close to the 700°C isotherm (Figure 26). Precision error for this geothermometer is within ±50°C.

3.1.3.2 Alumina solubility in orthopyroxene

On the basis of experiments in the system MgO-Al2O3-SiO2, it has been shown by Fujii (1976) that alumina solubility in orthopyroxene is useful as a geothermometer. In order to estimate geotemperature values, the T-P phase diagram of Gasparik & Lindsley (1980) is used instead of the diagram given by Fujii (1976) because the diagram of Fujii (1976) deals with temperatures above 800°C but the former one has a temperature range which covers the range of interest (Figure 27).

Extrapolated temperatures using Mg-Ts (mol.%) isopleths in the orthopyroxene solid solution are approximately 640°C. The reason for the low temperature is probably because of the limitation of the geothermometer. This geothermometer in the Al2O3-MgO-SiO2 system is an approximation to the ideal solid solution models. According to Danckwert & Newton (1978), ideal solution corrections for FeO and Cr2O3 in coexisting spinel would raise temperature estimates.

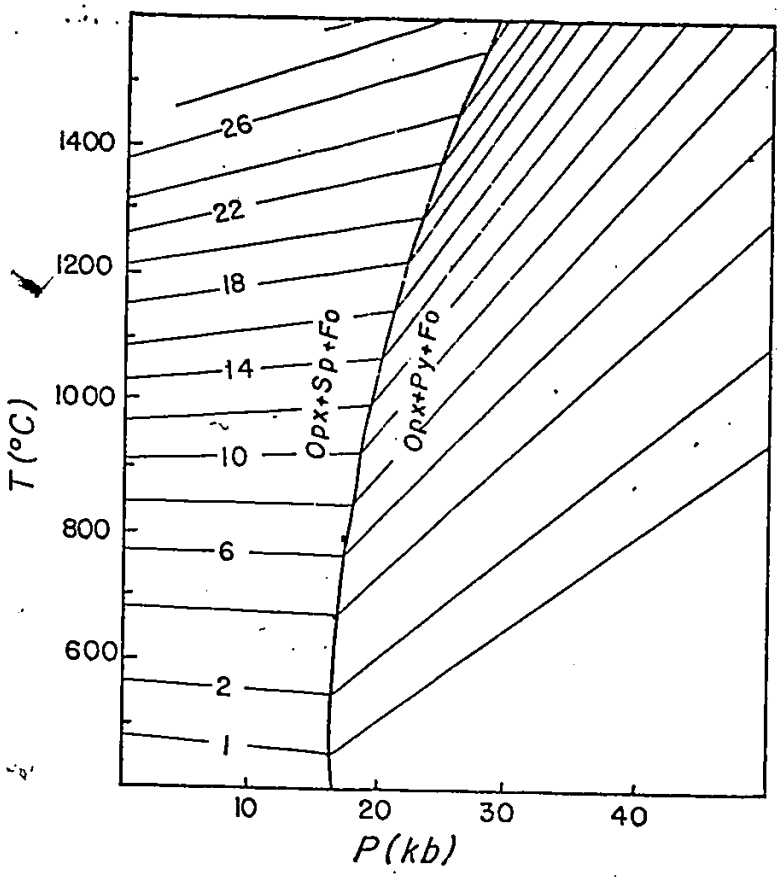

Figure 27: Magnesium-tschermak (mol%) isopleths in the T-P phase diagram for the system MgO-Al2O3-SiO2 after Gasparik & Lindsley (1980).

3.1.4 Rock Chemistry

Analytical procedure, precision and accuracy of the analyses are given in Appendix B, Tables 3 and 4. Complete sets of analyses are listed in Table 5.

The chemical data are plotted on various diagrams. It is seen on the Al2O3, FeO, CaO, TiO2 vs MgO (Figure 28), Al2O3

vs FeO/(FeO+MgO) (Figure 29), and Al2O3-CaO-MgO diagrams (Figure 30) that the rocks with a few exceptions, plot along distinct trends. The spread in plots along the trends is small. These coherent variations shown by most element pairs suggest that the original chemistry of the rocks has been preserved and not been greatly affected by metamorphism or alteration. If this was not the case, systematic changes in composition would not be apparent. This is justified in the cartesian diagrams of Pearce (1968 & 1969) on which the axes are represented by ratios of two elements with an immobile element (Figure 31). Al2O3 is chosen as the constant denominator since it is generally considered to be immobile. This is also suggested by the strong positive correlation of Al2O3 with other immobile elements such as TiO2 and Zr (Figure 32). Most of the rocks follow straight trends indicating little or no change to their major element chemistry. Several samples (T1.64, T1.68, T1.76) that plot away from the general trends in MgO/Al2O3, FeO/Al2O3, CaO/Al2O3, TiO2/Al2O3, MnO/Al2O3 vs SiO2/Al2O3 diagrams, are likely to represent altered samples.

The ultramafic rocks are compared with lherzolitic nodules, tectonite peridotites of ophiolite complexes, ultramafic komatiites and some inferred mantle compositions (Figure 28). Most of the oxide vs MgO variations show similar patterns to the regression lines of spinel lherzolites of which the field overlaps the peridotitic rocks. SiO2, MgO,

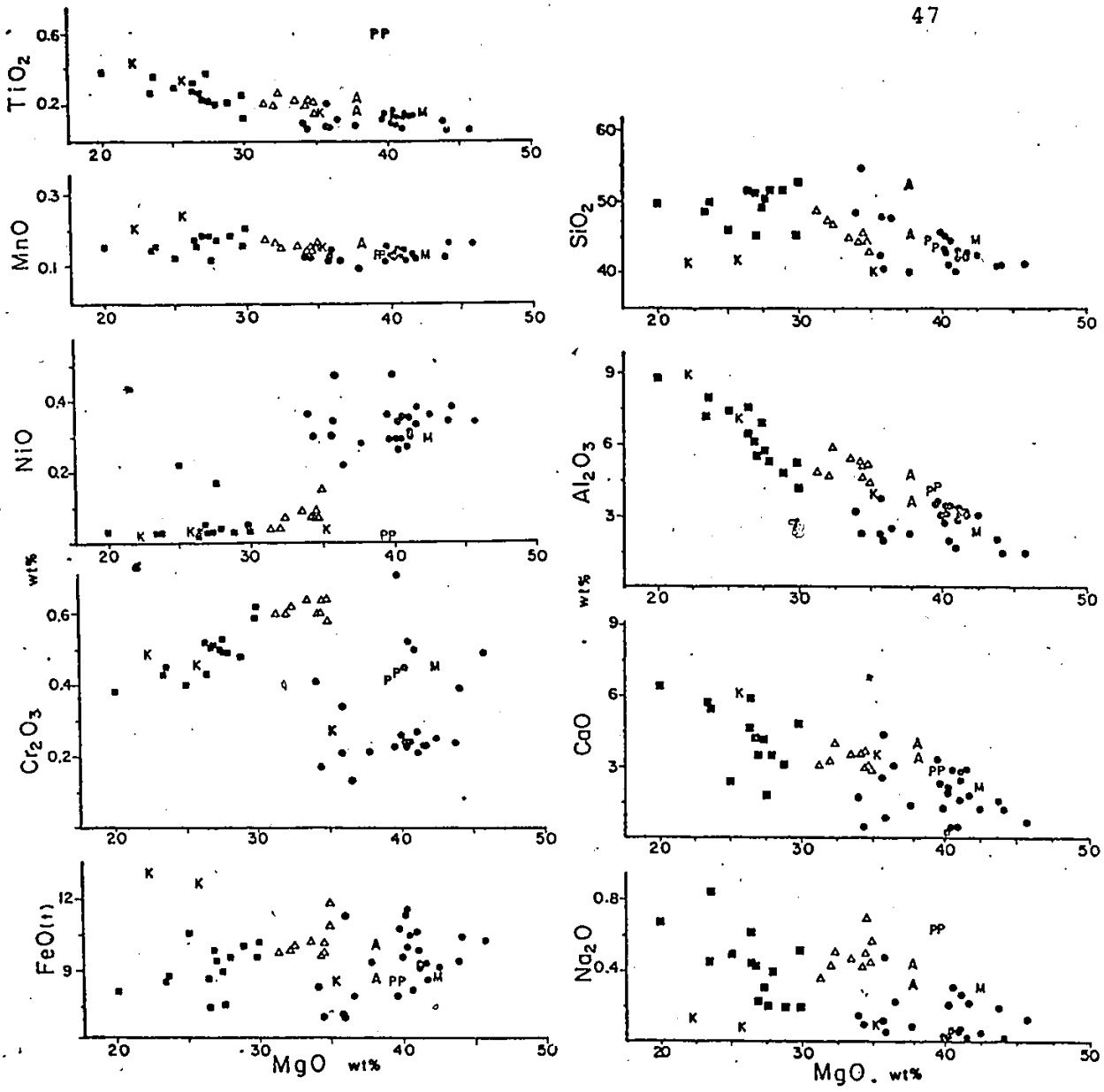

Figure 28: MgO variation diagrams. Filed circles, peridotitic rocks; triangles, olivine orthopyroxenitic rocks; squares, orthopyroxenitic rocks; A, estimated Archean mantle; K, representative peridotitic komatiites from Munro Township; M, average upper mantle composition; P, pyrolites (sources given in text)

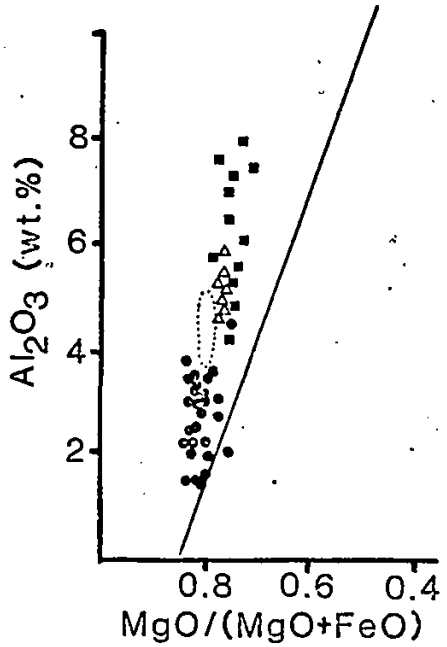

Figure 29: Al2O3 vs. MgO/(MgO+FeO) discrimination plot. Filled circles, peridotitic rocks; triangles, olivine orthopyroxenitic rocks; squares, orthopyroxenitic rocks; dotted area, estimated Archean mantle (Sun & Nesbitt 1977). Inclined line separating komatiites from tholeiites is after Naldrett & Cabri (1976).

FeO, CaO, Al2O3, Na2O and TiO2 concentrations of the inferred mantle (Maaloe & Aoki 1977) are very close to the peridotitic rocks. SiO2, MgO, FeO, Al2O3, CaO, MnO, and Cr2O3 concentrations of the calculated Archean mantle (Sun & Nesbitt 1977) and pyrolites (Ringwood 1966, Green & Ringwood 1970) plot in the peridotitic field, close to the olivine orthopyroxenitic rocks. TiO2 and Na2O concentrations are similar in the peridotitic rocks and the Archean mantle;

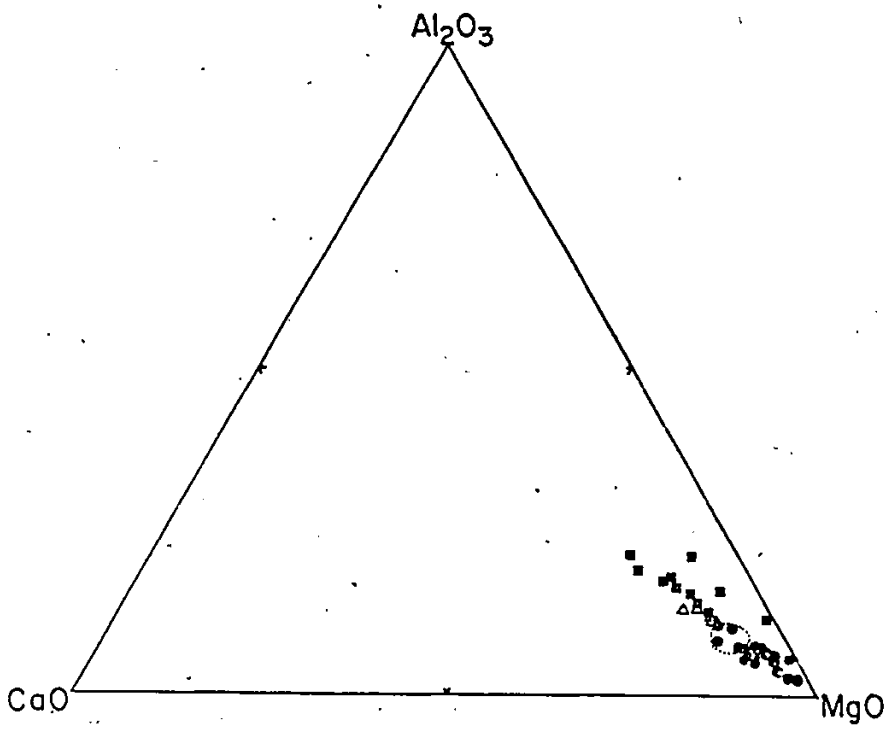

Figure 30: MgO-CaO-Al2O3 diagram. See Figure 29 for symbols.

however, they have higher abundances in the pyrolitic mantle. The trends of peridotitic komatiites[2] (Arndt et al 1977) in the SiO2, Al2O3, CaO, TiO2, MnO vs MgO diagrams are similar to those shown by the Thompson ultramafics. In the MgO-Cr2O3 diagram, peridotitic rocks plot away from the orthopyroxenitic and olivine orthopyroxenitic rocks and show scatter. However, a trend from peridotitic towards orthopy-

---

[2] Included here are three representative analyses: cumulate peridotite, spinifex-textured peridotitic komatiite and flow top of a spinifex-textured peridotitic komatiite flow, from Munro Township.

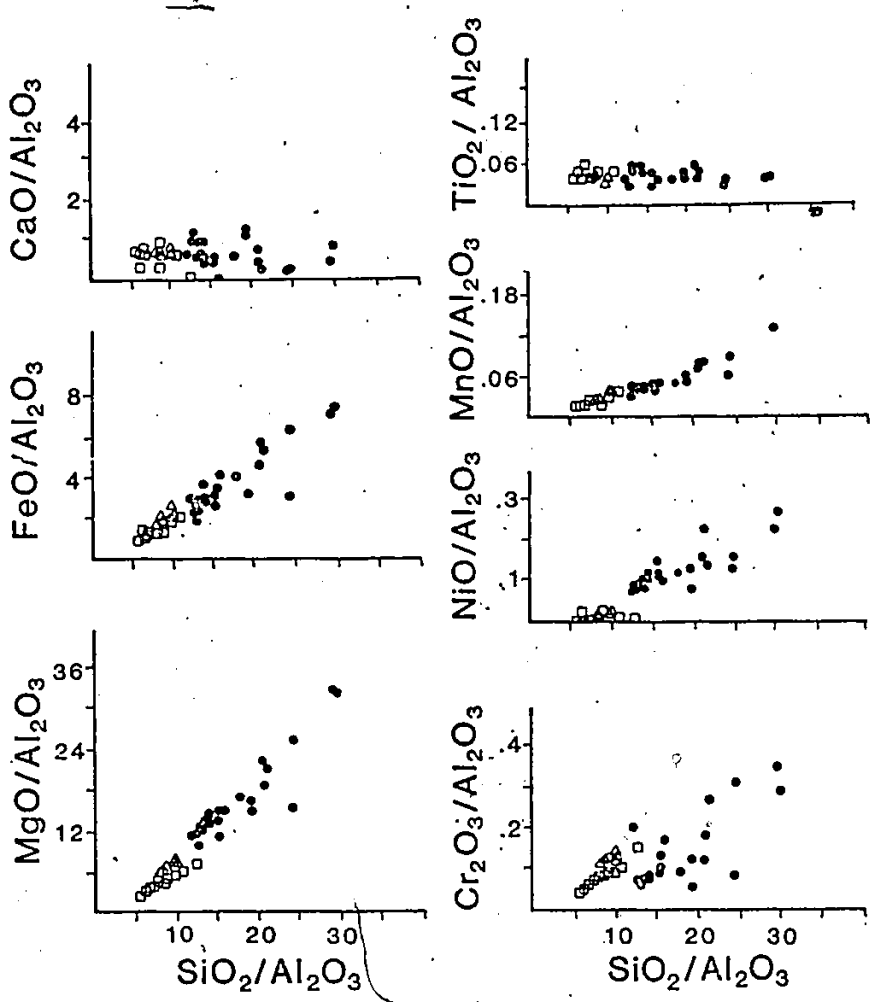

Figure 31: Pearce-type ratio diagrams (wt. % of oxides are used). Circles, peridotites; crosses, olivine orthopyroxenites; squares, orthopyroxenites.

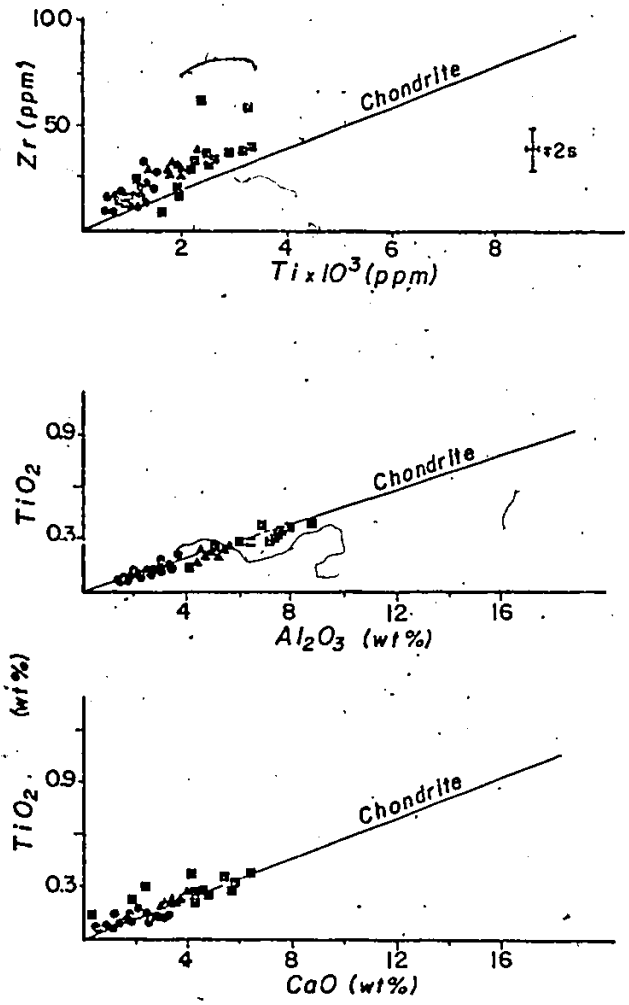

Figure 32: TiO2 vs. Al2O3 and CaO, and Ti vs. Zr plots. Circles, peridotitic rocks; triangles, olivine orthopyroxenitic rocks; squares, orthopyroxenitic rocks. Ti/Zr ratio of chondrites is after Kay & Hubbard (1978); CaO/TiO2 and Al2O3/TiO2 ratios of chondrites are after Sun & Nesbitt (1977).

roxenitic rocks, similar to the trend of the peridotitic komatiites is distinguished. Spinifex-textured peridotitic komatiites plot close to the orthopyroxenitic rocks whereas cumulate peridotite plot near the peridotitic rocks. Except for two samples (T1.26 and T2.56) with nickel sulfides, all orthopyroxenitic rocks have very low Ni content. There is an enrichment in Ni through the olivine orthopyroxenitic rocks to peridotitic rocks in the MgO-NiO diagram. Peridotitic rocks that are highly serpentinized or have some sulfide disseminations show scatter.

Ratios of Al_2O_3/TiO_2 and CaO/TiO_2 are similar to those of chondrites and komatiites from Munro, Rhodesia, and Scotia (Figure 32). Ti/Zr ratio is smaller than the chondritic ratio (Figure 32).

In the K-Rb diagram (Figure 33), orthopyroxenitic and olivine orthopyroxenitic rocks of the body plot along the trend of most igneous rocks defined by Shaw (1968). They have higher K and Rb contents compared to the peridotitic komatiiites. Peridotitic rocks, however, have very low Rb contents and show scatter. This scatter is probably due to analytical uncertainty for those samples with very low Rb contents and metasomatism for those with high K contents. Ba and Sr contents of the peridotitic rocks are similar to peridotitic komatiites whereas olivine orthopyroxenites and some of the orthopyroxenitic rocks have distinctly higher Ba contents (Figure 33).

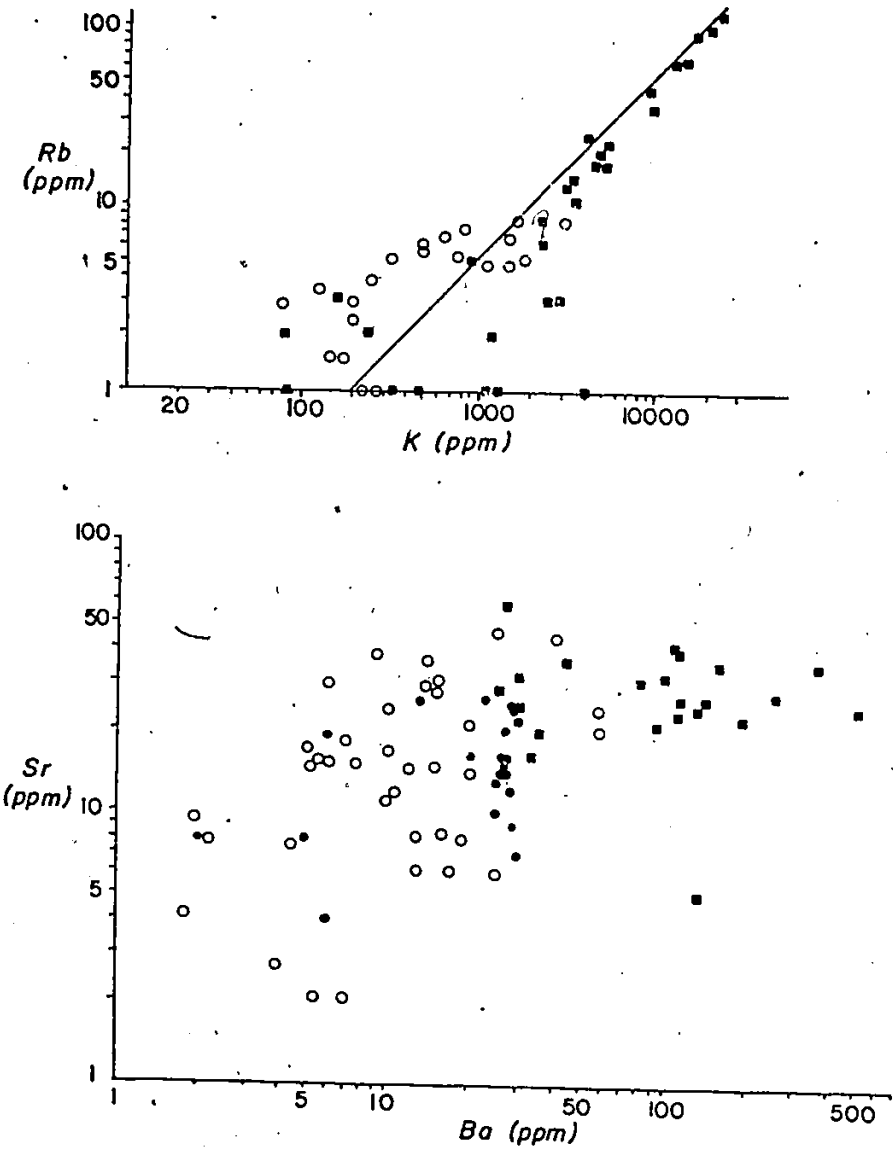

Figure 33: K vs. Rb and Ba vs. Sr plots. Filled circles, peridotitic rocks; filled squares, orthopyroxenitic rocks; open circles, komatiites from Canada, Africa, and Australia (Villaume & Rose 1977 and Nèsbitt et al 1979). The trend in the K-Rb diagram is for most igneous rocks defined by Shaw (1968).

Variations of major, minor and trace elements along the DDH 64599 and DDH 64816 are shown in Figures 34 and 35. One serpentinite sample in zone 2 and a schistose tremolite orthopyroxenite sample rich in phlogopite (zone 4) show abrupt changes in most of the variation patterns. They plot away from the general trends and are attributed to metasomatism as previously described. MgO decreases towards the margins of the body and from the peridotitic towards the orthopyroxenitic portions as expected. NiO exhibits variation pattern similar to that of MgO. Cr is enriched in the orthopyroxenitic rocks. There are abrupt increases in Cr content from the peridotitic towards the orthopyroxenitic portions, except in the dunitic portions with interstitial chromite. CaO, Al_2O_3 and TiO_2 show similar variations. Na_2O, K_2O, Rb and Ba are enriched on the margins of the body and in the orthopyroxenitic rocks compared to the peridotitic rocks. Mg/(Mg+Fe) ratio ranges from 0.88 in zone 2 to 0.84 near the contact of zone 4 with 5 and from 0.90 in zone 5a to 0.82 in zone 8. This type of variation suggests two magmatic cycles, formed by replenishment of magma. Similar variation is observed across a picritic body in the Upper Ospwagan Lake area (Peredery 1979). Cycle I includes zones 1 to 4 and cycle II zones 5 to 8. At the bottom of cycle II, in zone 5a, there is an increase in the Mg/(Mg+Fe) ratio. This increase is similar to what has been described by Irvine (1980) as a consequence of 'infiltration metasomatism'.

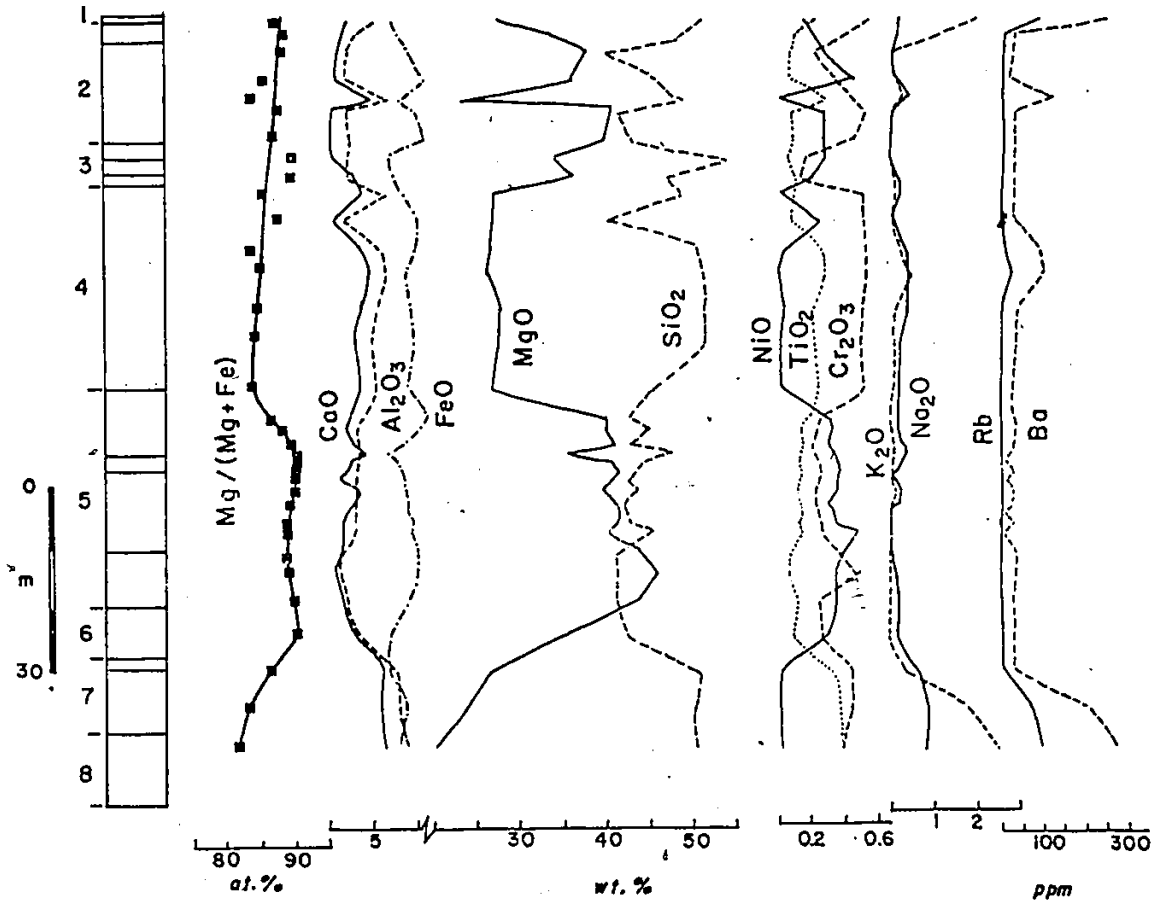

Figure 34: Chemical variation across the T-3 ultramafic body as seen along the DDH 64599.

However, oxide and elemental variations along the DDH 64816 are rather uniform, reflecting their uniform modal mineralogy and do not correlate with those of DDH 64599 (Figure 35). Precluding the possible effects of metamorphism, the relationship of the two intersections is now discussed. Mineralogical and chemical uniformity along the DDH 64816 and some irregular variations along the DDH 64599 can be interpreted as alternations of the same units due to tight folding. Actually, tight folding is commonly seen in less competent metasedimentary rocks and it is the major factor controlling the thickness of the biotite schist and nickel sulfide mineralization in the Thompson mine. Alternately, olivine orthopyroxenitic rocks seen along DDH 64816 may be interpreted as the result of migration of the residual liquid during crystallization of the peridotitic portion of the body. This is indicated by the fact that olivine orthopyroxenitic rocks plot between the peridotitic and orthopyroxenitic rocks in the variation diagrams. However, the latter possibility does not rule out the former interpretation. In other words, the thickness of the olivine orthopyroxenitic units, for instance, may still be due to tight folding. Magnesium shows a slight decrease from SE to NW side of the body. Cr and Ni variations are similar to MgO excluding several samples with Ni-disseminations. Although very little variation is seen in Mg/(Mg+Fe) ratio, it decreases slightly towards the NW side of the body.

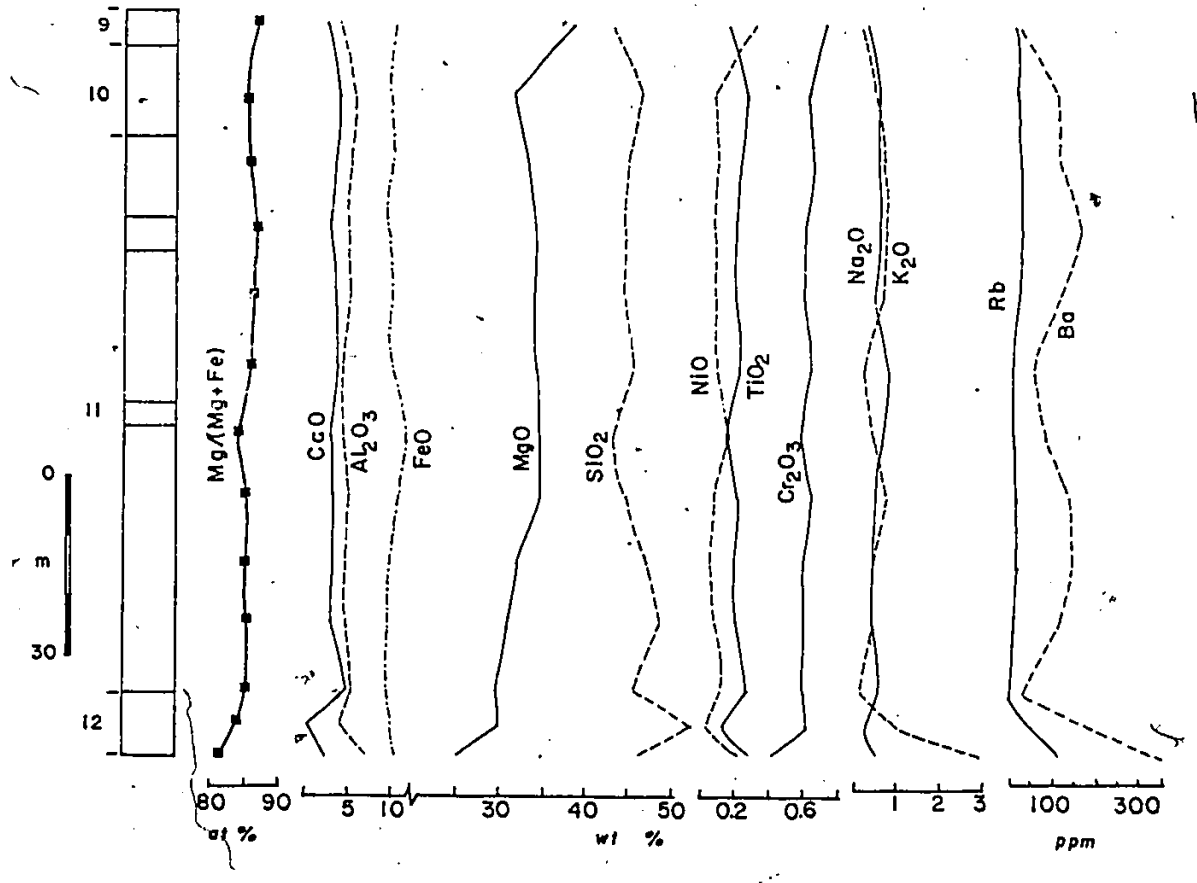

Figure 35: Chemical variation across the T-3 ultramafic body as seen along the DDH 64816.

3.2 PETROGENESIS

3.2.1 Igneous Petrogenesis

It appears that the ultramafic body was formed from a komatiitic liquid by crystal fractionation. Nearly all the rocks plot in the komatiite field in the Al_2O_3-FeO/(FeO+MgO) diagram (Figure 29), forming a linear trend from peridotitic rocks through olivine orthopyroxenitic rocks to orthopyroxenitic members where there is general FeO/(MgO+FeO) and alumina enrichment. In the MgO-CaO-Al_2O_3 diagram (Figure 30), the rocks form a trend from peridotitic to pyroxenitic rocks where there is general Al_2O_3 and CaO enrichments. This trend indicates an olivine control. Orthopyroxene may also be considered as a controlling phase if the fractionation takes place in a low-pressure environment. Controlling mineral phases in the bulk composition of the rocks are clearly justified in O'Hara's (1968) polybaric phase diagrams (Figure 36). In the clinopyroxene projection, the peridotitic and partly olivine-orthopyroxenitic rocks lie along an olivine-control line. This control line may represent the path of differentiated liquid during olivine fractionation. Alternately, the magma that is already olivine-rich, may be responsible for this trend. Orthopyroxenitic rocks form a distinct trend which is controlled by orthopyroxene and minor olivine. In the olivine projection, orthopyroxene control is evident. As seen on the enstatite and olivine projections, the olivine-orthopyroxene control line intersects

the 1 atmosphere phase boundary where plagioclase is the third phase to crystallize. These diagrams suggest that clinopyroxene does not seem to have been involved. Peridotitic komatiite samples from Munro Township (Arndt et al. 1977) also form an olivine control trend, although the trend is towards the clinopyroxene phase boundary (enstatite projection) or very close to the triple point (olivine projection). Average composition of continental and oceanic spinel lherzolites and the pyrolites plot close to the olivine control line. Basaltic rocks including a spinifex textured variety, lie around the olivine-orthopyroxene phase boundary in the diopside projection (Figure 37). On the olivine projection, they plot around the olivine-orthopyroxene control line but slightly more dispersed.

Among the first transition elements, V, Cr, Mn, Fe, Co, and Ni are considered as compatible during fractionation of mafic minerals; therefore, they are useful indicators for understanding the crystallization process in mafic and ultramafic suites. Abundances of transition elements (Ti,Cr,Mn,Fe,Ni,Zn) together with Ca and Al, relative to chondrites and a spinifex textured peridotitic komatiite are shown on Figure 38. Ca and Al are added in order to see the behaviour of plagioclase. Ca is also useful for clinopyroxene, since Sc analyses[3] are not available. From Ca to Cr,

[3] Sc strongly partitions into clinopyroxene (strongly compatible- its mineral/melt ratio is 3 -Frey et al.,1974).

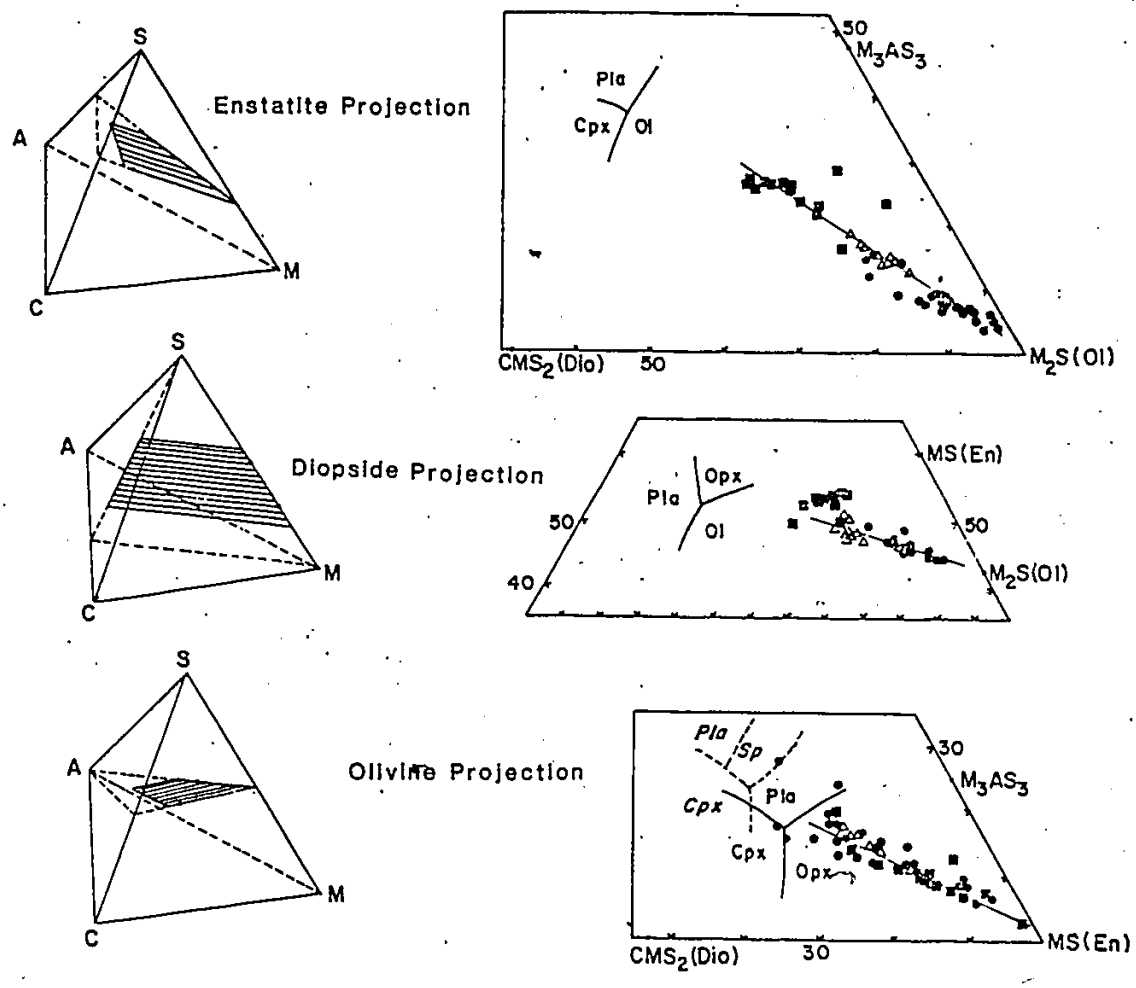

Figure 36: O'Hara's polybaric phase diagrams. Phase boundaries are at 1 atm. Also shown is the 9 kb phase boundary (dashed line). Circles, peridotitic rocks; triangles, olivine orthopyroxenitic rocks; squares, orthopyroxenitic rocks. Abbreviations: Dio, diopside; En, enstatite; Ol, olivine; Opx, orthopyroxene; Pla, plagioclase; Sp, spinel.

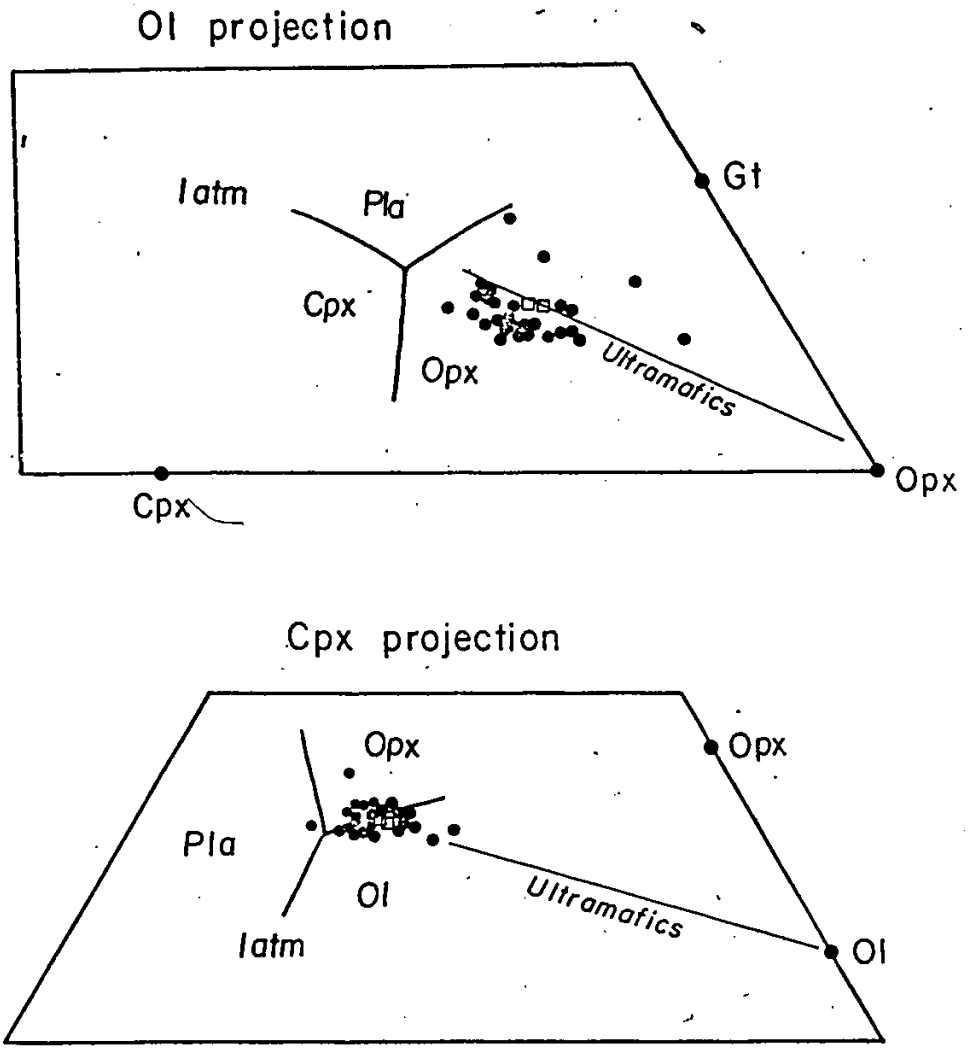

Figure 37: Olivine and clinopyroxene projections of the CMAS tetrahedron for the mafic rocks of the belt. Circles, mafic rocks; squares, quench textured magnesian basalts. Lines off the olivine and orthopyroxene corners are control lines of the ultramafic rocks (Figure 36).

the patterns of the three rock types are similar. There is a continuous enrichment of these elements from peridotites through olivine orthopyroxenitic rocks to orthopyroxenitic rocks. All three have similar abundances of Mn, Fe and Zn but differ in their Ni content. Both olivine orthopyroxenitic and orthopyroxenitic rocks have negative Ni anomalies. These patterns indicate that Ca, Al, Ti and partially Cr were relatively incompatible whereas Ni, Fe, Mn, and Zn were compatible during the crystallization of peridotitic parts. Ca /Al ratios of the peridotitic rocks are controlled by interstitial liquid trapped during fractionation of olivines. This ratio is similar to that of calcic plagioclase. Some patterns with Ca /Al ratios greater than 1 indicate some clinopyroxene fractionation. Cr with slight positive to negative anomalies is noteworthy and probably caused by a minor chromite fractionation and incompatible behaviour of Cr during fractionation. From these diagrams, it is inferred that olivine is the only fractionating mineral and is responsible for the chemical differentiation observed within the body.

The overall composition[4] of the ultramafic body is too magnesian to be representative of original liquid. Average MgO content of the body (34.11 wt%) is higher than suggested liquid compositions for komatiites which are in the range of

---

[4] Calculated assuming the two diamond-drill hole intersection represent the body.

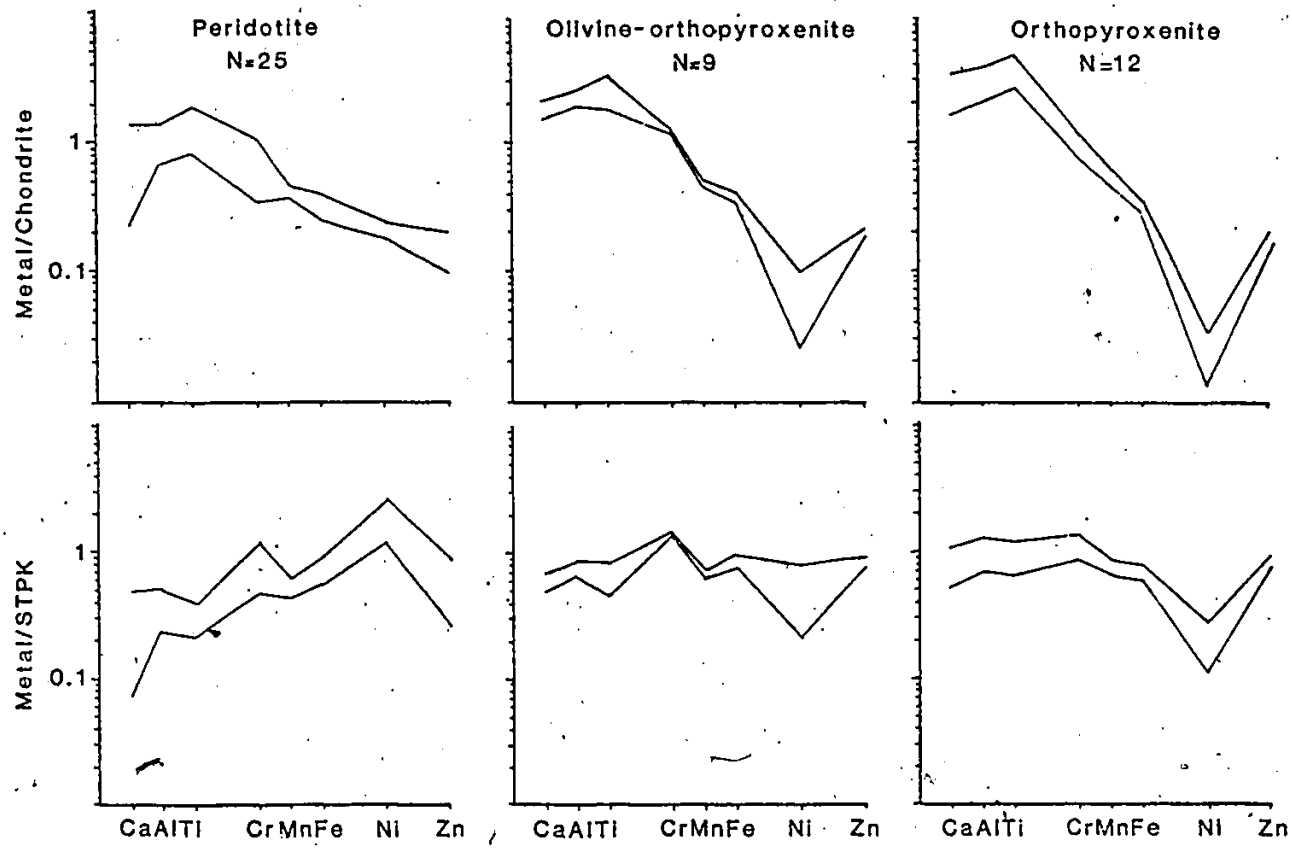

Figure 38: Ca, Al and transition metal abundances in the T-3 ultramafic body, plotted as multiples of chondrites and a spinifex-textured peridotitic komatiite (STPK).

20 to 30 wt %. The composition of the liquid, in equilibrium with the most magnesian olivine (Fo89) is calculated using a set of partition coefficient values. The partition coefficient Kd, where $Kd=(XMg/XFe)_{liq}/(XMg/XFe)_{ol}$ is practically independent of temperature and pressure (Irvine 1979). However it is worthwhile mentioning here that it is sensitive to temperature and pressure under upper mantle conditions (Mysen 1975). Kd values range from 0.30 to 0.36 for melt compositions encompassing terrestrial basaltic and ultrabasic liquids (Irvine 1979). Values of 0.345 for liquid without ferric iron and 0.293 for liquid with ferric iron which comprise 15 % of total iron, are suggested by Bickle (1982). Calculated XMg composition of liquid, in equilibrium with Fo89, ranges from 0.70 to 0.74 for the Kd values ranging from 0.293 to 0.36. This is much lower than the average composition (0.868) ; therefore, the average composition can not represent the original liquid. Consequently, alternate conclusions are as follows: 1) the body may have formed from a liquid containing an appreciable amount of olivine phenocrysts, 2) some differentiated liquid may have escaped, 3) less magnesian parts of the body may have been sliced off during deformation. The second possibility is a likely case, since XMg composition of the ultramafic amphibolites described by Peredery (1979) cover the range of XMg of liquids with which the most magnesian olivine equilibrated. In fact, ultramafic amphibolites (pi-

crites) associated with serpentinites are interpreted as fractional differentiates of an ultrabasic magma by Peredery (1982).

3.2.2 Metamorphism

As deduced from the mineral assemblages and textures, the ultramafic body has experienced a series of complex hydration and dehydration reactions during, before and following progressive metamorphism. The dominant mineral assemblage is olivine+tremolite+orthopyroxene+aluminous spinel, suggesting upper amphibolite facies conditions. The presence of tremolite as a Ca-bearing silicate instead of diopside, and the absence of talc and cordierite constrain the pressure and temperature conditions for the ultramafic rocks in the MgO-CaO-Al2O3-SiO2-H2O system (Figure 39). This corresponds to the amp-anth-chl peridotite, amp-chl peridotite and amp-peridotite rock types of Jenkins (1981). Occurrence of minerals representing lower grades such as aluminian-chromite, chlorite, Ca-poor amphibole together with olivine and orthopyroxene may be explained by polymetamorphism or locally varying fluid phase composition according to Evans (1977). The fine opaque material as previously discussed, can be relict magnetite stringers formed during serpentinization and enclosed in olivine during deserpentinization, or alternately, it may be a result of high-temperature oxidation of olivine. Since high-temperature oxidation products

usually form more regular patterns (Haggerty & Baker 1967), pyroxene and magnetite usually forming a dendritic intergrowth (Putnis 1979), the former possibility is favoured for the formation of the fine opaque material. In addition to these relict magnetite stringers, amphibole and chlorite inclusions forming parallel oriented flakes, optically continuous with grains adjacent to enclosing olivine megacrysts indicate metamorphic growth of olivine. Similarly, very irregular grain boundary relations of anhedral olivine with other metamorphic minerals strongly suggest this. Subhedral and euhedral olivine megacrysts, partly forming cumulus texture, may be interpreted as recrystallized igneous olivines with minor metamorphic modification, since formation of equant olivine grains by metamorphic processes would be unlikely. This is supported by relatively uniform forsterite content of olivines within individual specimens and uniform MgO-NiO and MgO-MnO relationships of subhedral-euhedral olivines.

Low CaO and Al_2O_3 content of the orthopyroxene megacrysts and their poikiloblastic nature indicate that they are metamorphic, not relict igneous. Minute inclusions of amphibole, chlorite and phlogopite are similar to the matrix material but smaller in size. They probably resulted from high growth rate of orthopyroxene relative to the rate of diffusion of components of the inclusions through the host orthopyroxene. According to the phase relations in Figure

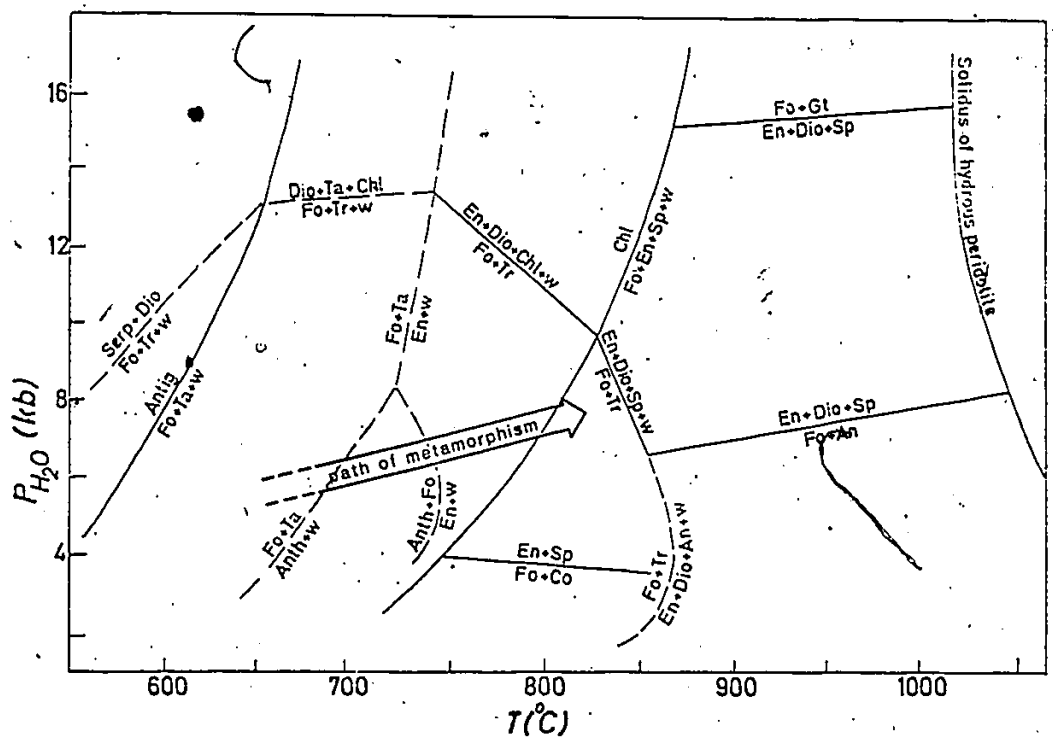

Figure 39: T-P(H20) phase diagram for the ultramafic rock assemblages. Mineral assemblages indicate that conditions of metamorphism are to the right of the Fo+Ta field and within the Fo+Tr field, i.e between about 700 and 900°C at 6 kb. A possible path of increasing metamorphism is shown. Solid lines are experimentally determined curves; dashed lines are theoretical (calculated) curves, after Evans (1977) and Jenkins (1981). Abbreviations: Anth, anthophyllite; Antig, antigorite; Chl, chlorite; Co, cordierite; Dio, diopside; En, enstatite; Fo, forsterite; Gt, garnet; Serp, serpentine; Sp, spinel; Ta, talc; Tr, tremolite; w, water.

39, enstatite forms from forsterite and anthophyllite at temperatures above 700°C, below 8 kb pressure.

During progressive metamorphism spinel changed in composition from Al-chromite through picotite and Cr-spinel to Mg-Al-spinel as suggested already by Evans (1977). Equilibration of coexisting Al-chromite and olivines was probably achieved at approximately 660°C. This opaque Al-chromite changed to a dark brownish-red semiopaque variety at its margin which became more Al- and Mg-rich relative to Cr and Fe during an increase of temperature. Pale brownish yellow and yellowish green spinels, on the other hand, have probably formed at temperatures of 685°C and 720°C respectively. Spinel may be formed from chlorite according to the dehydration reaction:

clinochlore=forsterite+2enstatite+spinel+4H2O

This reaction in the MgO-CaO-Al2O3-SiO2-H2O system (Evans 1977, Jenkins 1981) takes place between 750°C and 800°C at 4-6 kb pressure. Addition of iron into this 5 component system, however, shifts the reaction curves towards lower temperatures. Additionally reaction boundaries in the system will be shifted to lower temperatures and pressures if the activity of H2O in the ambient fluid is not close to unity for ultramafics (Jenkins 1981). As a result, geotemperature results of approximately 720°C, obtained from Mg-Al-spinel and olivine pairs would be realistic for the formation of spinel.

Anhedral chlorite (chromium bearing clinochlore) inclusions developed along certain crystallographic directions of host olivine are interpreted as being a reaction product of host olivine and spinel inclusions which are still present as pseudomorphs enclosed by chlorite (Figure 15).

Serpentinization seen in zones 2 and 6 is a late stage event, developed following metamorphism and deformation. This is indicated by thin serpentine veins cutting olivine neoblasts as well as other metamorphic minerals. On the margin of the body (zone 12), recrystallized phlogopites are pseudomorphed by later green chlorite.

Deformation of the body is indicated by the fabric, kink banding and undulatory extinction of olivine and orthopyroxene megacrysts. According to Poirier & Nicolas (1975) spinel in peridotite nodules is progressively scattered with increasing flow since it is less ductile than the silicates. From their interpretation, the scatter seen in Mg-Al-spinel may be due to increasing deformation. However, the situation is different in zone 5b where the spinel is Al-chromite occupying the interstices of olivine megacrysts. This zone is probably the least deformed part of the body. This fact is further supported by the unrecrystallized olivine grains.

Deformation was followed or accompanied by recrystallization processes. It is not clear whether the recrystallization was of annealing (static) or syntectonic (dynamic)

character. It may be an annealing type because of the large grain size, equant grain shapes, polygonal grain boundaries, and the absence of intragranular strain features (Green et al. 1970) as opposed to inequant grain shapes and strong preferred orientation which are characteristics of syntectonic recrystallization. The presence of bimodal texture seen in zone 5a, however, suggests that it is syntectonic recrystallization (Goetze 1975). If this is the case, some features such as equant and large grain size may have been formed with the help of small amounts of water (Green et al. 1970) during the recovery stage. The driving force of primary recrystallization is strain energy stored in megacrysts and has developed along grain boundaries and dislocations, some of which are obscured by the development of fine grained neoblasts (Figure 13). Where the secondary recrystallization is evident, olivine forms equigranular mosaics in which the grains have 120° interfacial angles or xenomorphic outlines, well developed in zone 11. The driving force for this secondary recrystallization is grain boundary and surface energy but not strain energy.

3.3 ULTRAMAFIC AND MAFIC MAGMATISM

Coherent chemical variations shown by ultramafic, picritic and basaltic rocks of the belt suggest that they may be cogenetic (Figure 40). Most of the ultramafic rocks found as discrete bodies have some mafic portions. The transition

zones from ultramafic to mafic portions are chemically gradational, implying formation from a differentiating magma. Chemical variations across sill-like ultramafic bodies and relict textures suggest that crystal fractionation has occurred in-situ. Variation of MgO/(MgO+FeO) ratios across individual bodies differs considerably; that is, some show less variation (e.g. South Manasan: 0.84 to 0.88) whereas some others show great variation (e.g. Pipe 2: 0.40 to 0.86) (Figure 41). These differing compositional variations may reflect the extent of differentiation; that is, the amount of the differentiated liquid that is separated and/or the time when it is separated, may differ among individual intrusions. On the other hand, the range of most magnesian composition may suggest some range in the composition of the liquid producing individual bodies. Alternately, it may be that some parts of the ultramafic bodies have been tectonically sliced off after formation.

On the chondrite normalized transition element diagram (Figure 42), there are progressive enrichments in Ca, Al, and Ti and progressive depletions in Cr, and Ni from ultramafics through picritic and Mg-basalts to basaltic rocks. The patterns indicate crystal fractionation as a viable process. Otherwise, rapid decrease of compatible transition metals (Cr and Ni) in liquids would not have been expected. Ni depletion is due to olivine fractionation whereas minor chromite fractionation seems to be responsible for the Cr

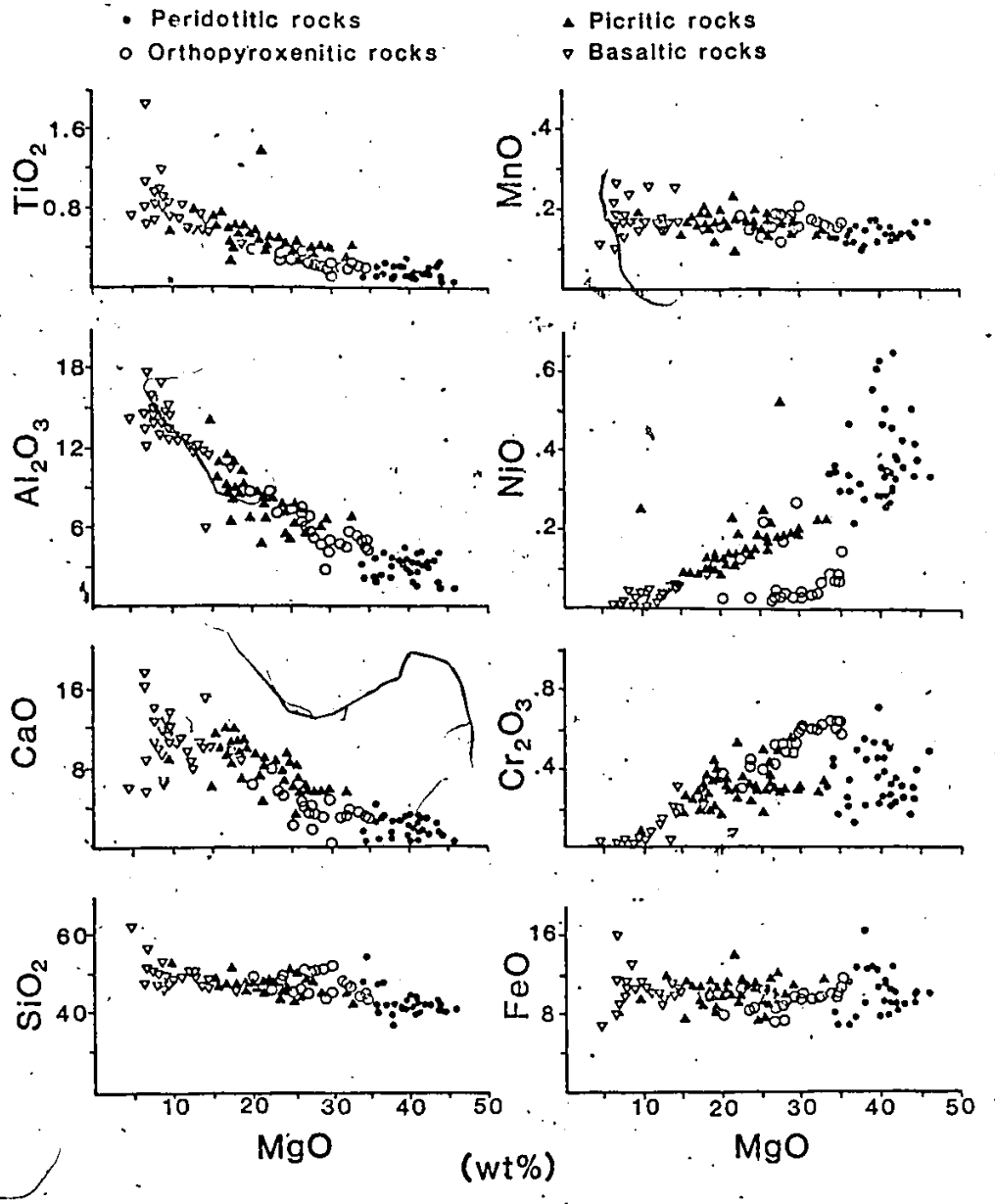

Figure 40: MgO variation diagrams for the Thompson ultramafic and mafic rocks. Included are data from Peredery (1979) and Stephenson (1974).

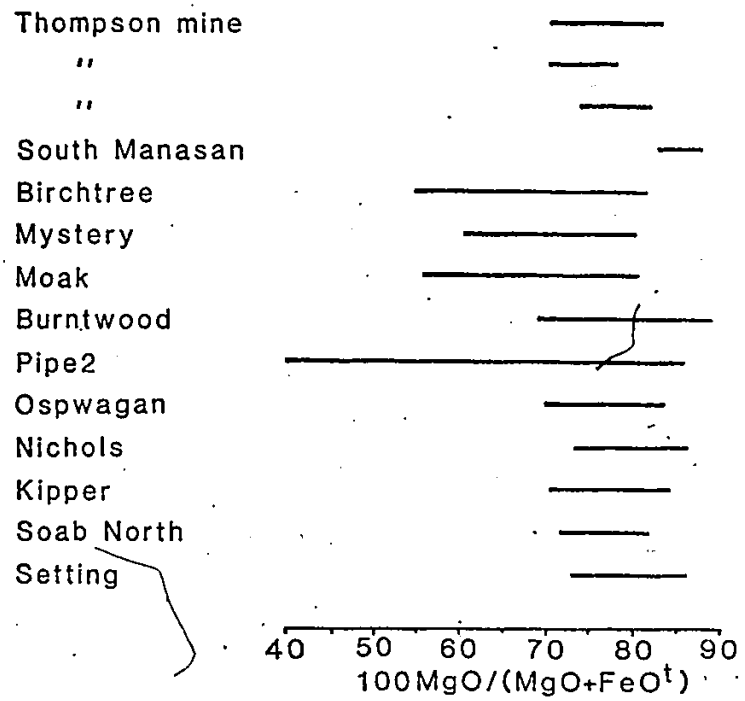

Figure 41: Variation of MgO/(MgO+FeO) across individual ultramafic bodies. Data sources: S.Manasan, Birchtree, Mystery, Moak, Burntwood, Pipe2, Ospwagan, Nichols, Kipper and Soab North are after Peredery (1982); Setting is after Coats (1966).

depletion. In the ultramafic rocks the Ca /Al ratio is less than 1 and this is similar to the calcic plagioclase ratio. This ratio, in the picritic and basaltic rocks is greater than 1 and may indicate involvement of clinopyroxene.

On the Mg-variation diagrams, the ultramafic and mafic rocks of the belt display coherent and serial chemical variations, suggesting that they are petrogenetically linked.

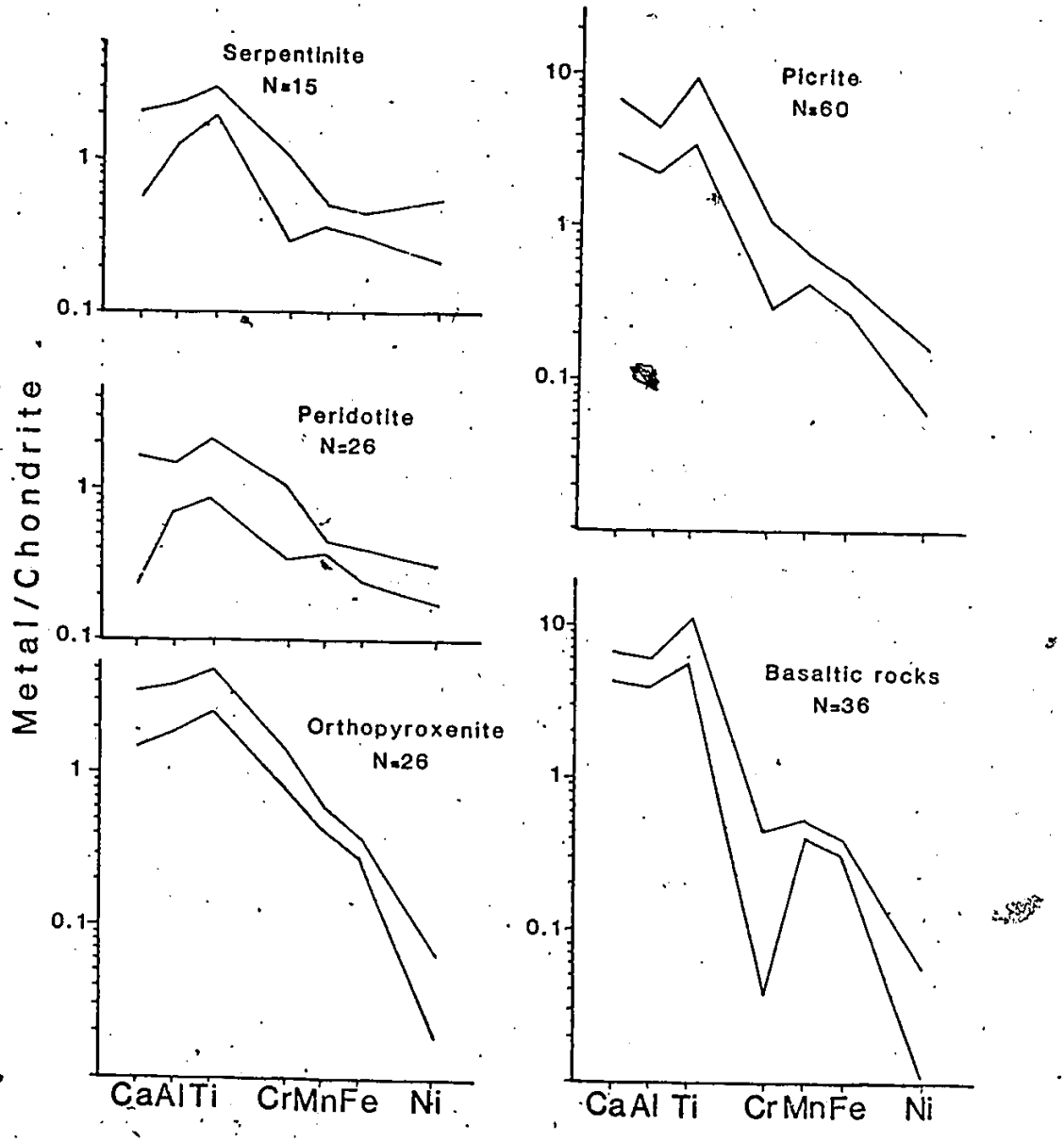

Figure 42: Chondrite normalized Ca, Al and transition metal abundances in the Thompson ultramafic and mafic rocks.

The trends are broadly consistent with either partial melting or fractional crystallization models. Scatter of some of the ultramafic rocks in the MgO vs. NiO and MgO vs. Cr2O3 diagrams is due to low-pressure fractionation. Olivine-orthopyroxenitic and orthopyroxenitic rocks plot away from the general trend in the MgO vs. NiO diagram. It is unlikely that this rapid depletion may only be due to seperation of olivine alone, but it becomes more acceptable when it is accompanied by molten sulfide fractionation from a sulfide-saturated liquid by analogy with the model fractionation trends of Duke & Naldrett (1978).

The basaltic rocks of the belt plot near the low-pressure olivine-orthopyroxene boundary and the low-pressure invariant point in the clinopyroxene projection of the CMAS tetrahedron (Figure 37). This may indicate derivation of mafic rocks from peridotitic komatiite liquid by low-pressure olivine and orthopyroxene fractionation.

Apart from the effects of low-pressure fractionation, there are imprints of an early partial melting event as indicated by some element pairs with chondritic ratios, such as CaO/TiO2 and Al2O3/TiO2 (Figure 43). To produce a komatiitic liquid with chondritic CaO/TiO2 and Al2O3/TiO2 ratios, the degree of melting should be at a level where clinopyroxene and an aluminum bearing phase (garnet, spinel or plagioclase depending upon the depth where the liquid was

produced) must be completely melted. The residuum should be highly refractory in order not to retain significant amounts of these elements. Since orthopyroxene can hold some aluminum at certain depths, it should not be regarded as an important residual mineral. This requires approximately 40-50 % melting (Jaques & Green 1980; Scarfe et al., 1978) where olivine is the principal residual mineral.

In summary, petrogenesis of the ultramafic rocks can be explained in two stages: 1) High degrees of partial melting of mantle material with chondritic abundances of CaO, Al2O3, TiO2 producing a komatiitic melt. 2) Emplacement of the melt, followed by low-pressure fractionation in which olivine and orthopyroxene played important roles.

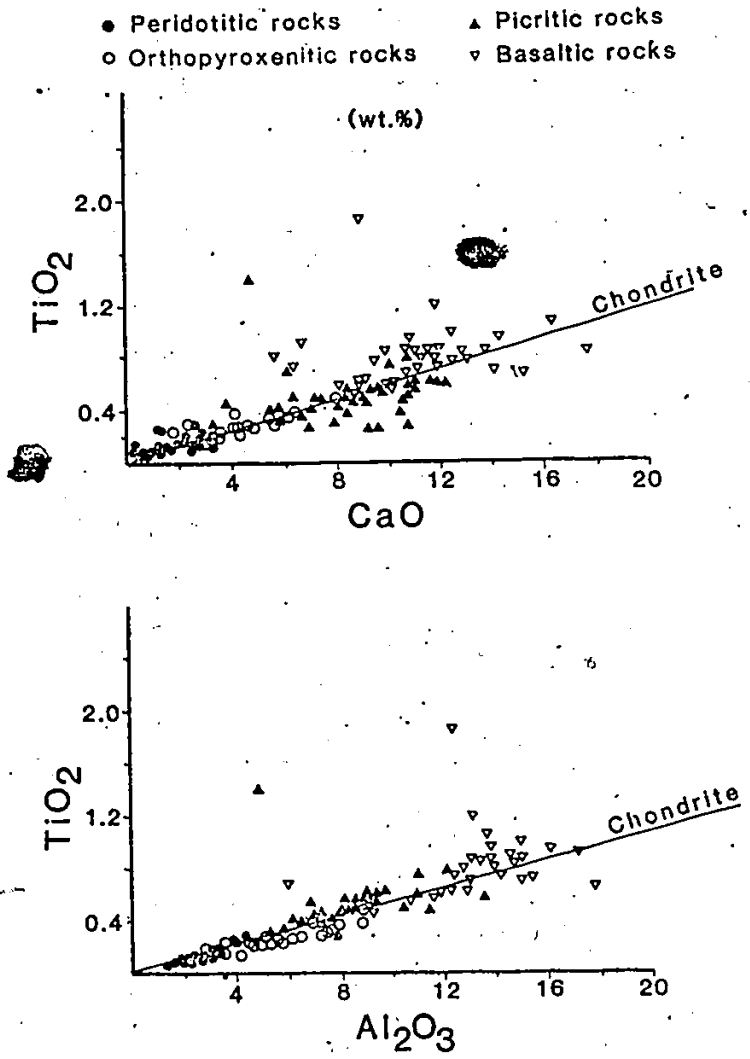

Figure 43: TiO2 vs. CaO and Al2O3 plots for the Thompson ultramafic and mafic rocks.

3.4 GENETIC MODELS FOR THE NICKEL SULFIDE DEPOSITS

The Pipe II, Mystery, and Moak deposits are mainly in the form of disseminated sulfides in the ultramafic rocks. In the Thompson mine, nickel sulfides are found mainly as massive sulfide bodies together with ultramafic rocks in pelitic metasedimentary rocks. The main ore zone corresponds to the biotite-schist unit, and is continuous for a length of 5.5 km. Although larger ultramafic bodies are not uncommon in the Thompson mine, their volume is small relative to the amount of sulfides. The features observed (e.g. ore-host rock relationships, texture) in the Pipe II, Mystery, and Moak deposits are suggestive of magmatic origin. However, these features are rare at the Thompson mine, which has led some people (e.g. Gale, pers. comm. 1980; Sangster, pers. comm. 1980) to consider a volcanogenic-exhalative origin.

According to the magmatic theory, sulfides are carried as immiscible droplets in a sulfur-saturated ascending magma that is generally komatiitic in composition. Separation of immiscible sulfides from the silicate magma occurs either following emplacement, due to density difference between the silicate and the sulfide phases (Naldrett 1973), or during ascent of the magma, due to viscosity difference between the two phases (Ross & Hopkins 1975). The volcanic-exhalative model was proposed by Lusk (1976) for lenticular nickel sulfide deposits to explain some features which are similar to

volcanogenic Cu-Zn deposits (e.g. occurence of pyrite in massive sulfide, mineralogical layering, stringer ore). However, most of the features used by Lusk (1976) to support volcanogenic-exhalative model were largely due to metamorphism (Groves et al 1976). Peredery (1982) also explains that the presence of similar features (e.g. occurence of pyrite, mineralogical layering, stringer ore) in the Thompson mine has been largely due to secondary processes (e.g. metamorphism). Additionally, hydrothermally altered footwall rocks are absent in the Thompson mine. Moreover, the presence of source rocks from which Ni can be extracted is uncertain. Generally speaking, features supporting a volcanogenic origin are rare as well in the Thompson mine. Thus, one must unravel the effects of complex metamorphism and deformation on the nickel sulfides and their host rocks before attempting to favour any genetic model.

Chapter IV

THE CUTHBERT LAKE DIKES

The Cuthbert Lake dikes are a number of vertically dipping parallel dikes, striking approximately N30°E. They can be traced along their strikes for about 160 km on the geological map of Manitoba (Manitoba Department of Mines 1980). The dikes consist of a number of 'en-echelon' dike segments, a feature which was mentioned in McDonald (1960). The composition of the dikes range from ultramafic to mafic and they cut the Pikwitonei granulites which consist of gneisses, gabbro and minor pyroxenites (Figure 44).

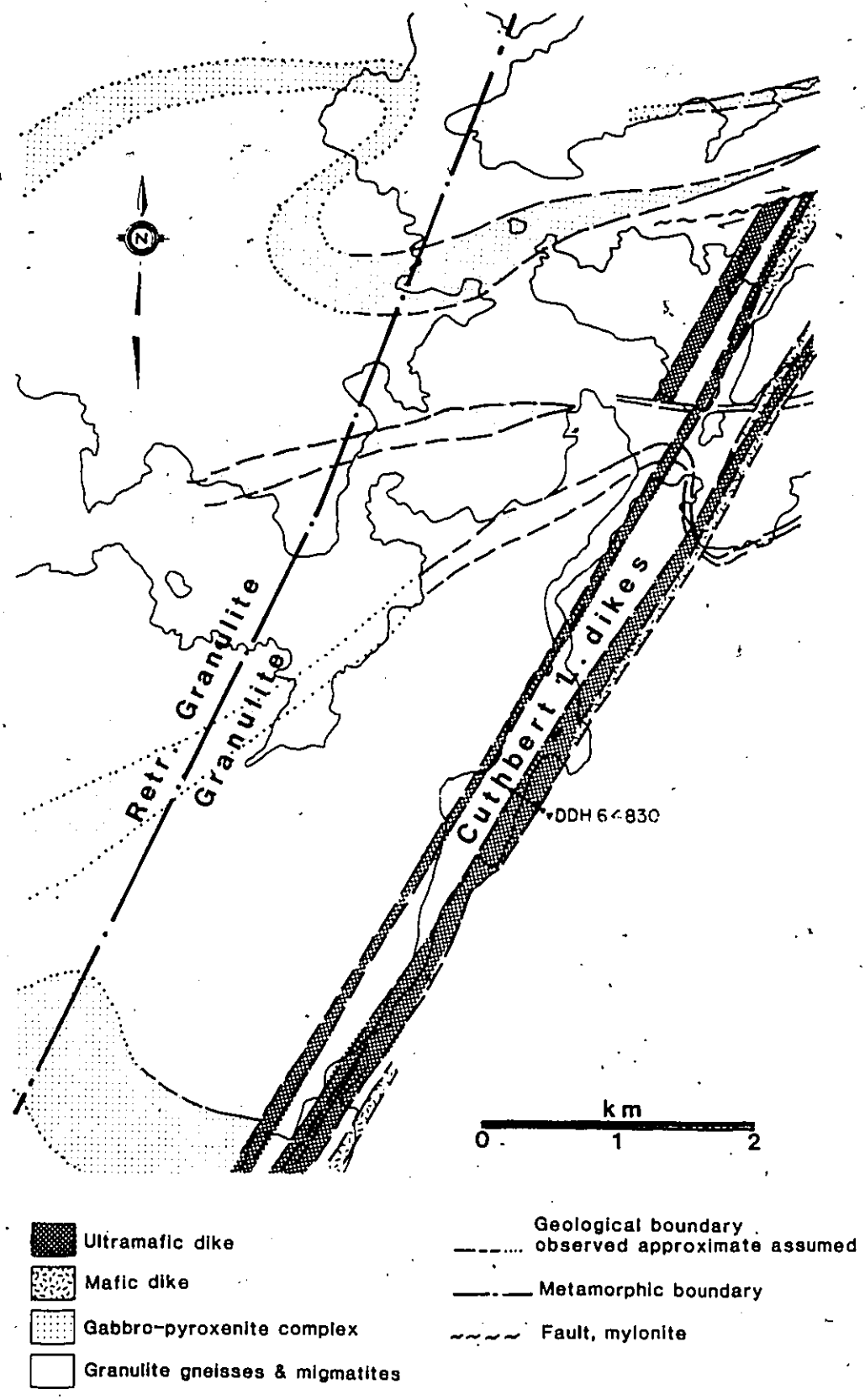

Figure 44: Geological map of the area around Cuthbert Lake. Simplified from the Geological Map of INCO Metals Ltd. Manitoba Division.

4.1 PETROLOGY AND GEOCHEMISTRY

The Cuthbert Lake dikes were studied as seen along DDH 64830. The diamond-drill hole intersected a 10 meter thick mafic dike which will be referred as the minor dike and a 60 meter thick ultramafic dike which will be referred as the major dike throughout the text.

4.1.1 Mineralogy and Petrography

4.1.1.1 The major dike

The major dike, as observed along the diamond-drill hole intersection is composed mainly of olivine-pyroxenite. A minor websterite unit is present near the northwestern contact (Figure 45). A thin pyroxene-picritic unit close to the southeastern side of the major dike does not seem to be part of the major dike and will be discussed later.

The chilled margin is composed of fine grained chlorites that show weak foliation and finely disseminated iron oxides (Figure 46). Fine grained chlorites may represent devitrified glass.

There is a mineralogical zonation across the major dike. The modal amount of olivine appears to show an increase, whereas that of plagioclase seems to decrease toward the

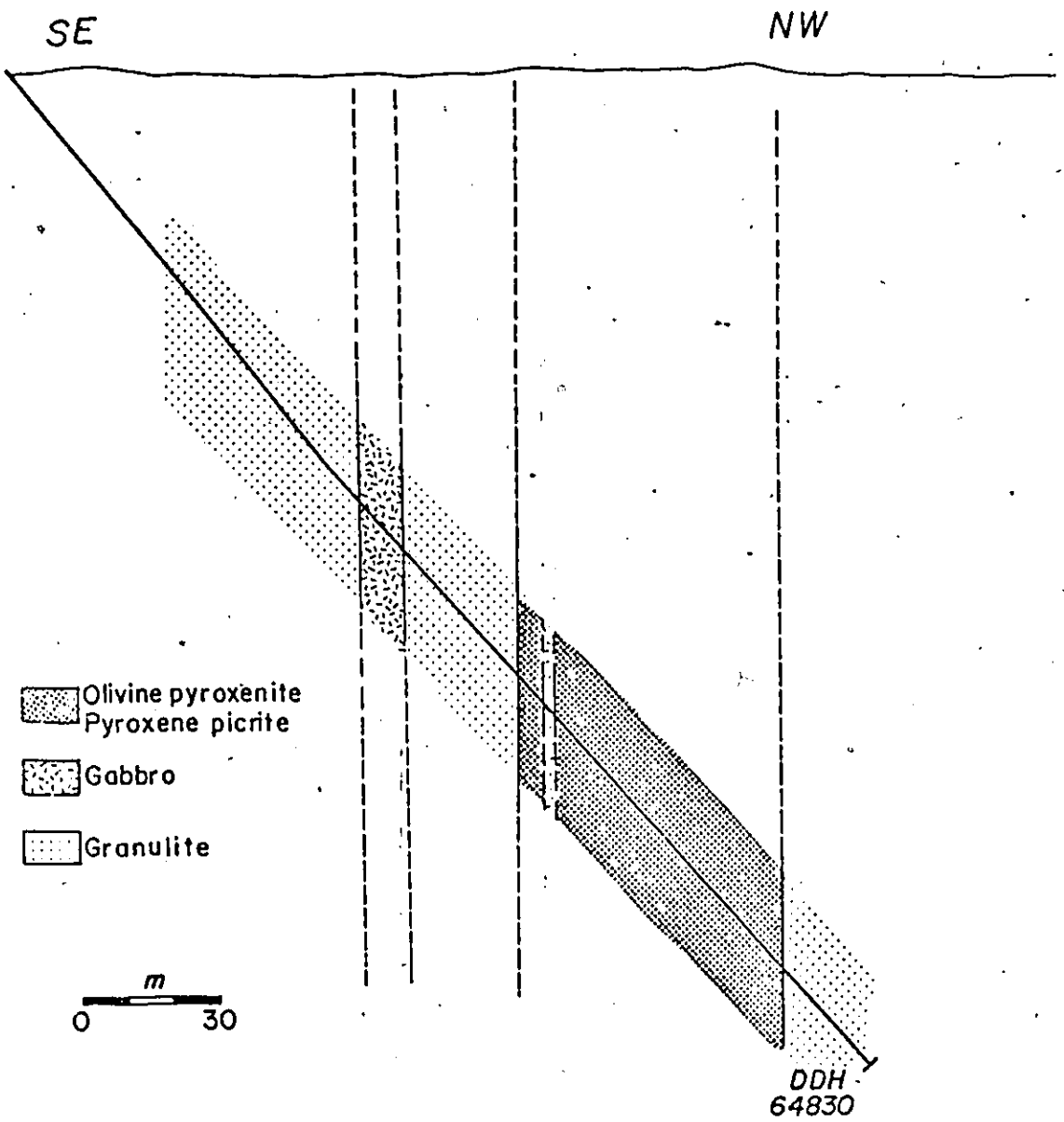

Figure 45: Cross section of the Cuthbert Lake dike as seen along the DDH 64830. Contacts are drawn as measured from the angle of the DDH axis with the contact.

Figure 46: Margin of the major dike. Crossed polars.

dike center, similar to those found by Scoates & Macek (1978) in another dike of the swarm. According to them, orthopyroxene shows a distribution similar to that of plagioclase, and to some extent, clinopyroxene distribution is similar to that of olivine. Similar mineralogical variation has been noted in the ultrabasic dikes of the Isle of Skye, Scotland (Gibb, 1968); that is, olivine increases toward the center whereas plagioclase and clinopyroxene decrease in that direction.

Olivine is found as subhedral-euhedral prismatic crystals. Some of them form elongate crystals of which the long axes are up to 4 times longer than their short axes (Figure 47). Commonly, they display rounded corners and some show

embayed outlines (Figure 48), indicating partial resorption of olivine during the magmatic stage. Grain size is not uniform, varying from 0.1 to 2 mm, even within the limit of a thin section. There does not seem to be a systematic variation in the grain size of olivine across the dike. Near the margin, however, the olivines are mostly small (averaging 0.2 mm) with a few coarse grains. In the center of the dike, the amount of coarse grains (1-2 mm) increases. Ermanovics & Fahrig (1975) have also noted that coarse olivine and orthopyroxene are concentrated in the center of the Molson dikes.

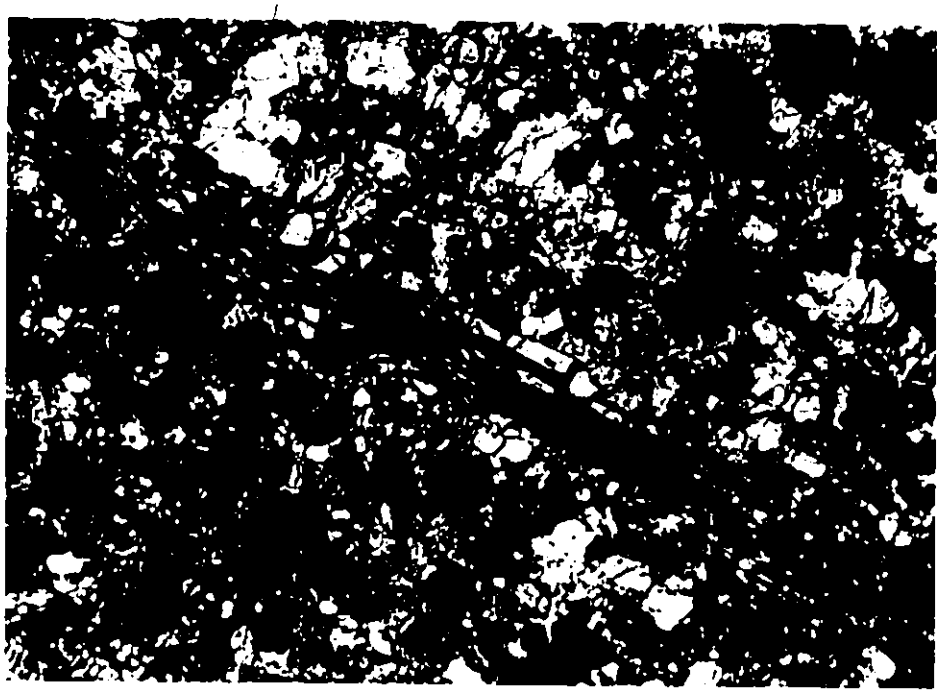

Figure 47: Elongate olivine crystals sitting in finer grained olivines, pyroxenes(white-grey) and plagioclase.

Figure 48: Olivine crystals with rounded outlines. Large euhedral crystal is orthopyroxene. Interstitial mineral is amphibole.

Close to the SE side of the major dike, coarse elongate olivine crystals show a preferred orientation; that is, the long dimensions of the elongate olivine crystals are oriented parallel to the dike margin. This fabric may indicate flow direction.

Thin serpentine veins and magnetite stringers are found cutting olivine grains. In some places, the serpentinization is complete leaving no relicts of olivine.

Orthopyroxene is pinkish, weakly pleochroic and forms equant euhedral and subhedral grains (Figure 49). The grain size also varies considerably (0.2 to 1.5 mm), like that of

olivine. Some grains display zonation. Exsolution blebs and oriented platelets parallel to the c-axis of the host orthopyroxene have been observed in some grains. These platelets have oblique extinction. Orthopyroxenes rarely enclose olivines. Where they are in grain to grain contact, the grain boundary is usually straight indicating equilibrium between these two minerals.

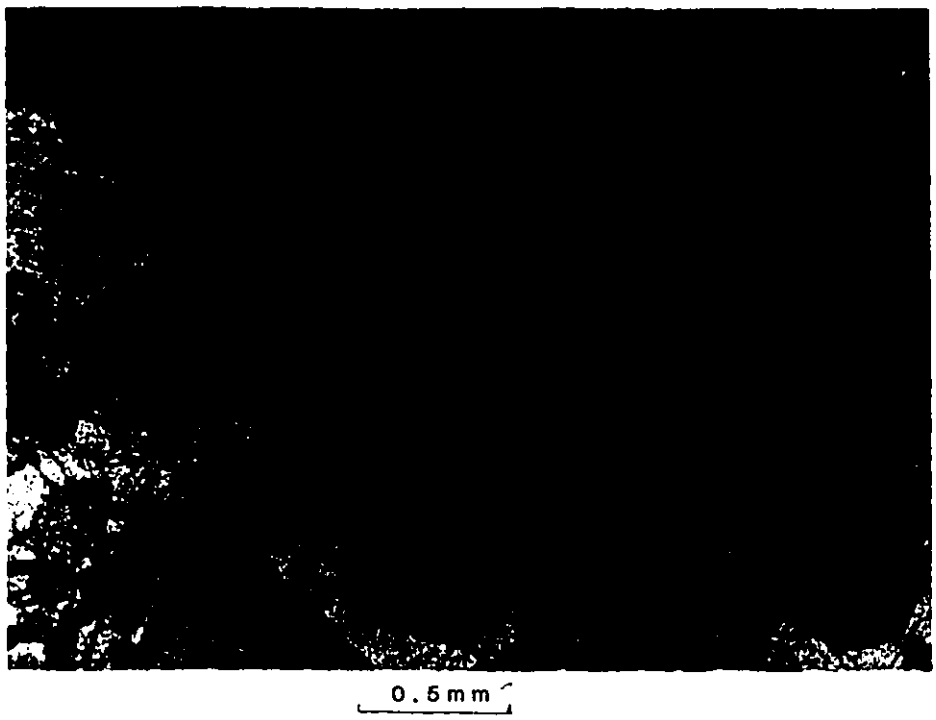

Figure 49: Euhedral-subhedral orthopyroxene grains (x), clinopyroxene (c), olivine (o) , and plagioclase (p). Note rounded olivines are surrounded by brownish corona in plagioclase.

Clinopyroxene is in the form of equant subhedral grains, similar to orthopyroxene. It is usually coarse grained (0.5 to 1.6 mm) compared to other minerals nearby. It is weakly pleochroic with shades of light green (Figure 49). Some of

the grains have tiny blebs concentrated near the margin, and oriented platelets similar to those observed in the orthopyroxenes (Figure 50). Alteration preferentially developed in the exsolution-rich parts of the clinopyroxenes, complicating the texture and positive identification of the exsolving phase. However, parallel extinction of the oriented platelets suggests that they are orthopyroxene. Grain boundary relationship with amphiboles indicates partial replacement of clinopyroxene by amphibole.

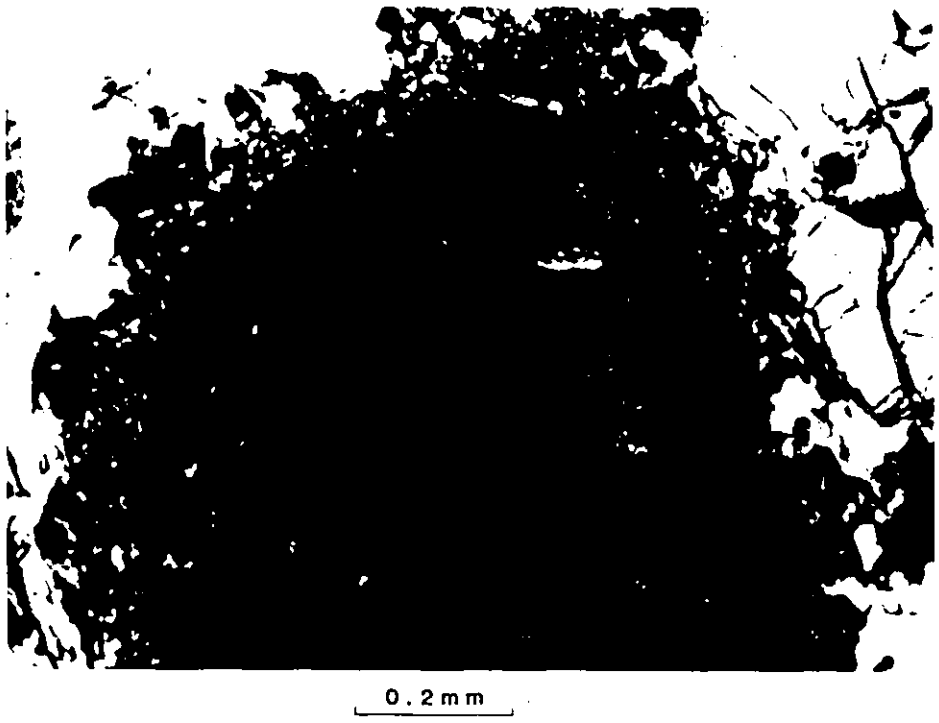

Figure 50: Fine exsolution blebs and rods developed around the margin of clinopyroxene.

Plagioclase occurs as medium to coarse anhedral, interstitial grains. Several small laths of plagioclase are also observed. The former type poikilitically encloses olivine,

orthopyroxene and clinopyroxene (Figure 51). Olivines enclosed in plagioclase have reaction rims. Two types of reaction rims are present. One is a kelyphitic rim with radial fibrous texture (Figure 52). The other type seems to be a corona structure which consists of two silicate layers (Figure 53). The inner layer, adjacent to olivine, is an orthopyroxene. The outer layer consists mainly of an amphibole, intergrown with a dark brownish phase, forming a vermicular texture. Similar textures have been noted in the Michael Gabbro, Labrador by Emslie (1983). He explains the double coronas separating olivine from plagioclase as an inner corona which consists of prismatic, colourless hyperstene with elongation perpendicular to olivine margins and an outer rim which is an amphibole (pale-medium green) and may contain very fine spinel near the inner corona. The kelyphitic rims are interpreted as secondary, whereas the other reaction rim is believed to be a subsolidus phenomenon. No reaction rim was observed between pyroxene and plagioclase.

Amphibole, a hornblende, is always in the form of large interstitial grains (Figure 54). It is characteristically brownish to greenish with distinct pleochroism.

Opaque chromian spinel is fine grained, generally smaller than 0.1 mm. It occurs as euhedral crystals which are evenly disseminated and found to be enclosed by olivine and other silicates. Some of these fine grained spinels have tiny

Figure 51: Coarse plagioclase grain poikilitically enclosing clinopyroxene, orthopyroxene and olivine.

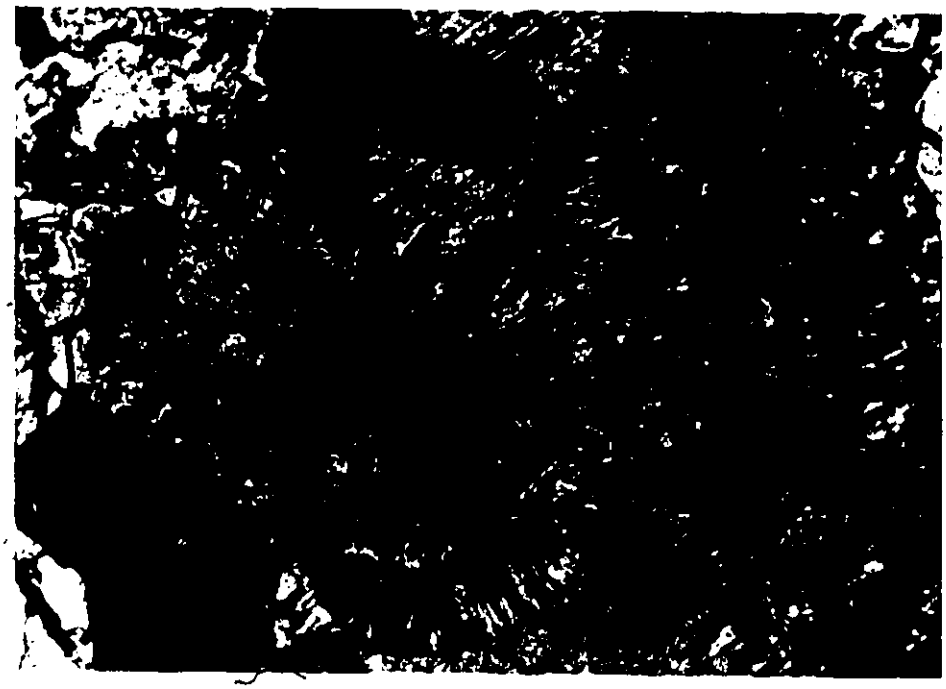

Figure 52: Kelyphitic rims around olivine grains enclosed in plagioclase.

Figure 53: Corona with double layers between olivine and plagioclase.

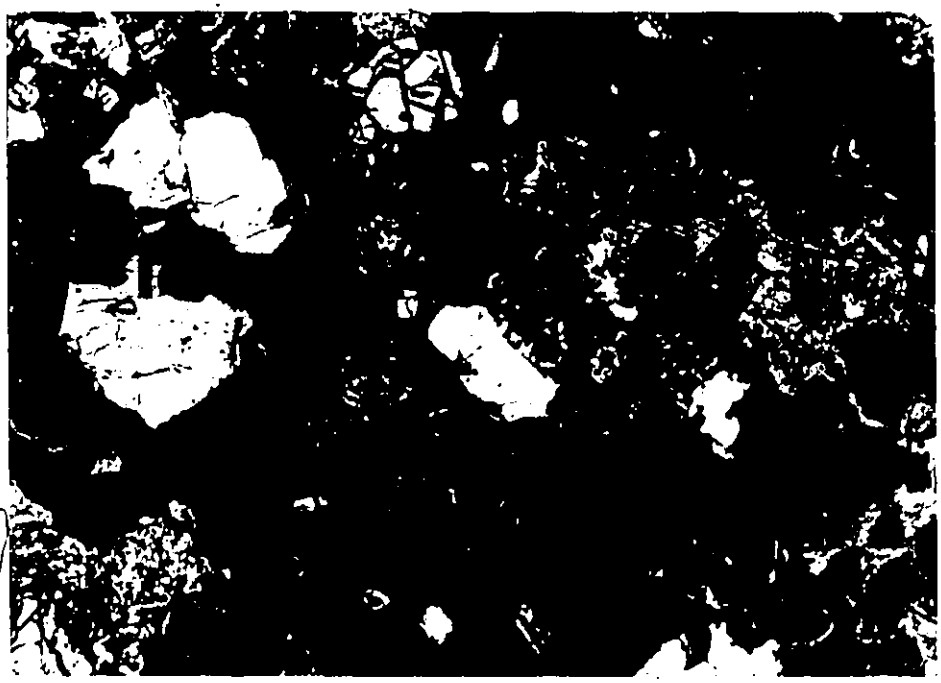

Figure 54: Coarse interstitial amphibole enclosing rounded olivines, subhedral pyroxenes and plagioclase laths.

silicate inclusions (Figure 55) which are identified as olivine and amphibole by microprobe analyses. Chromian spinels display zonation where the enclosing material is highly altered. Zoned spinels have opaque core and semi-opaque rims, indicating alteration that starts at the margin and develops inward. Among these zoned spinels, there are also some semi-opaque dirty-greenish spinels. They are believed to represent completely altered varieties. Under reflected light, chromian spinels are light grey in colour. Almost all the grains contain needle-like, highly reflective exsolved phases which are arranged preferentially along crystallographic directions of the host chromian-spinel. That phase is interpreted to be hematite. A similar exsolved phase is found in chromian-spinels in basalts (Haggerty,1976) and in chromites of the Bird River Sill, southern Manitoba (Paktunc, unpublished). The exsolved phase was interpreted as the result of high temperature oxidation of chromian-spinel by Haggerty (1976).

Minor pyrrhotite and chalcopyrite occur as fine anhedral grains.

4.1.1.2 The minor dike

The minor dike is composed of pyroxene picrite and gabbro. Pyroxene picrite forms the central portion whereas the marginal phase is gabbroic. The boundary between these

COLOURED PICTURES
Images en couleur

Figure 55: Olivine inclusion in euhedral chromian spinel. o, olivine; p, plagioclase; s, chromian spinel; x, orthopyroxene.

units is gradational. The margin of the dike contains abundant phenocrysts of clinopyroxene of which the size reaches up to 2 mm (Figure 56). Some of the clinopyroxene phenocrysts are partly altered around their margins. Others are completely altered to a greenish pleochroic material. Plagioclase, minor olivine and orthopyroxene phenocrysts are also present. The matrix is composed of fine plagioclase microlites, opaque material and fine greenish chlorite.

The rest of the dike is fine grained and shows ophitic texture (Figure 57). Clinopyroxene is coarse grained with subhedral outlines, partly surrounded by secondary microcrystalline rims (ophitic rims). Some of the grains show optical zonation and twinning. Several grains are found to

COLOURED PICTURES
Images en couleur

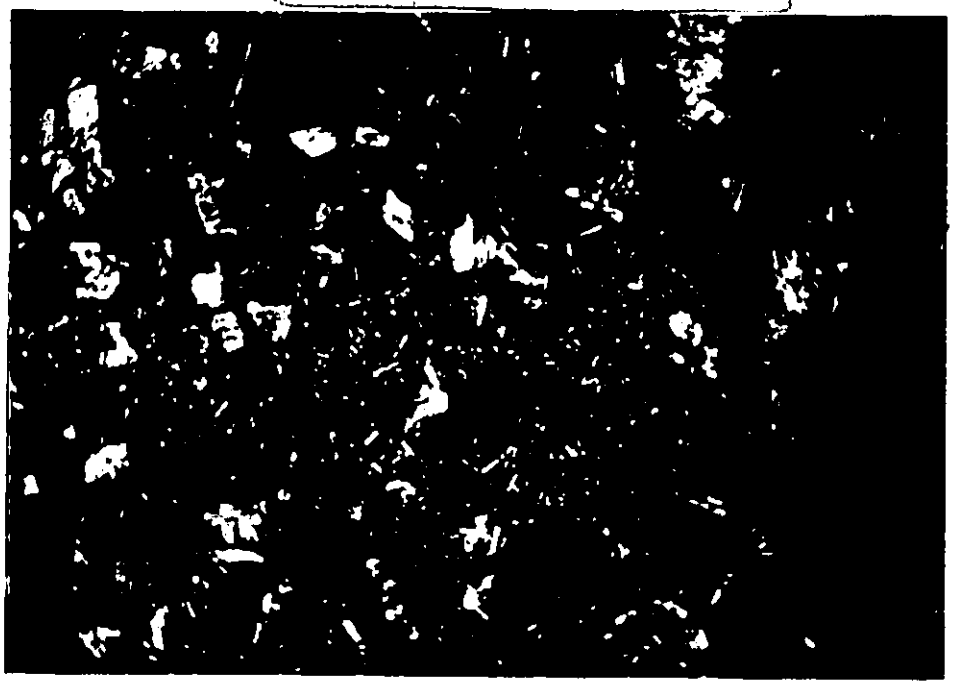

Figure 56: Margin of the minor dike containing phenocrysts of clinopyroxene.

be composed of small irregular mosaics of clinopyroxenes. This is similar to the 'multigrain aggregate' of Scoates & Macek (1978). Fine exsolution lamellae have been observed in several grains.

Figure 57: Minor dike showing ophitic texture.

4.1.2 Mineral Chemistry

4.1.2.1 Olivine

The composition of olivine in the major dike ranges from Fo76.5 to Fo81. This range corresponds to the change of Fo content from the dike margins inward. Mg/(Mg+Fe) ratios (XMg) of olivines are identical to those of the bulk-rock. In other words, olivines seem to control the XMg of the bulk-rock. A chromian-spinel grain which is enclosed in olivine, has a tiny olivine inclusion in it. This tiny olivine inclusion (Fo80.5) is more magnesian than the olivine that encloses spinel (Fo79.3). Similarly, an olivine inclusion in a euhedral clinopyroxene grain is more magnesian than the olivines not enclosed by clinopyroxene. This may

indicate that the olivines that are trapped preserve their composition while others reacting with the magma in which they are suspended, change their composition. However, the difference in composition is too small to be important.

The NiO content of olivine ranges from 0.11 to 0.41 (wt. %), unrelated to MgO content. This variation is even shown among individual grains in a given thin section. MnO displays less variation, ranging from 0.20 to 0.43 and shows a weak negative correlation with the MgO content.

4.1.2.2 Pyroxenes

The compositions of the pyroxenes are shown on the pyroxene quadrilateral diagram (Figure 58). Orthopyroxenes plot close to the enstatite corner; whereas clinopyroxenes are near the diopside corner. The composition of orthopyroxenes in a given sample is variable. However, the variation observed among individual grains in a given sample may be complicated due to the presence of finely exsolved pyroxenes. The Mg/(Mg+Fe) ratio of the orthopyroxenes, ranging from 0.80 to 0.84 is generally higher than that of coexisting olivines. This feature, acccording to Bowen & Schairer (1935) suggests that equilibrium conditions have been reached at low pressures.

Several clinopyroxene analyses indicate that their Mg/(Mg+Fe) ratios are slightly higher than those of orthopyroxenes.

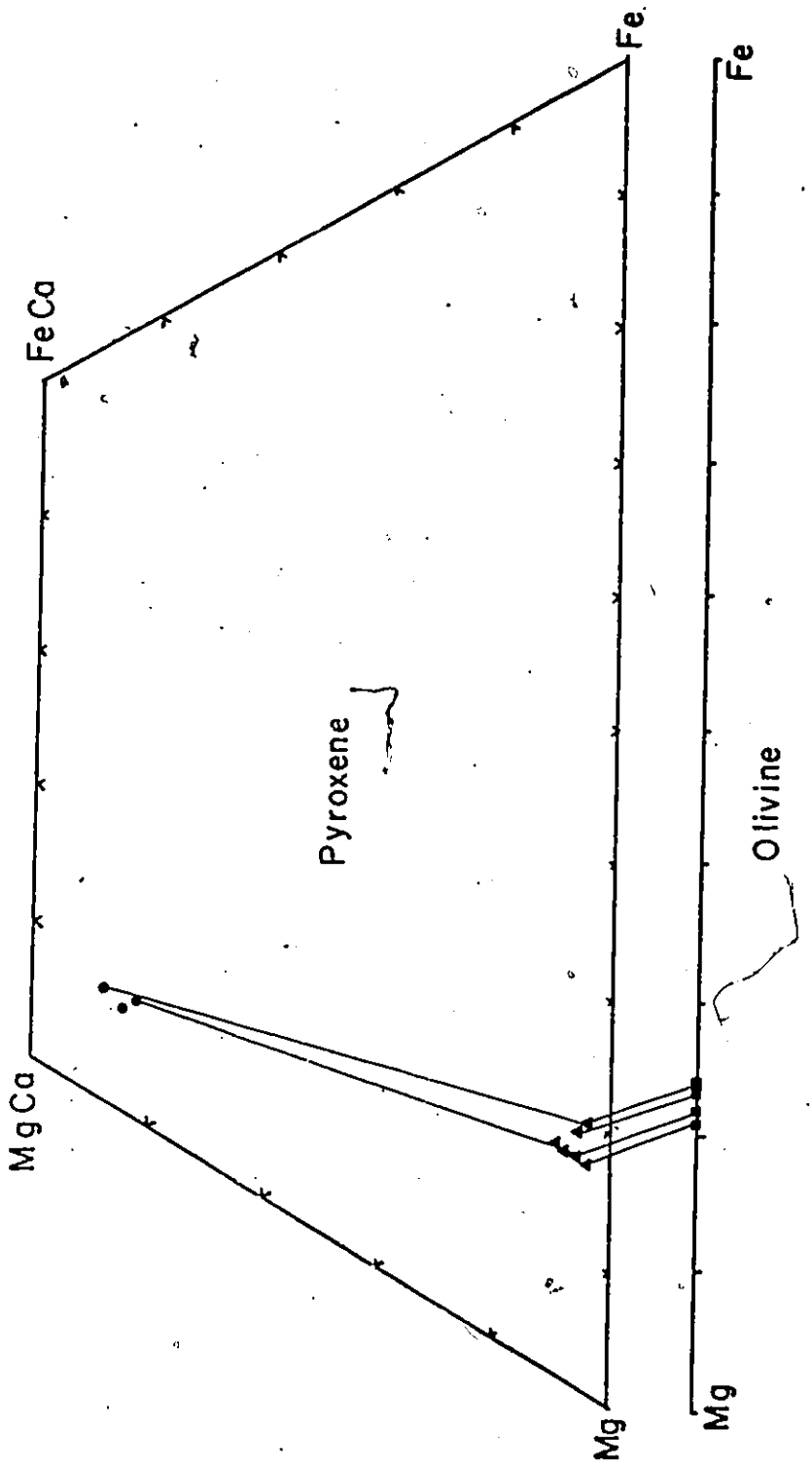

Figure 58: Pyroxene quadrilateral diagram and the composition of olivines. Lines connect coexisting orthopyroxene (triangles), clinopyroxene (circles) and olivine (squares).

CaO and Al2O3 concentrations of the orthopyroxenes are high, ranging from 1.07 to 2,28 (wt. %) and 0.30 to 4.46 (wt. %) respectively. On the Al2O3 vs Mg/(Mg+Fe) diagram (Figure 59) it is observed that there is a weak negative correlation between these two parameters.

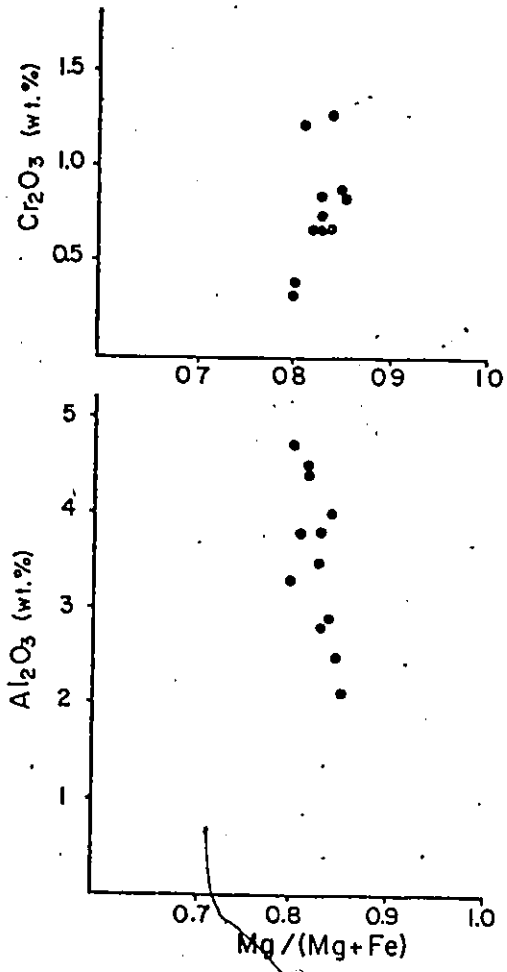

Figure 59: Mg/(Mg+Fe) vs. Al2O3 and Cr2O3 plots for pyroxenes.

4.1.2.3 Amphibole

Amphibole analyses plot linearly between the pargasite and tremolite end members on the Al^{IV} -(Na+K) diagram (Figure 60). They are distinctly richer in Al2O3 (9.45-13.94 wt. %) and slightly less calcic (9.22-11.27 wt. %) than the amphiboles of the Thompson ultramafic body. The Mg/(Mg+Fe) ratios (0.74-0.82) are in the range of those of the olivines.

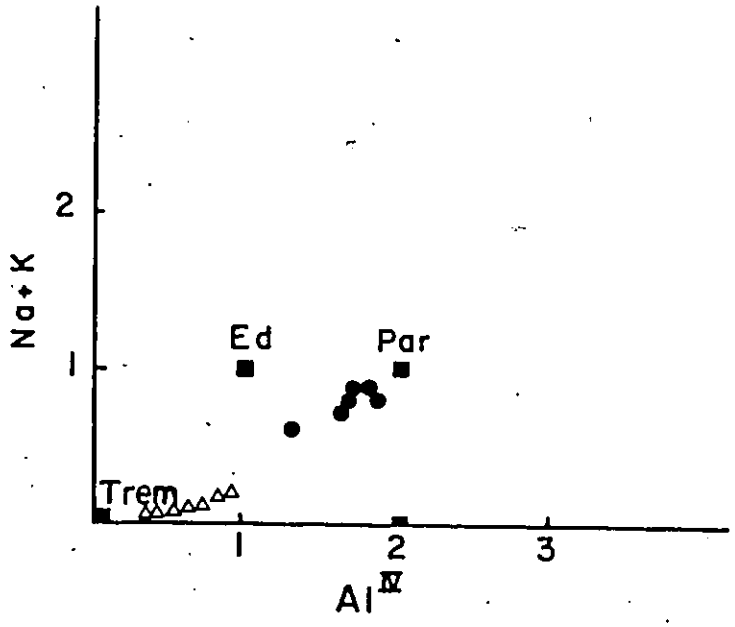

Figure 60: Composition of amphiboles (solid dots). Also shown are the Thompson amphiboles (triangles). Number of atoms per 23 oxygen ions. Ed, edenite; Par, pargasite; Trem, tremolite.

4.1.2.4 Plagioclase

Only two plagioclase grains have been analysed. The one in the major dike, near the margin is bytownite whereas the other in the minor dike is labradorite in composition.

4.1.2.5 Chromian-spinel

Variation of trivalent ions in the opaque spinels is shown on Figure 61. It is seen that the chromian spinels are rich in ferric iron which requires formation under high oxygen fugacity conditions. As pointed out earlier, the chromian-spinels have experienced a high temperature oxidation which has resulted in the formation of hematite exsolution lamellae. The $Cr/(Cr+Al+Fe^{+++})$ ratios range from 0.24 to 0.40. On the $Mg/(Mg+Fe^{++})$ vs $Cr/(Cr+Al+Fe^{+++})$ diagram (Figure 62), they form a linear trend which is parallel to but distinctly different from the trend of the spinels of the Thompson ultramafic body. Their V_2O_3 content is high, around 2 % wt.

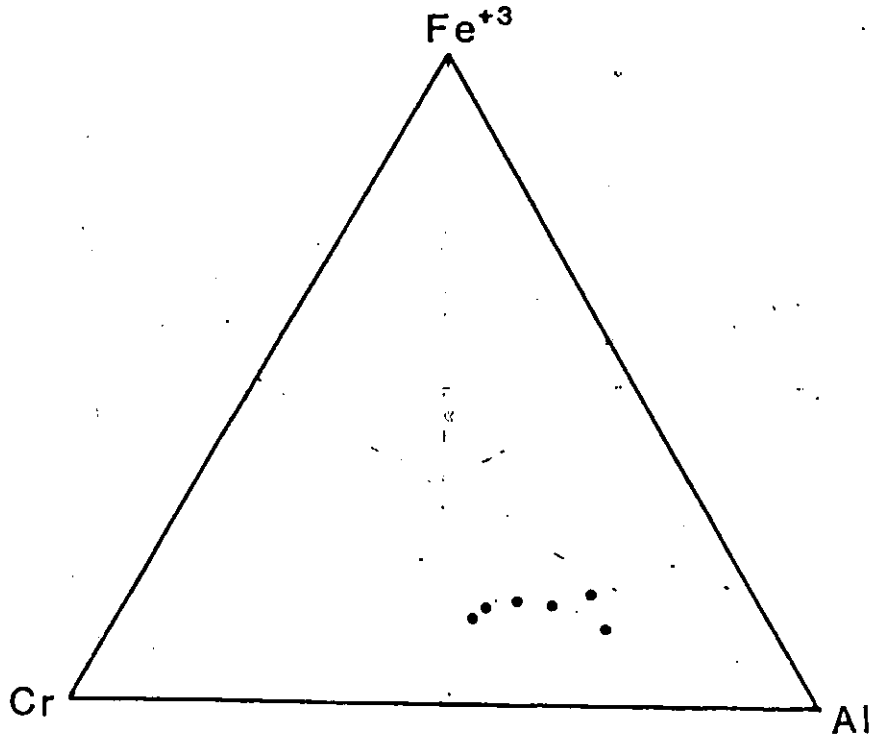

Figure 61: Variation of trivalent ions in spinels. Fe^{+++} is calculated assuming ideal spinel stoichiometry.

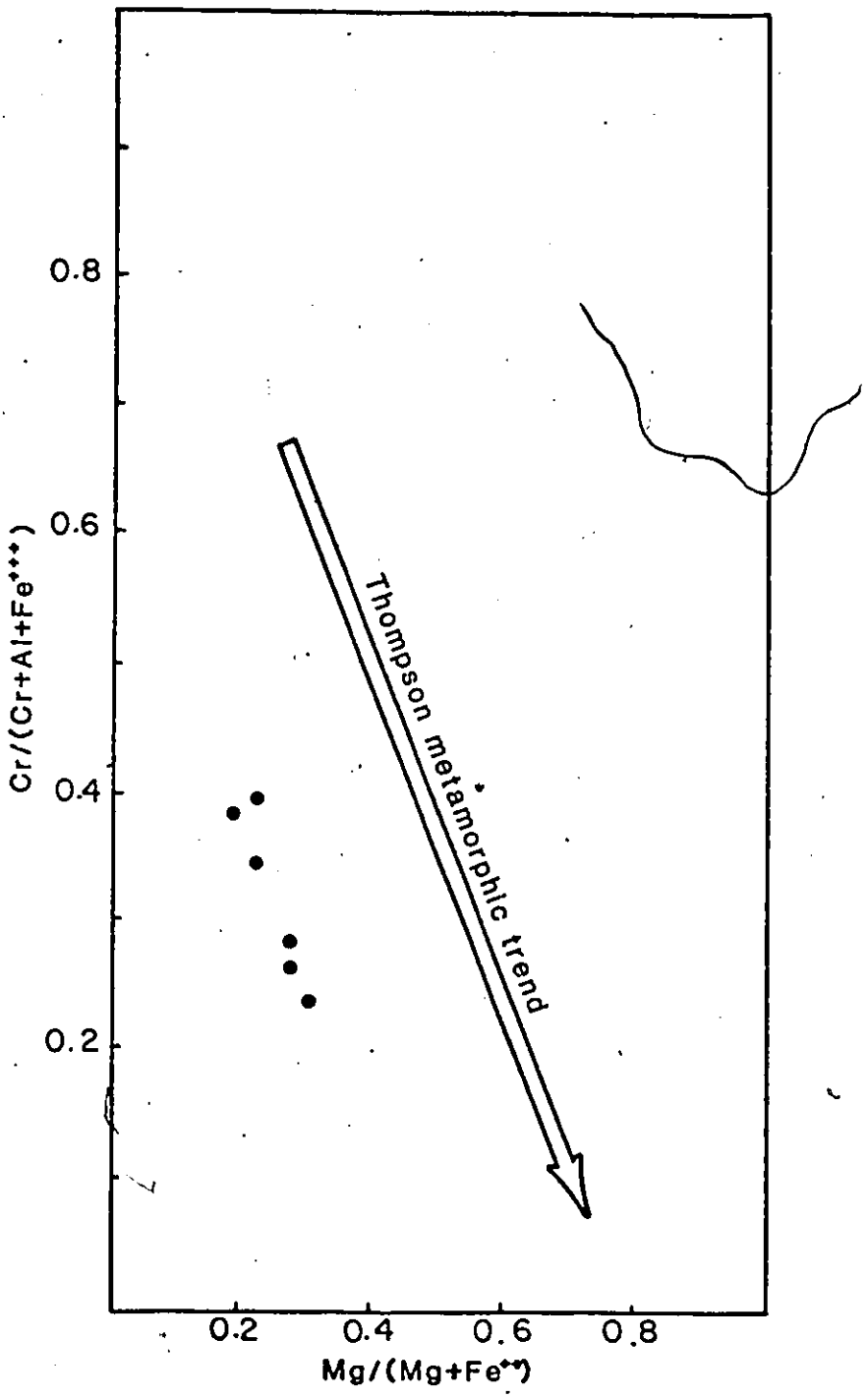

Figure 62: Plot of Mg/(Mg+Fe^{++}) vs Cr/(Cr+Al+Fe^{+++}) of spinels. Metamorphic trend is shown for reference only.

4.1.3 Geotemperature Estimates

Alumina solubility in orthopyroxene, single pyroxene and two pyroxene geothermometers have been used to estimate temperature conditions. Olivine-spinel geothermometry could not be used since the chromian spinels have been intensely oxidized; that is, most of the ferrous iron has been converted to ferric iron.

4.1.3.1 Alumina solubility in orthopyroxene

The magnesium-tschermak component of the orthopyroxene is used to extrapolate temperature values from the temperature-pressure phase diagram of Gasparik & Lindsley (1980) (Figure 27). Alumina solubility in orthopyroxenes coexisting with forsterite and spinel in the system $MgO-Al_2O_3-SiO_2$ is practically independent of pressure in the range of interest (i.e. below 15 kb. and 1100°C). Extrapolated values are in the range of 900°C to 1000°C.

4.1.3.2 Single pyroxene geothermometer

The single pyroxene geothermometer (Mercier, 1976 and 1980) is based on alumina solubility in pyroxenes coexisting with an Al-rich phase. The details of this method are given in Mercier (1976) with some revised thermodynamic parameters and formulae in Mercier (1980).

The equations for enstatite coexisting with spinel are:

$A=(Al-Na)/2$

$W=Ca/(Ca+Mg+Fe+Mn)$

$FCr=Cr/(Al+Cr-Na)$

$Ka=(A/(1-A))/(1-2.87FCr)^2$

$Kw=6W/(1-2W)$

$D=\ln Ka \times \ln Kw - 8.6751 \ln Kw + 2.2595 \ln Ka + 24.568$

$T(°K)=(-6308.5 \ln Kw + 45449)/D$

The equations for diopside coexisting with spinel are:

$Kw=(1-2W)/(0.667+0.667W)$

$Ka=(A/(1-A))/(1-1.27FCr)^2$

$D=\ln Ka \times \ln Kw - 11.2724 \ln Kw + 2.2595 \ln Ka + 32.371$

$T(°K)=(-7537.5 \ln Kw + 61152)/D$

(element symbols represent number of atoms per 6 oxygen ions).

Temperatures obtained range from 1093 to 1324°C, peaking at 1150°C (Figure 63). Precision is estimated to be ±70°C.

4.1.3.3 Two pyroxene geothermometer

Transfer and exchange equations derived by Kretz (1982) are used to estimate geotemperature conditions.

The transfer reaction is a change in the solubility of the enstatite component in diopside crystals.

The equation for temperatures above 1080°C :

$T(°K)=1000/(0.468+0.246XFe-0.304 \ln(1-2YCa))$

for temperatures below 1080°C :

$T(°K)=1000/(0.054+0.608XFe-0.304 \ln(1-2YCa))$

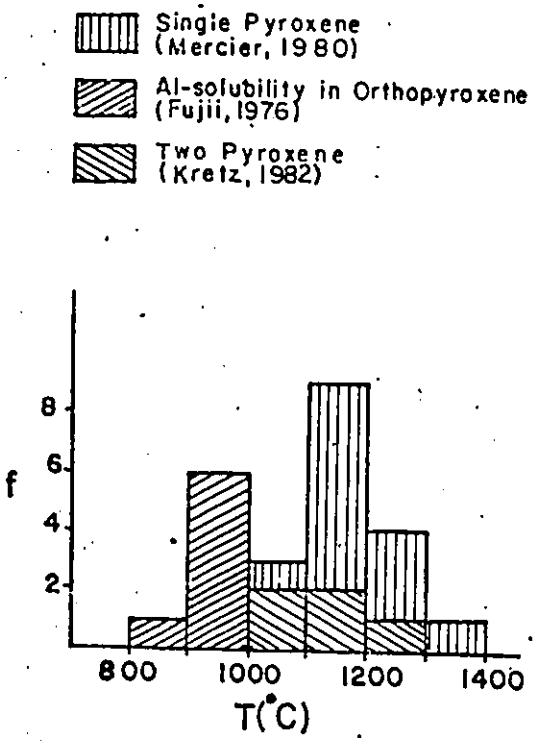

Figure 63: Frequency histogram of the geotemperature estimates.

where; XFe and YCa are fractions of Fe^{**} and Ca in clinopyroxene.

$XFe=Fe^{**}/(Mg+Fe^{**})$

$YCa=Ca/(Mg+Fe^{**}+Ca)$

The exchange reaction is based on Mg-Fe^{**} partition between clinopyroxene and orthopyroxene.

The equation:

$T(°K)=1130/(\ln Kd+0.505)$

where;

$Kd=(XFe/XMg)_{opx} \times (XMg/XFe)_{cpx}$

$XFe=Fe^{++}/(Mg+Fe^{++})$

$XMg=Mg/(Mg+Fe^{++})$

Temperatures calculated using the transfer equation give 1040±60°C and 1220±60°C whereas estimates obtained from the exchange equation give 980°C and 1540°C. This large variation may result from failure to analyse for ferrous iron.

4.1.3.4 Comparison of the geotemperature estimates

Temperatures obtained from the single pyroxene geothermometer and from the transfer equation are consistent. They peak at 1150°C (Figure 63); therefore, this value can be taken as the equilibration temperature of the orthopyroxene and clinopyroxene. Low temperatures (900-1000°C) obtained from the alumina solubility in orthopyroxene are probably because of the effects of FeO, Fe_2O_3, Cr_2O_3 and CaO which are ignored in the method.

4.1.4 Rock Chemistry

The dike rocks were sampled and analysed approximately every 6 meters along DDH 64830. The chemical analyses are given in Table 5.

The effect of alteration seems to be negligible, because several altered samples display sympathetic variation patterns with the unaltered rocks for most of the oxides and elements.

Contamination of the dike from the enclosing gneisses is also negligible for most of the oxides and elements. The gneissic country rock on the NW side of the dike is low in TiO2, whereas the other side (SE) of the dike is rich in TiO2. Ba, Sr, Rb appear to have been enriched in the country rock (see Table 5, samples 908 and 955); however, no apparent increase of these elements is seen along the dike margins.

Unusual enrichment of TiO2 near the minor pyroxene-picritic-gabbroic dike which is found to be intruding into the major dike, close to the SE margin, is observed. The minor dike itself is rich in TiO2 (1.97 wt. %); therefore, it is likely that the titanium has been introduced during the emplacement of the minor dike.

Chemical variation across the major dike and minor dike nearby is seen on Figure 64. MgO, ranging from 20 to 28 (wt. %), increases toward the center of the major dike. Similarly, FeO (total), Ni and Cr display enrichments inward. SiO2 seems to slightly decrease in the same direction. Al2O3 and CaO show variations similar to those of SiO2. MnO is uniform (around 0.2 wt. %) whereas TiO2 shows large vari-

ation. Concentrations of Na2O, K2O, Ba are rather uniform across the major dike. Variations of oxides across the minor dike are not as regular as in the major dike, although similar variations seem to be present for most of the oxides from the gabbroic margins toward the thin pyroxene-picritic center.

On the MgO-CaO-Al2O3 and AFM digrams (Figure 65), the major and minor dikes follow the trend of the Molson dike swarm given by Scoates & Macek (1978). Olivine control on the MgO-CaO-Al2O3 diagram for the major dike samples, with a few exceptions, is obvious. The samples from the minor dike plot along the trend of the major dike on the MgO vs NiO, Cr2O3 and Al2O3 diagrams (Figure 66). On the MgO-CaO plot, samples from the minor dike form a trend indicating clinopyroxene fractionation. This trend which has a positive slope, is different from the negative sloped trend of the major dike. On Pearce diagrams, some of the scatter shown by some element pairs is eliminated, resulting in more distinct trends for most of the oxides (Figure 67). The trends on the MgO/Al2O3, FeO/Al2O3, MnO/Al2O3, NiO/Al2O3 vs SiO2/Al2O3 diagrams are similar to those of the Thompson ultramafic body. The trend on the Cr2O3/Al2O3 vs SiO2/Al2O3 diagram is similar to the trend of the orthopyroxenitic rocks of the Thompson ultramafic body.

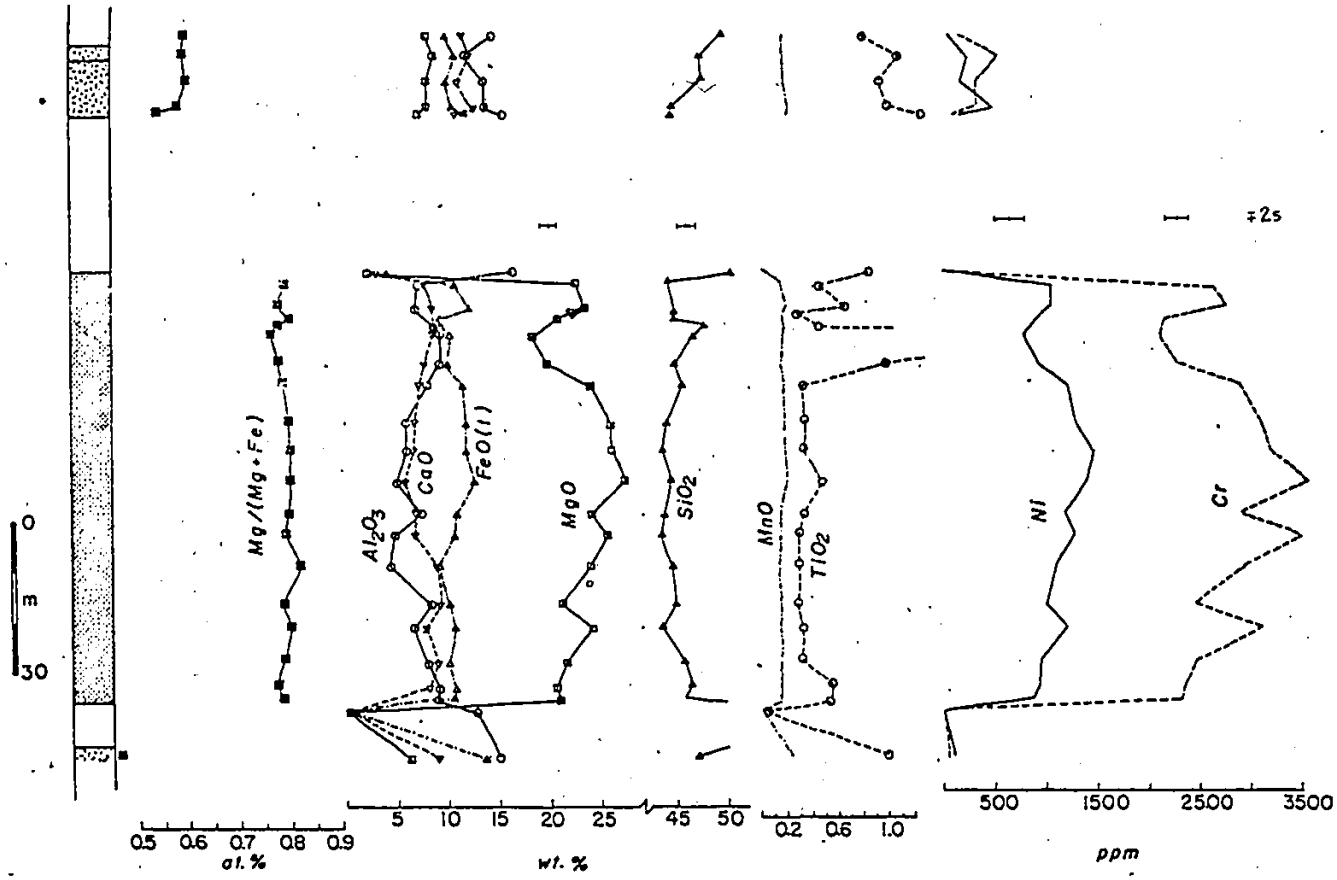

Figure 64: Chemical variation across the dikes as seen along the DDH 64830.

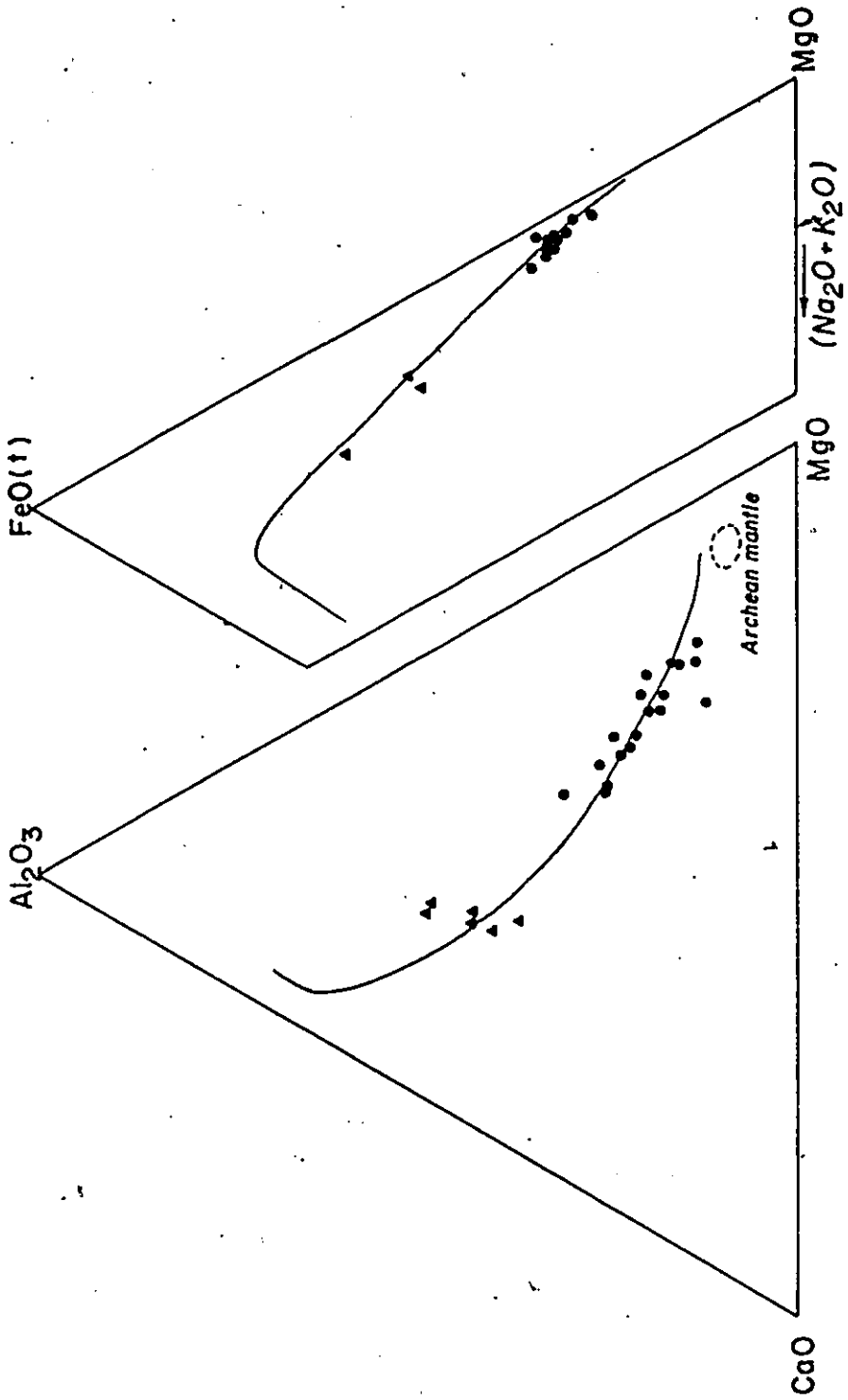

Figure 65: MgO-CaO-Al2O3 and AFM diagrams. Circle, major dike; triangle, minor dike. Lines are the regression lines of the Molson dike swarm after Scoates & Macek (1978).

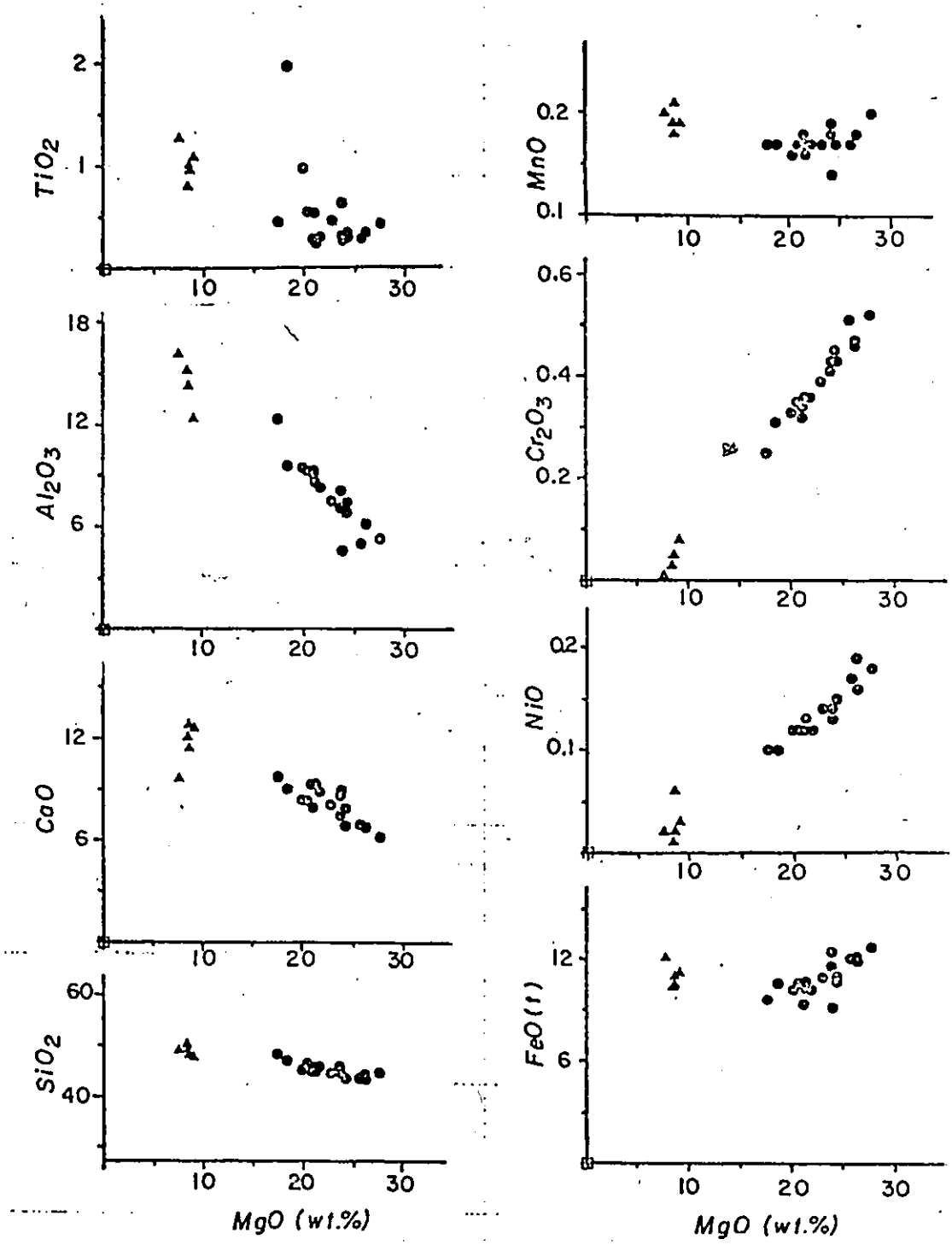

Figure 66: MgO variation diagrams. Circle, major dike; triangle, minor dike.

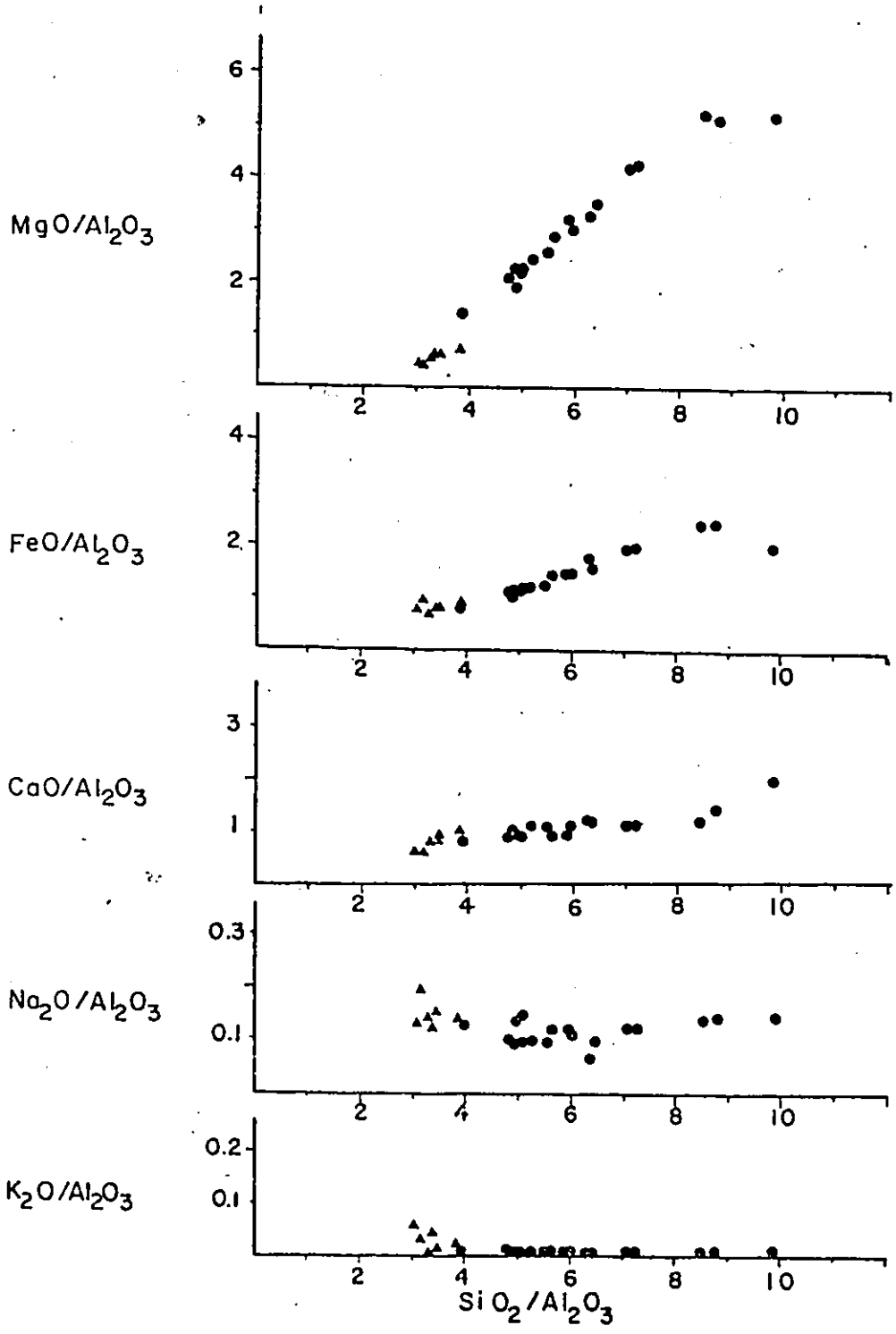

Figure 67: Pearce-type ratio plots. Circle, major dike; triangle, minor dike.

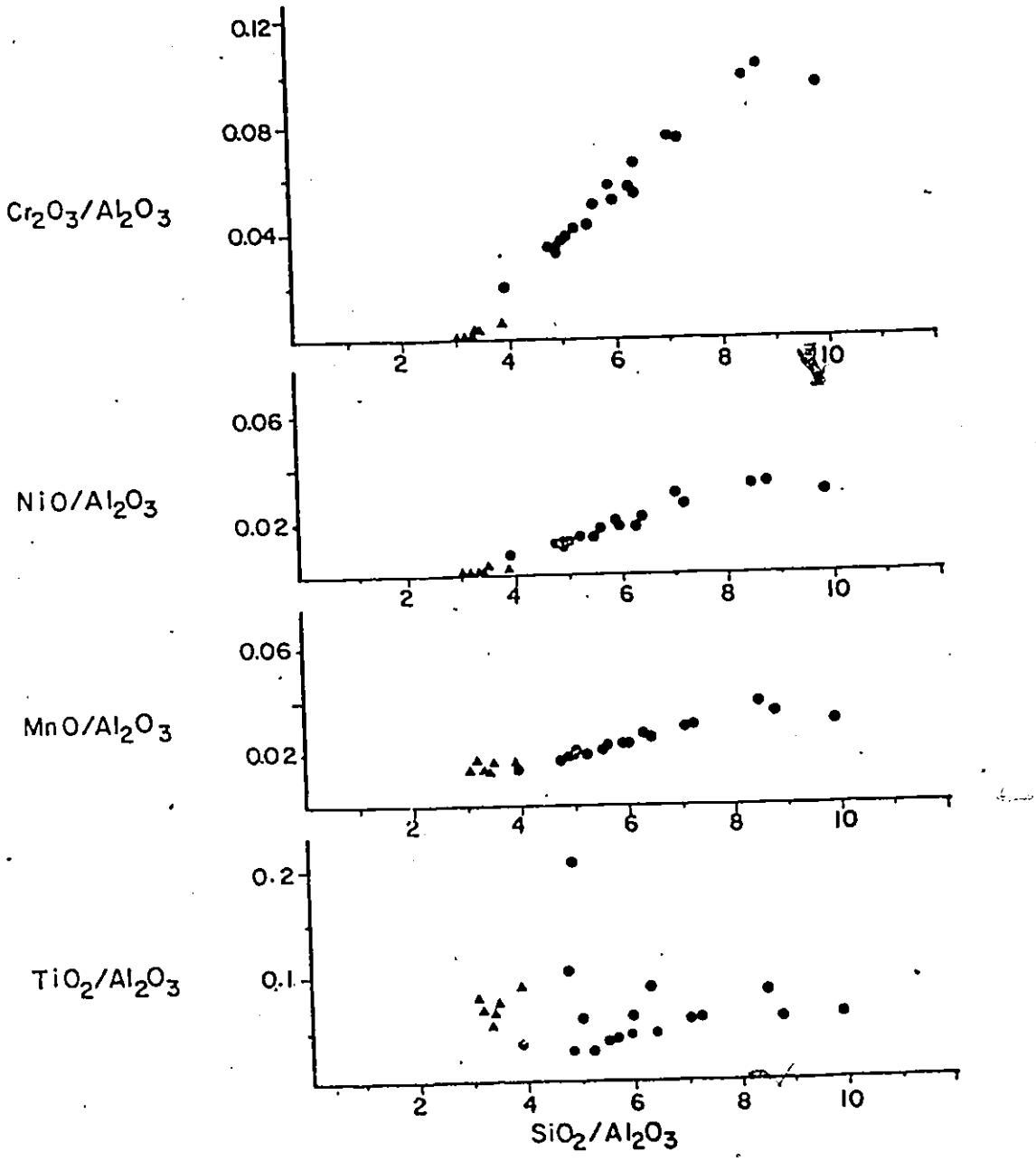

Figure 67 cont.

The data show scatter on the CaO-TiO2 and Al2O3-TiO2 diagrams (Figure 68). Al_2O_3/TiO_2 and CaO/TiO2 ratios of the chilled margin, 16.8 and 14.7 respectively are slightly lower than chondritic ratios. The samples form a trend with positive correlation on the Ti-Zr diagram (Figure 68). Ti/Zr ratio of the chilled margin (145) is higher than the chondritic ratio (110) and much higher than the ratio of the Thompson ultramafic body (80).

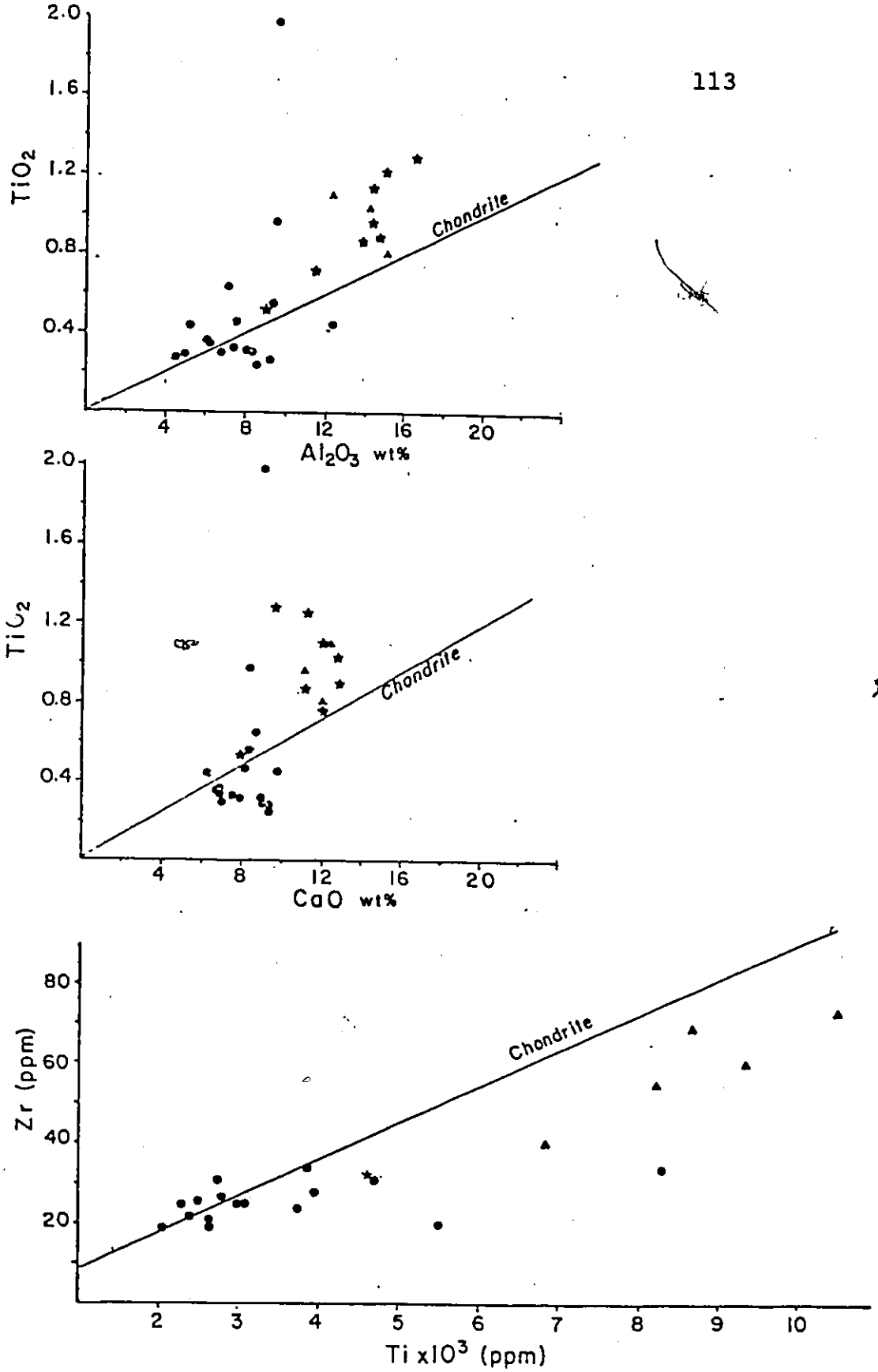

Figure 68: Plots of TiO2 vs. CaO and Al2O3 and Ti vs. Zr. Stars, dike margins.

4.2 PETROGENESIS

4.2.1 Petrogenesis of Individual Dikes

It appears that most of the olivine has formed before and/or during the emplacement of the dike and has been carried in suspension , segregating away from the walls of the vertical conduit due to a flowage effect. This is indicated by (1) increase in modal olivine toward the dike interior, coupled with an increase of bulk MgO, (2) alignment of some early-formed olivines along their long axis, (3) olivines with resorbed outlines, (4) strong similarity of XMg between olivine and whole rock.

Abundances of transition metals, Ca and Al relative to chondrites give nearly parallel patterns with a narrow range of variation for each element across the dike (Figure 69). When they are normalized to the spinifex-textured peridotitic komatiite (STPK) from Munro Township (Arndt et al 1977), they form a nearly flat pattern with concentrations being more or less similar to the STPK. The dike margin is slightly enriched in Ca, Al, and Ti and slightly depleted in Cr, Fe, Mn, Ni, and Zn compared to the STPK and to the rest of the dike samples. This indicates that the chilled margin has experienced a slight olivine fractionation during flow. However, the flow differentiation does not seem to have changed the bulk composition of the magma. The bulk composition of the samples across the dike lie along an olivine

control line on O'Hara's polybaric phase diagram and Irvine's phase diagram (Figures 70 & 71). This is partly consistent with the observed modal mineralogy across the dike showing that the olivine is an abundant phase. However, clinopyroxene and orthopyroxene forming euhedral-subhedral crystals are also abundant as early-formed minerals. If the presence of clinopyroxene and orthopyroxene in the dike is simply due to fractionation, either by removal or accumulation of phases, the observed fractionation trend of the bulk composition would have been destroyed. Euhedral-subhedral clinopyroxene and orthopyroxene crystals displaying straight grain boundaries with the enclosing interstitial material suggest equilibrium conditions during crystallization. Thus, clinopyroxene and orthopyroxene crystals equilibrate with the liquid and simultaneously settle through a distance which is much smaller than the height of the vertical conduit, similar to the 'compensated crystal settling' hypothesis of Cox et al (1979). Since the magma chamber is actually a vertical conduit, crystals that are settling down would not have a chance to accumulate, probably those reaching to deep levels would have dissolved in hotter liquids. Providing that crystals that settle down are replaced by settling of similar crystals from above, the bulk composition of the magma does not change significantly, as already mentioned.

Here the dike rocks may be termed 'accumulates' following the terminology of Irvine (1979). Accumulates are rocks in

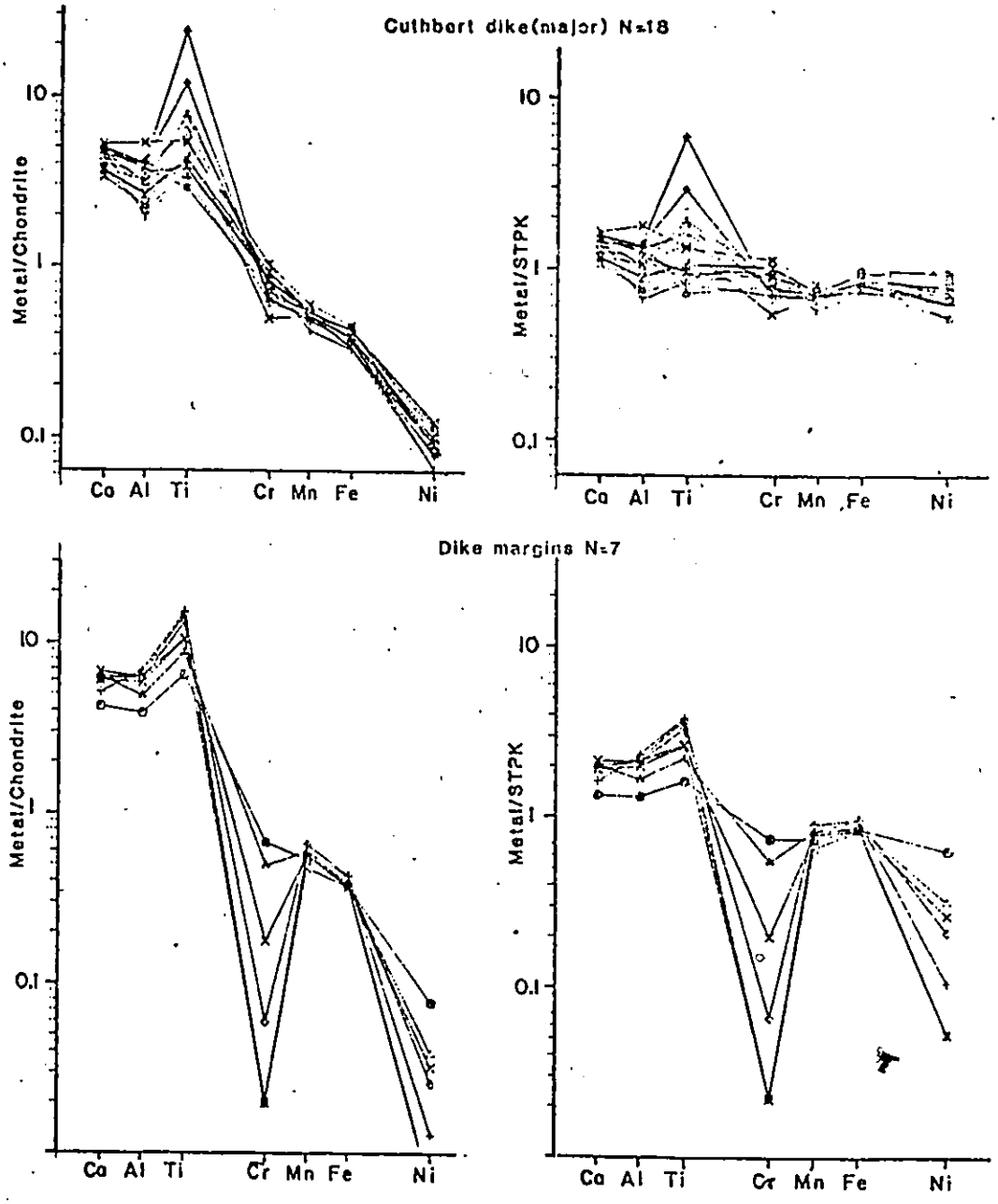

Figure 69: Ca, Al, and transition metal abundances normalized to chondrites and STPK.

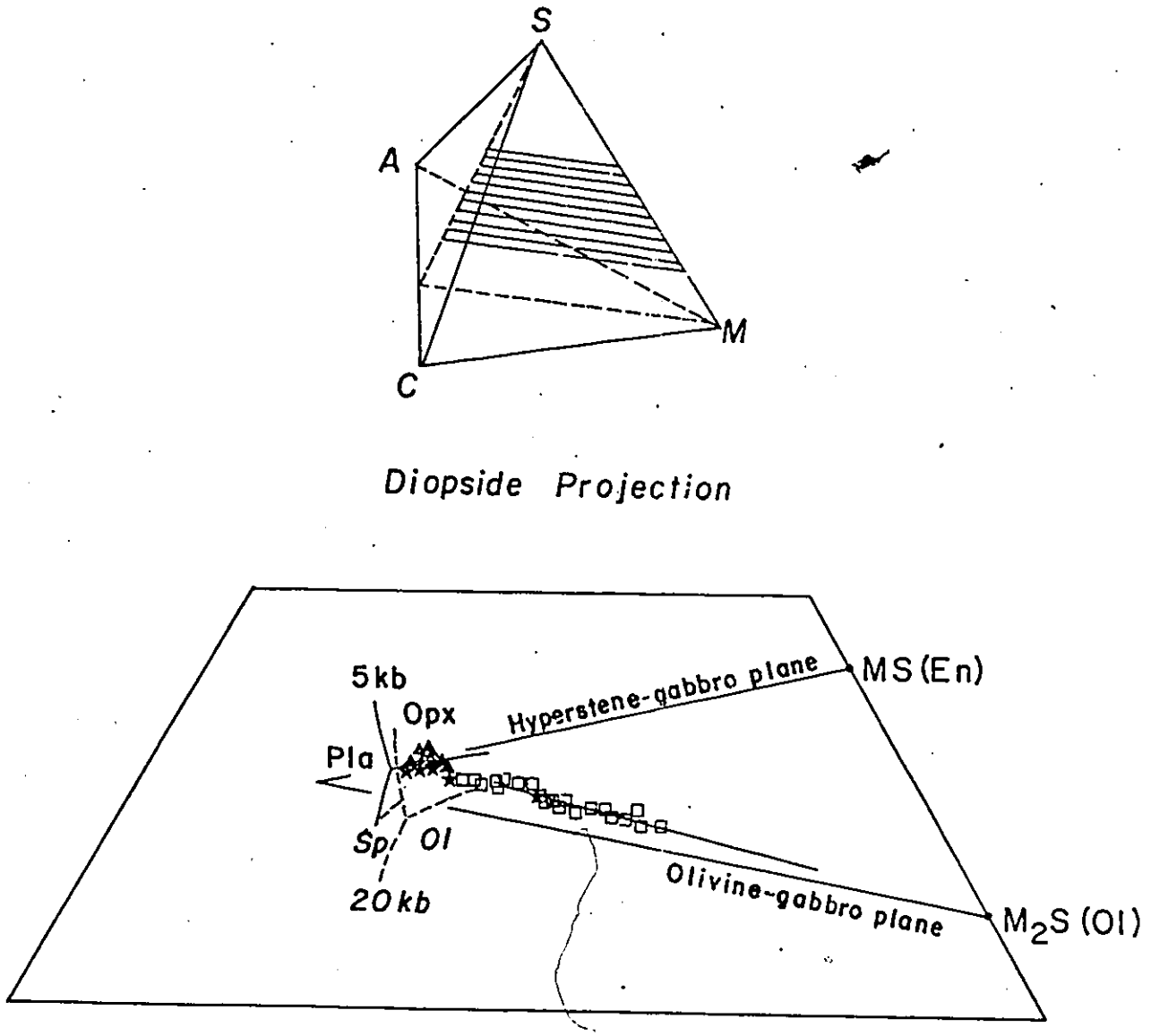

Figure 70: Diopside projection of CMAS tetrahedron. Squares, major dike; triangles, minor dike; stars, dike margins. Note that minor dikes and their margins plot near the 5 kb olivine-orthopyroxene boundary. Hyperstene- and olivine-gabbro planes are shown for reference.

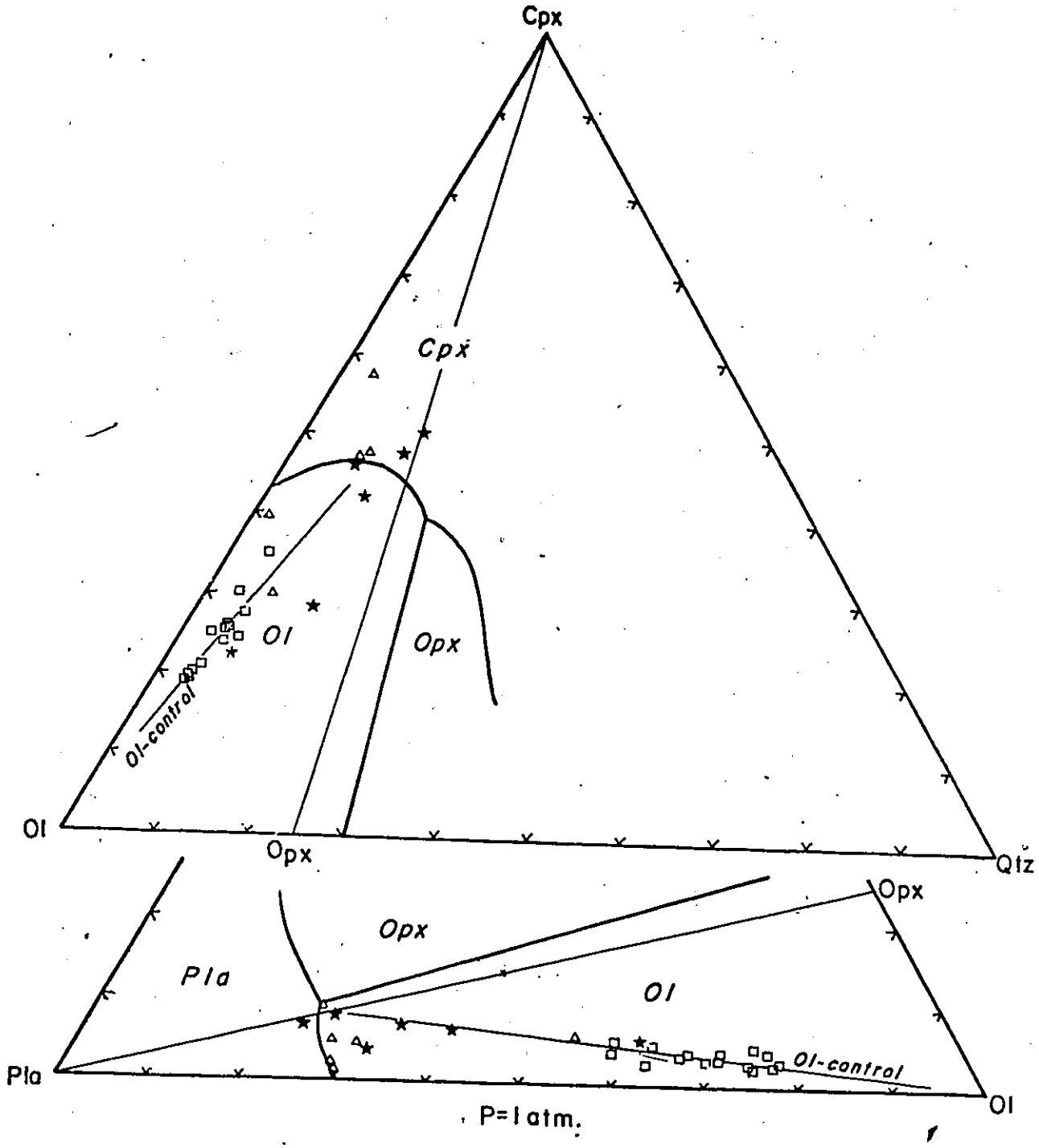

Figure 71: Clinopyroxene and plagioclase projections of the Ol-Cpx-Pla-Qz system. Liquidus boundaries are at 1 atm. Squares, major dike; triangles, minor dike; stars, dike margins. For construction method see Irvine (1979).

which the separation of crystals and liquid is less complete as opposed to fractionated rocks that have only small amounts of trapped liquid. Actually, the dike rocks plot in the field of picritic-peridotitic accumulates on the Irvine's Al/(Mg+Fe) vs Mg/(Mg+Fe) diagram (Figure 72).

The composition of the chilled margin is not in chemical equilibrium with the most magnesian olivine (Fo81) in the dike. This is much smaller than the forsterite composition of 92 which is calculated for the olivine in equilibrium with the composition of the chilled margin by using the Mg/Fe distribution coefficient (Kd) of 0.33 (Irvine, 1979). Thus, it is concluded that the olivines have reacted with the magma in which they are suspended and have changed composition. This is also supported by the texture of the dike rocks (i.e. rounded, resorbed outlines of olivines).

The crystallization sequence can be inferred from the quarternary phase diagram of the system olivine-clinopyroxene-plagioclase-quartz after Irvine (1979).[3] Olivine with composition of Fo92 forms first from the liquid of which the composition is similar to the chilled margin (Figure 73). The composition of the remaining liquid moves directly away from the olivine corner along the path 'ij', as crystallization of olivine proceeds. When the liquid and the suspended

---

[3] Crystallization sequences that are inferred from the three projections (olivine, clinopyroxene, and plagioclase projections) are combined in the quarternary diagram.

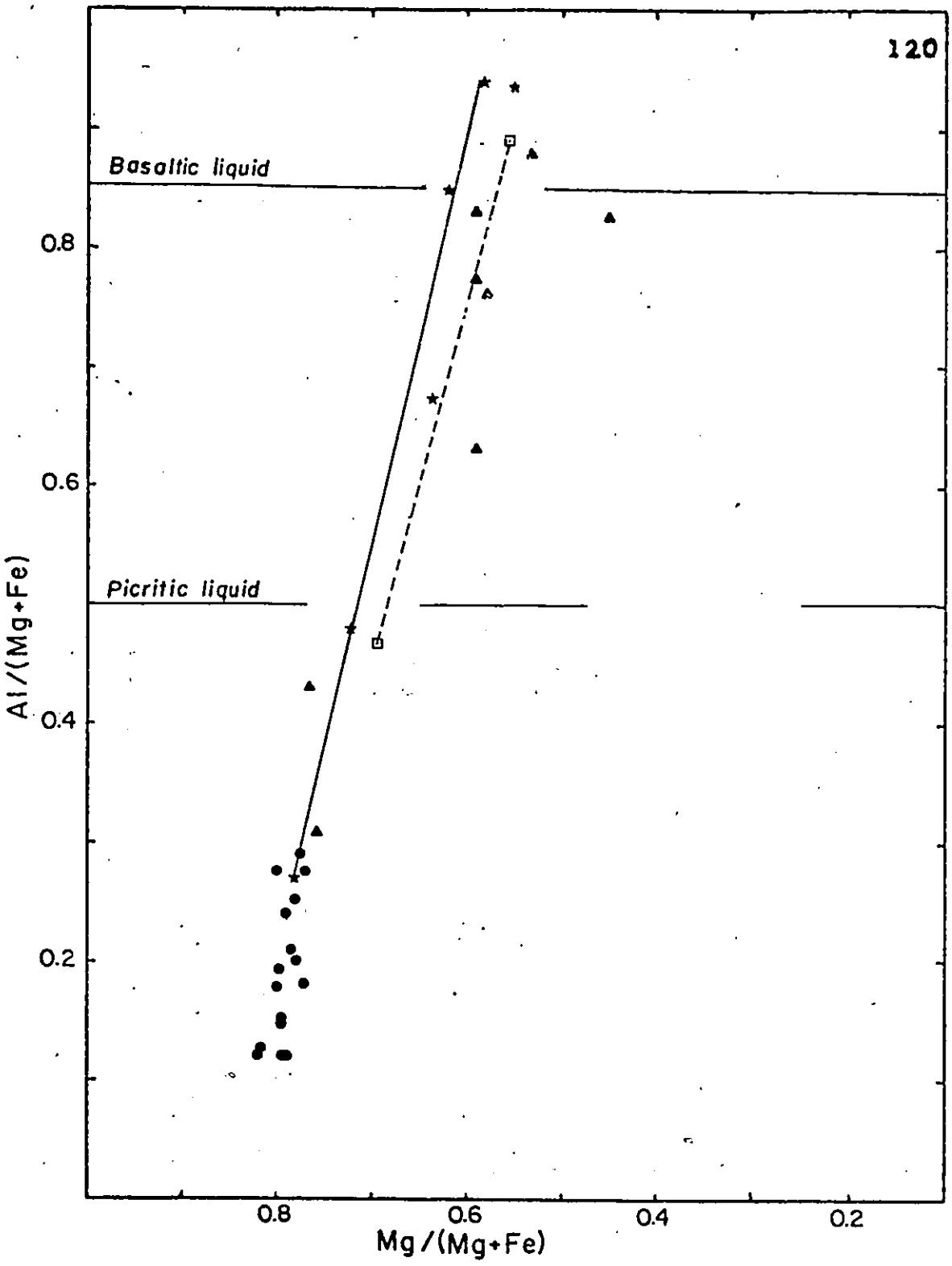

Figure 72: Plot of Mg/(Mg+Fe) vs. Al/(Mg+Fe). Circles, major dike; triangles, minor dike; stars, dike margin. Two squares connected with a dashed line are assumed derivative and calculated primitive liquid compositions for the Kilauea and Mauno Loa lavas (Irvine 1979). Model basaltic and picritic liquids are also from Irvine (1979).

olivine mixture reach the olivine-clinopyroxene plane, clinopyroxene starts to crystallize. Along the path 'jk', olivine reacts with the liquid, changes its composition and becomes resorbed while clinopyroxene is crystallizing. Crystallization of orthopyroxene begins where the olivine-clinopyroxene-orthopyroxene boundary, 'dc', is reached and continues along it toward the point 'd'. At that point, four phases; olivine, clinopyroxene, orthopyroxene and plagioclase are in equilibrium with the remaining liquid. The crystallization sequence would then be:

(i-j) ol

(j-k) ol+cpx

(k-d) ol+cpx+opx

(d) ol+cpx+opx+pla

However, this crystallization sequence differs slightly at higher pressures. The pyroxene volumes expand as the pressure increases (Irvine 1979). Use of phase boundaries at 4.5 kb (Irvine 1970) causes crystallization of orthopyroxene following olivine. The inferred crystallization sequence at 4.5 kb would be:

ol

ol+opx

ol+opx+cpx

ol+opx+cpx+pla

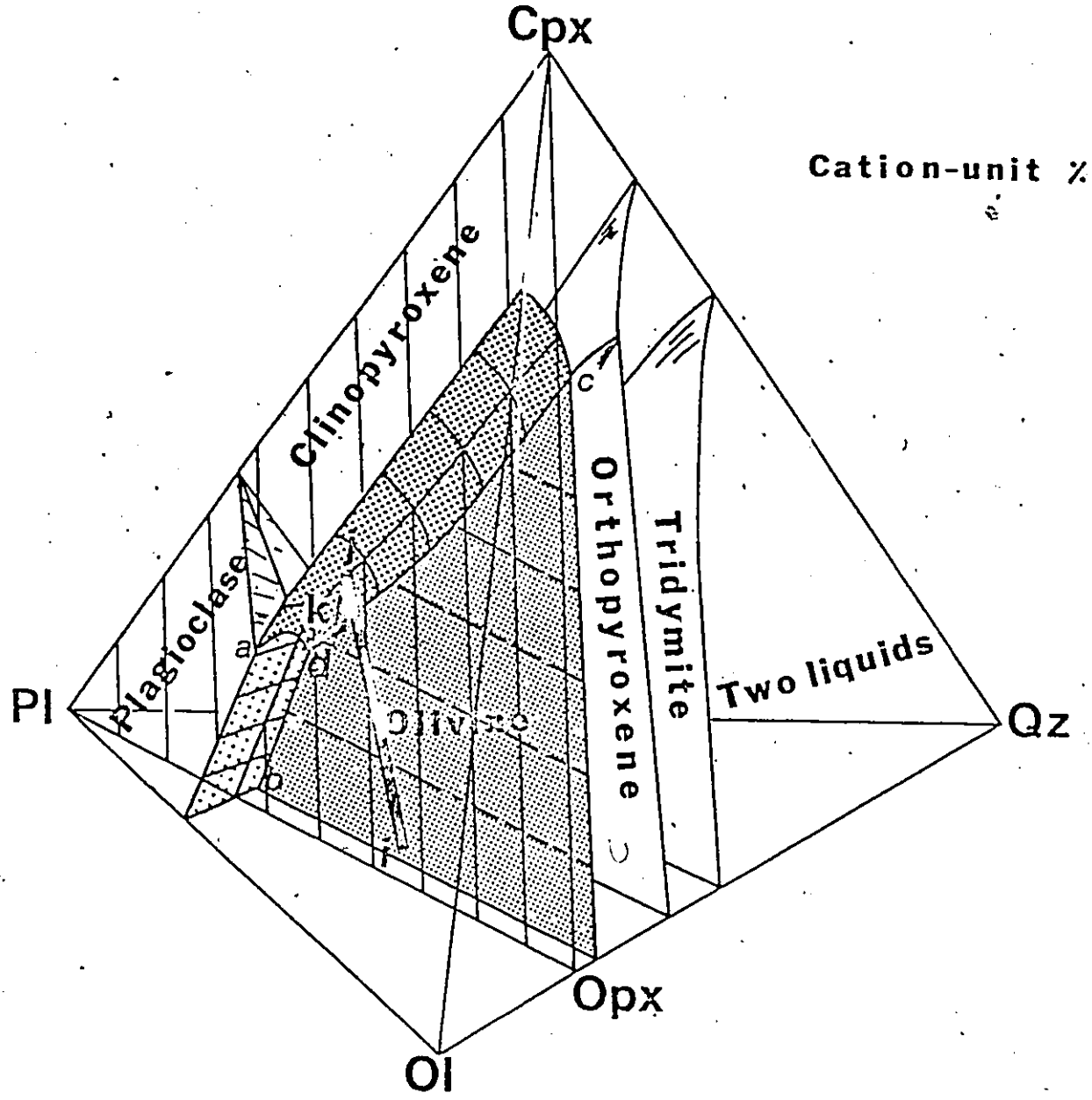

Figure 73: Inferred liquid path of the major dike in the Olivine-Clinopyroxene-Plagioclase-Quartz system (after Irvine, 1979).

The crystallization sequence deduced from O'Hara's polybaric phase diagrams is: (Figure 70)

ol

ol+opx

ol+opx+pla

Chilled margins of the minor dikes' plot close to point 'd' (1 atm) where the four phases are in equlibrium with liquid; therefore, it is difficult to infer a liquid path. At 1 atmosphere pressure, the crstallization sequence would roughly be:

ol+cpx

ol+cpx+pla

At 4.5 kb pressure, it would be:

ol+opx

ol+opx+cpx

This sequence is consistent with the one inferred from O'-Hara's polybaric phase diagram. The chilled margins plot along the olivine-orthopyroxene 5 kb boundary, indicating coprecipitation of orthopyroxene and olivine. Most of the minor dike samples cluster around the olivine-orthopyroxene boundary.

' Includes diabase dikes of Ermanovics & Fahrig (1975) and 'intermediate' and 'minor' dikes of Scoates & Macek (1978).

4.2.2 Petrogenesis of the Dike Swarm

Chilled margins of the major and minor dikes are plotted on the Mg/(Mg+Fe) vs Al/(Mg+Fe) diagram and compared with the 'calculated primitive liquids' and 'assumed derivative liquids' of the Muskox intrusion, Kilauea, Mauna Loa volcanoes and abyssal tholeiites (Irvine 1979). One of the chilled margins of the major dikes plots near the 'calculated primitive liquids' which corresponds to the model picritic liquid of Irvine (1979). The tie-line connecting the chilled margin of the major dike with the chilled margins of the minor dikes is parallel to the tie-lines connecting primitive and derivative liquid compositions. Al/(Mg+Fe) ratio of the other dike margin is similar to that of STPK (e.g. flowtop of a STPK flow; Arndt et al. 1977); therefore, it may be regarded as a komatiitic liquid. From these, one can interpret that the major dikes are formed from komatiitic and picritic liquids whereas the minor dikes are formed from more evolved basaltic liquids.

These liquids with different compositions can represent batches of magmas derived by partial melting of mantle, or alternately, a spectrum produced by differentiation of magma in a subcrustal magma chamber. The latter hypothesis is favoured since the relationship of the chondrite normalized transition element patterns of the chilled margins (Figure 69) is more compatible with it (i.e. progressive depletion

of Cr and Ni, indicating olivine and minor chromite fractionation). CaO/TiO_2 ratio of one of the two major dike margins is similar to chondritic ratio and that of the other is slightly smaller. Al_2O_3/TiO_2 ratios of the two dike margins, on the other hand, are similar to each other and smaller than chondritic ratio. This is consistent with the proposed model dealing with a minor chromite fractionation as well as of olivine. This fractionation changes the original alumina content of the liquid without altering CaO content of the liquid. The texture of the dikes also suggests the existence of olivine and minor chromite prior to intrusion. Thus, the liquid that produced the major dikes must have originated from a zone accumulating olivine and minor chromite.

The ultramafic dikes are usually thicker and longer than mafic ones; therefore, emplacement of the ultramafic dikes is related to major breakups in the crust during tensional failure. Whether major tensional failure occurred first and was followed by minor fracture or major breakups followed the minor fracturing which led the emplacement of mafic dikes, is not known. Scoates and Macek (1978) speculate that the major dikes are earlier than the minor dikes. However, any model concerning magmatism and emplacement of the dike swarm can not be based on such a relationship, since they do not give any supporting evidence to their hypothesis.

Chapter V

CONCLUSION

5.1 THE THOMPSON ULTRAMAFIC ROCKS

Ultramafic rocks of the Thompson Mine were altered prior to metamorphism, as indicated by 1) relict magnetite stringers in olivine megacrysts, 2) parallel orientation of amphibole and chlorite flakes in olivine megacrysts, 3) abundant minute inclusions of amphibole, chlorite, and phlogopite in orthopyroxene megacrysts.

Olivine megacrysts may have recrystallized from partly altered olivines during progressive metamorphism. Orthopyroxene may have formed at the expense of olivine and probably anthophyllite at temperatures above 700°C.

$Mg-Fe^{++}$ partitioning between olivine and Al-chromite was blocked at 670°C. Formation of more Al- and Mg-rich margins relative to Cr- and Fe-rich cores of spinels probably took place at higher grades of progressive metamorphism. This could be considered as a partial reequilibration of $Mg-Fe^{++}$ exchange reaction between olivine and spinel at higher temperatures.

Geotemperature estimates and the mineral assemblage of olivine+tremolite+orthopyroxene+Al-spinel correspond to upper amphibolite facies metamorphism. During or following metamorphism, the ultramafic body was deformed and subsequently recrystallized.

Localized secondary serpentinization is the latest event observed. This secondary serpentinization probably accounts for the extensive serpentinization of peridotitic rocks elsewhere in the belt.

Complex metamorphism and tectonism, however, do not seem to have affected the chemistry of some of the rocks, especially those that were slightly altered or not altered during the retrogressive metamorphism. Chemical variation across the bodies suggests in-situ differentiation. Chemical evolution of the bodies was controlled mainly by olivine and orthopyroxene. Relative abundances of some of the incompatible elements for olivine and orthopyroxene suggest that the original liquid was komatiitic in composition. Differing compositional variations among individual bodies may be explained either by the extent of differentiation, and/or by varying amounts of differentiated liquid that is separated. Another possibility is that some parts of the bodies may have been sliced off during deformation.

Ultramafic and mafic rocks of the belt are linked by a combination of partial melting and crystal fractionation

processes. It is believed that high degrees of partial melting of mantle material, with chondritic abundances of CaO, Al2O3, and TiO2, may have produced the komatiitic melt. Emplacement of the melt seems to have been followed by low-pressure olivine and orthopyroxene fractionation that resulted in the formation of a suite of rocks ranging in composition from ultramafic to mafic.

5.2 THE CUTHBERT LAKE DIKE

Olivine formed before and/or during the emplacement of major dikes and was carried in suspension, concentrating toward the center of the dike due to a flowage effect. Bulk chemistry of dike rocks is controlled mainly by olivine. Although flowage differentiation seems to have been effective, the bulk composition of the magma along the vertical conduit does not seem to have changed significantly, indicating that crystals settling down are replaced by a settling of similar crystals from above. Equilibrium crystallization is favoured to explain the chemistry and texture of these rocks.

Crystallization sequence, as inferred from the 1 atm liquidus relationships is: Ol, Cpx, Opx, Pla. At higher pressures (e.g. 4.5 kb) orthopyroxene replaces the position of clinopyroxene; that is, orthopyroxene crystallizes before clinopyroxene. Equilibration of orthopyroxene with clinopyroxene was reached at 1150°C.

From dike margin compositions, it is concluded that the major dikes were formed from komatiitic liquids whereas the minor dikes were formed from more evolved basaltic liquids. These liquids are regarded as the spectrum produced by differentiation of magma in a subcrustal magma chamber.

5.3 RELATIONSHIP OF THE DIKE SWARM TO THE THOMPSON ULTRAMAFICS

The possibility of a genetic link between the Thompson ultramafics and Cuthbert Lake dikes has been mentioned elsewhere (eg. Bell, 1971; Scoates & Macek, 1978). Bell (1971) suggested the dike swarm could form feeders to ultramafic rocks of the Thompson Nickel Belt. To warrant this possibility, the two suites of rocks must be related in space and time and show similar chemical affinities.

Parallelism of the dike swarm to the Thompson Nickel Belt and the presence of deformed dikes in the belt may indicate that they are spatially related. However, the major concentration of dikes occurs in the Pikwitonei region, whereas the Thompson ultramafic rocks are concentrated near the western margin of the belt. The distance between these two is about 30-35 km and should be taken into consideration.

Age relationships between the two suites are poorly understood. The age of metasedimentary rocks enclosing ultramafic rocks is interpreted to be 2.1 Ga using a Sr-evolution

diagram (Brooks & Theyer 1981). Pb-ages from nickel sulfides which are believed to be cogenetic with the ultramafics, suggest emplacement at 2.3 Ga (Cummings et al. 1982). These relationships have led Cummings et al.(1982) to postulate a relative age of 2.3 Ga for ultramafic rocks of the belt. Ages for the dike swarm are rather tenuous. A range from 1.8 to 2.0 Ga is given as the magnetisation age of the Molson dikes (Ermanovics & Fahrig 1975). Thus, the dike swarm and Thompson ultramafics appear to be Aphebian in age.

Apart from the effects of in-situ differentiation on both the dikes and Thompson ultramafics, it has been shown that both suite of rocks have komatiitic affinities. Chemistry of the orthopyroxenitic and picritic rocks of the belt is similar to that of the Cuthbert Lake dike. This suggests that they may have a common origin. Since Thompson ultramafics have experienced low-pressure olivine and orthopyroxene fractionation, elements that are incompatible for these minerals (e.g. CaO, Al_2O_3, TiO_2) should provide some information about the composition of the liquid. Thus, comparision of the concentration of these elements gives some constraints about the possible genetic relationship of the two suites. Al_2O_3/TiO_2 and CaO/TiO_2 ratios of the Thompson ultramafics are chondritic, whereas those of the dike margins are found to be smaller. As pointed out earlier, the dike margins have experienced olivine and minor chromite fractionation; the latter being responsible for the low

Al_2O_3/TiO_2 ratio. Thus, these relationships preclude the possibility of Cuthbert Lake dikes being feeders to the Thompson ultramafic rocks. However, two suites of rocks may be related by some other means during the mafic-ultramafic magmatic activity along the northwestern edge of the Superior Province. Both suites may be the products of the same partial melting event; however, they may have experienced different fractionation histories during their ascent and/or emplacement. This requires establishment of better age relationships of the ultramafic and mafic rocks in the region.

REFERENCES

Abbey, S. (1977): Studies in 'standard samples' for use in the general analysis of silicate rocks and minerals. Geol. Surv. Canada, Paper 77-34, 31p.

Arai, S. (1975): Contact metamorphosed dunite-harzburgite complex in the Chugoku district, western Japan. Contr. Mineral. Petrology 52, 1-16.

Arndt, N. T., Naldrett, A. J. & Pyke, D. R. (1977): Komatiiitic and iron-rich tholeiitic lavas from Munro Township, northeast Ontario. J. Petrology 18, 319-369.

Baragar, W. R. A. & Scoates, R. F. J. (1981): The Circum-Superior belt: a Proterozoic plate margin? In Precambrian plate tectonics (A. Kroner, ed.), Elsevier, Amsterdam, 297-330.

Bell, C. K. (1971): Boundary geology, upper Nelson River area, Manitoba and northwestern Ontario. Geol. Assoc. Can., Spec. Pap., 9, 11-39.

Bickle, M. J. (1982): The magnesium contents of komatiitic liquids. In Komatiites (N.T. Arndt & E.G. Nisbett eds.) George Allen & Unwin (London), 479-493.

Bliss, N. W. (1972): A comparative study of two ultramafic bodies at the southwest end of the Manitoba nickel belt, with special reference to the chromite mineralogy. Ph.D. thesis, McGill University, Montreal.

Bowen, N. L. & Schairer, J. F. (1935): The system MgO-FeO-SiO2. Amer. J. Sci. 29, 151-217.

Brooks, C. & Theyer, P. (1981): Rb/Sr geochronology in the Thompson belt, Manitoba: implications for Aphebian crustal

development and metallogenesis. Can. J. Earth Sci. 18, 932-943.

Champness, P. E. (1970): Nucleation and growth of iron oxides in olivines. Mineral. Magazine 37, 790-800.

Coats, C. J. A. (1966): Serpentinized ultramafic rocks of the Manitoba nickel belt. Ph.D. thesis, University of Manitoba, Winnipeg.

_____, Quirke, T. T., Jr., Bell, C. K., Cranstone, D. A. & Campbell, F. H. A. (1972): Geology and mineral deposits of the Flin Flon, Lynn Lake and Thompson areas, Manitoba, and the Churchill-Superior front of the western Precambrian Shield. Guidebook, Field excursion A31-C31. 24th International Geological Congress, Montreal, 1-96.

Cox, K. G., Bell, J. D. & Pankhurst, R. J. (1979): The interpretation of igneous rocks. George Allen & Unwin Ltd., London, 450p.

Cranstone, D. A. & Turek, A. T. (1976): Geological and geochronological relationships of the Thompson nickel belt, Manitoba. Can. J. Earth Sci. 13, 1058-1069.

Cummings, G. L., Eckstrand, O. R. & Peredery, W. V. (1982): Geochronological interpretations of Pb isotope ratios in nickel sulfides of the Thompson belt, Manitoba. Can. J. Earth Sci. 19, 2306-2324.

Danckwert, P. A. & Newton, R. C. (1978): Experimental determination of the spinel peridotite to garnet peridotite reaction in the system MgO-Al2O3-SiO2 in the range 900°C-1100°C and Al2O3 isopleths of enstatite in the spinel field. Contr. Mineral. Petrology 66, 189-201.

Deer, W. A., Howie, R. A. & Zussman, J. (1966): An introduction to the rock forming minerals. Longman's London.

DeJongh W. K. (1975): Table of influence coefficients. Unpubl. Report for Philips's application laboratory, Eindhoven, Holland.

DeSaboia, L. A. (1978): The West Manasan and the Pipe mine 2 ultramafic bodies of the Thompson nickel belt. M.Sc. thesis, University of Western Ontario, London.

Dobretsov, N. L. (1968): Paragenetic types and compositions of metamorphic pyroxenes. J. Petrology 9, 358-377.

Duke, J. M. & Naldrett, A. J. (1978): A numerical model of the fractionation of olivine and molten sulfide from komatiite magma. Earth Planet Sci. Lett.,39, 255-266.

Emslie, R. F. (1983): The coronitic Michael Gabbros, Labrador: Assessment of Grenvillian metamorphism in northeastern Grenville Province. Geol. Surv. Canada, Paper 83-1A, Current Res. part A, 139-145.

Engi, M. & Evans, B. W. (1980): A re-evaluation of the olivine-spinel geothermometer: Discussion. Contr. Mineral. Petrology 73, 201-203.

Ermanovics, I. & Fahrig, W. F. (1975): The petrochemistry and paleomagnetism of the Molson dikes, Manitoba. Can. J. Earth Sci. 12, 1564-1575.

Evans, B. W. (1977): Metamorphism of alpine peridotite and serpentinite. Ann. Rev. Earth Planet. Sci. 5, 397-447.

_____ & Frost, B. R. (1975): Chrome-spinel in progressive metamorphism-a preliminary analysis. Geochim.

Cosmochim. Acta 39, 959-972.

_____ & Trommsdorff, V. (1974): Stability of enstatite plus talc, and CO2 metasomatism of metaperidotite, Val d' Efra, Lepontine Alps. Amer. J. Sci. 274, 274-296.

Fabries, J. (1979): Spinel-olivine geothermometry in peridotites from ultramafic complexes. Contr. Mineral. Petrology 69, 329-336.

Frey, F. A., Bryan, W. B. & Thompson, G. (1974): Atlantic Ocean Floor: Geochemistry and petrology of basalts from legs 2 and 3 of the Deep-Sea Drilling Project. J. Geophy. Res. 79, 5507-5527.

Frost, B. R. (1975): Contact metamorphism of serpentinite, chloritic blackwall and rodingite at Paddy-Go-Easy Pass, Central Cascades, Washington. J. Petrology 16, 272-313.

Fujii, T. (1976): Solubility of Al2O3 in enstatite coexisting with forsterite and spinel. Carnegie Inst. Washington Yearb. 75, 566-571.

Gasparik, T. & Lindsley, D. H. (1980): Phase equilibria at high pressure of pyroxenes containing monovalent and trivalent ions. In Pyroxenes (C. T. Prewitt, ed.). Mineral. Soc. Amer. Pap. v.7, 309-339.

Gibb, F. G. F. (1968): Flow differentiation in the xenolithic ultrabasic dykes of the Cuillins and the Strathaird Peninsula, Isle of Skye, Scotland. J. Petrology 9, 411-443.

Goetze, C. (1975): Sheared lherzolites: from the point of view of rock mechanics. Geol. 3, 172-173.

Green, D. H. & Ringwood, A. E. (1970): Mineralogy of peridotitic compositions under upper mantle conditions. Phys. Earth Planet

Inter. 3, 359-371.

Green, H. W., Griggs, D. T. & Christie, J. M. (1970): Syntectonic and annealing recrystallization of fine grained quartz aggregates. In Experimental and natural rock deformation (P. Paulitsch, ed.), Springer, New York, 272-335.

Groves, D. I., Barrett, F. M., Binns, R. A., Marston, R. J. & McQueen, K. G. (1976): A possible volcanic-exhalative origin for lenticular nickel sulfide deposits of volcanic association with special reference to those in Western Australia: discussion. Can. J. Earth Sci. 13, 1646-1650.

Haggerty, S. E. (1976): Oxidation of opaque mineral oxides in basalts. In Oxide minerals (Shorth Course Notes) (D. Rumble III ed.), Mineral. Soc. Amer., 3, 1-100.

_____ & Baker, I. (1967): The alteration of olivine in basaltic and associated lavas, part I: high temperature alteration. Contr. Mineral. Petrology 16, 233-257.

Irvine, T. N. (1965): Chromian spinel as a petrogenetic indicator I: Theory. Can. J. Earth Sci. 2, 648-672.

_____ (1970): Crystallization sequences in the Muscox Intrusion and other layered intrusions, I. Olivine-pyroxene-plagioclase relations. Spec. Publ. Geol. Soc. S. Afr. 1, 441-476.

_____ (1979): Rocks whose compositions are determined by crystal accumulation and sorting. In: Evolution of the Igneous Rocks (H. S. Yoder, ed.). Princeton University Press, 245-306.

_____ (1980): Magmatic infiltration metasomatism, double-diffusive fractional crystallization, and adcumulus growth in the Muskox Intrusion and other layered intrusions. In Physics

of Magmatic Processes (R. B. Hargraves, ed.). Princeton University Press, 325-383.

Jackson, E. D. (1969): Chemical variation in coexisting chromite and olivine in the chromitite zones of the Stillwater Complex. Econ. Geol. Monograph 4, 41-71.

Jamieson, R. A. (1981): Metamorphism during ophiolite emplacement-the petrology of the St. Anthony Complex. J. Petrology 22, 397-449.

Jaques, A. L. & Green, D. H. (1980): Anhydrous melting of peridotite at 0-15 kb pressure and the genesis of tholeiitic basalts. Contr. Mineral. Petrology 73, 287-310.

Jenkins, D. M. (1981): Experimental phase relations of hydrous peridotites, modelled in the system H2O-CaO-MgO-Al2O3-SiO2. Contr. Mineral. Petrology 77, 166-176.

Kay, R. W. & Hubbard, N. J. (1978): Trace elements in ocean ridge basalts. Earth Planet. Sci. Lett. 38, 95-116.

Kretz, R. (1982): Transfer and exchange equilibria in a portion of the pyroxene quadrilateral as deduced from natural and experimental data. Geochim. Cosmochim. Acta 46, 411-421.

Lusk, J. (1976): A possible volcanic-exhalative origin for lenticular nickel sulfide deposits of volcanic association, with special reference to those in Western Australia. Can. J. Earth Sci. 13, 451-458.

Maaloe, S. & Aoki, K. (1977): The major element composition of the upper mantle estimated from the composition of lherzolites. Contr. Mineral. Petrology 63, 161-173.

McDonald, J. A. (1960): A petrological study of the Cuthbert

Lake ultrabasic and basic dike swarms. M.Sc. thesis, University of Manitoba, Winnipeg.

Manitoba Mineral Resources Division (1979): Geological Map of Manitoba. Scale 1:1 000 000 Map 79-2.

Medaris, L. G. (1969): Partitioning of Fe^{++} and Mg between coexisting synthetic olivine and orthopyroxene. Amer. J. Sci., 267, 945-968.

Mercier, J-C. C. (1976): Single pyroxene geothermometry and barometry. Amer. Mineral. 61, 603-615.

_____ (1980): Single pyroxene thermobarometry. Tectonophys. 70, 1-37.

_____ & Nicolas, A. (1975): Textures and fabrics of upper-mantle peridotites as illustrated by xenoliths from basalts. J. Petrology 16, 454-487.

Mysen, B. (1975): Partitioning of iron and magnesium between crystals and partial melts in peridotite upper mantle. Contr. Mineral. Petrology 52, 69-76.

Naldrett, A. J. (1973): Nickel sulfide deposits- their classification and genesis, with special emphasis on deposits of volcanic association. Can. Inst. Mining Met. Bull. 76, 183-201.

Naldrett, A. J. & Cabri, L. J. (1976): Ultramafic and related mafic rocks: Their classification and genesis with special reference to the concentration of nickel sulfides and platinum-group elements. Econ. Geol., 71 1131-1158.

Nesbitt, R. W., Sun, S. S., & Purvis, A. C. (1979):

Komatiites: Geochemistry and genesis. Can. Mineral. 17, 165-186.

O'Hara, M. J. (1968): The bearing of phase equilibria studies in synthetic and natural systems on the origin and evolution of basic and ultrabasic rocks. Earth Sci. Rev. 4, 69-133.

Pearce, T. H. (1968): A contribution to the theory of variation diagrams. Contr. Mineral. Petrology 19, 142-157.

_____ (1969): Some comments on the differentiation of the Dundonald sill, Ontario. Can. J. Earth Sci. 6, 75-80.

Peredery, W. V. (1979): Relationship of ultramafic amphibolites to metavolcanic rocks and serpentinites in the Thompson belt, Manitoba. Can. Mineral. 17, 187-200.

_____ (1982): Geology and nickel sulphide deposits of the Thompson belt, Manitoba. In Precambrian Sulphide deposits, Geol. Assoc. Can. Robinson vol. (R. W. Hutchinson, C. D. Spence & J. M. Franklin eds.), 165-209.

Peters, TJ. (1968): Distribution of Mg, Fe, Al, Ca and Na in coexisting olivine, orthopyroxene and clinopyroxene in the Totalp serpentinite (Davos, Switzerland) and in the Alpine metamorphosed Melanco serpentinite (N. Italy). Contr. Mineral. Petrology 18, 65-75.

Poirier, J. P. & Nicolas, A. (1975): Deformation-induced recrystallization due to progressive misorientation of subgrains, with special reference to mantle peridotites. J. Geol. 83, 707-720.

Putnis, A. (1979): Electron petrography of high-temperature oxidation in olivine from the Rhum Layered Intrusion. Mineral. Mag. 43, 293-296.

Rance, H. (1966): Superior-Churchill structural boundary, Wabowden, Manitoba. Ph.D. thesis, University of Western Ontario, London.

Ringwood, A. E. (1966): The chemical composition and origin of the earth. In Advances in Earth Science (P. Hurley, ed.). M.I.T. Press, Cambridge, Mass., 287-356.

Roeder, P. L., Campbell, I. H. & Jamieson, H. E. (1979): A re-evaluation of the olivine-spinel geothermometer. Contr. Mineral. Petrology 68, 325-334.

Ross, J. R. & Hopkins, G. M. F. (1975): Kambalda nickel sulfide deposits. In Economic Geology of Australia and Papua-New Guinea, vol I, Metals (C. L. Knight, ed.), Austral. Inst. Mining Met. Mon. 5, 100-121.

Russell, J. K. (1981): Metamorphism of the Thompson nickel belt gneisses: Paint Lake, Manitoba. Can. J. Earth Sci. 18, 191-209.

Sack, R. O. (1980): Some constraints on the thermodynamic mixing properties of Fe-Mg orthopyroxenes and olivines. Contr. Mineral. Petrology 71, 257-269.

Scarfe, C. M., Mysen, B. O. & Rai, C. S. (1978): Invariant melting behavior of mantle material: Partial melting of two lherzolite nodules. Carnegie Inst. Washington Yearbook, 498-501.

Scoates, R. F. J. & Macek, J. J. (1978): Molson dike swarm. Manitoba Mineral Res. Div. Geol. Surv. paper 78-1, 53p.

Shaw, D. M. (1968): A rewiev of K-Rb fractionation trends by covariance analysis. Geochim. Cosmochim. Acta 32, 573-601.

Smith, D. G. W. & Gold, C. M. (1979): EDATA2: A Fortran IV computer program for processing wavelength- and/or energy-dispersive electron microprobe analysis. In Microbeam Anal. Soc. Proc. 14th Ann. Conf. San Antonio 1979 (D. E. Newbury, ed.), 273-278.

Stephenson, J. F. (1974): Geology of the Ospwagan Lake (East half) area. Manitoba Mineral Res. Publ., 74-1.

Sun, S. S. & Nesbitt, R. W. (1977): Chemical heterogeneity of the Archean mantle, composition of the earth and mantle evolution. Earth Planet. Sci. Lett. 35, 429-448.

Trommsdorff, V. & Evans, B. W. (1974): Alpine metamorphism of peridotitic rocks. Schweiz. Mineral. Petrog. Mitt. 54, 333-352.

_____ & _____ (1980): Titanian hydroxyl-clinohumite: Formation and breakdown in antigorite rocks (Melanco, Italy). Contr. Mineral. Petrology 72, 229-242.

Vance, J. A. & Dungan, M. A. (1977): Formation of peridotites by deserpentinization in the Darrington and Sultan areas, Cascade Mountains, Washington. Geol. Soc. Amer. Bull. 88, 1497-1508.

Villaume, J. F. & Rose, A. W. (1977): The geochemistry of some Archean ultramafic lavas. Chem. Geol. 10, 43-50.

Weber, W. & Scoates, R. F. J. (1978): Archean and proterozoic metamorphism in the northwestern Superior province and along the Churchill-Superior boundary, Manitoba.

In Metamorphism in the Canadian Shield (J. A. Fraser & W. W. Heywood, eds.). Geol. Surv. Can. Pap. 78-10, 5-16.

Wilson, H. D. B. & Brisbin, W. C. (1961): Regional structure of the Thompson-Moak Lake nickel belt. Can. Inst. Mining Met. Bull. 54, 815-822.

Zurbrigg, H. F. (1963): Thompson mine geology. Can. Inst. Mining Met. Bull. 56, 451-460.

Appendix A

MINERAL ANALYSES

Mineral analysis was performed with a Cambridge Mark-V electron microprobe at the Department of Geology, Dalhousie University. The instrument is equipped with an Ortec energy dispersive spectrometer and it is automated to produce simultaneous multi-element analyses and data reduction using program 'EDATA 2' of Smith & Gold (1979). Natural and synthetic minerals were used as standards. Precision of the analyses obtained from replicate determinations is given in Table 1. Mineral analyses are listed in Table 2.

Since it was impossible to have subscripts printed with the text editor used, some of the chemical formulas with subscripts were written informally throughout the thesis. Their formal equivalents are as follows: SiO2, SiO_2; TiO2, TiO_2; Al2O3, Al_2O_3; Cr2O3, Cr_2O_3; V2O3, V_2O_3; Fe2O3, Fe_2O_3; Na2O, Na_2O.

TABLE 1

Precision of Mineral Analyses

		R.M	2s	v
SiO2	Ol, Opx, Amp	40-58	±0.23	0.2
TiO2	Opx, Sp	0.30-0.50	±0.04	5.4
Al2O3	Opx	0.33	±0.19	28.8
	Amp	5.35	±0.17	1.6
	Sp	14-17	±0.89	3.1
Cr2O3	Opx	0.05	±0.06	60
	Amp	0.44	±0.07	8
	Sp	47-54	±1.20	1.1
V2O3	Sp	0.25	±0.04	8
MgO	Ol, Opx, Amp	20-50	±0.23	0.5
	Sp	6-12	±0.30	2.1
FeO(t)	Ol, Opx	6-12	±0.15	0.7
	Amp	2.59	±0.01	0.2
	Sp	22-25	±0.28	0.8
CaO	Opx	0.11	±0.04	18
	Amp	12.34	±0.03	0.1
MnO	Amp	0.07	±0.03	23
	Ol	0.14	±0.02	5.7
	Opx	0.21	±0.04	9.5
	Sp	0.5	±0.32	32
NiO	Ol	0.13	±0.08	30
	Opx, Amp	0.1	±0.2	95
Na2O	Amp	0.66	±0.04	3

R.M, Range or mean; 2s, confidence limit given as 2 times standard deviation; v, coefficient of variation (%): v=100s/mean.

MICROPROBE ANALYSES OF OLIVINE

S.NO	63.10	63.11	63.20	63.21	100.11	100.11	100.12	100.12	100.21	100.21	100.22	
SIO2	39.76	41.36	39.71	41.23	38.81	39.74	39.13	39.37	38.82	39.58	38.69	SIO2
TIO2	0.0	0.0	0.0	0.0	0.0	0.0	0.0	0.0	0.0	0.0	0.0	TIO2
AL2O3	0.0	0.03	0.0	0.03	0.0	0.0	0.0	0.0	0.0	0.0	0.0	AL2O3
CR2O3	0.0	0.03	0.0	0.02	0.0	0.0	0.07	0.0	0.0	0.0	0.0	CR2O3
FEO	9.73	10.35	9.84	10.17	13.97	14.42	14.15	14.41	14.09	14.38	13.97	FEO
MGO	48.73	48.28	48.88	48.77	45.70	45.37	45.69	46.47	45.44	45.88	45.68	MGO
CAO	0.0	0.02	0.0	0.02	0.0	0.0	0.0	0.01	0.0	0.0	0.0	CAO
MNO	0.13	0.10	0.11	0.09	0.29	0.31	0.27	0.31	0.23	0.32	0.25	MNO
NIO	0.25	0.18	0.22	0.16	0.15	0.10	0.07	0.07	0.07	0.07	0.0	NIO
TOTAL	98.60	100.35	98.76	100.49	98.92	99.94	99.38	100.64	98.65	100.23	98.59	TOTAL

CATION PROPORTIONS ON THE BASIS OF 4 OXYGENS

SI	0.990	1.011	0.988	1.006	0.984	0.997	0.987	0.982	0.987	0.990	0.984	SI
TI	0.0	0.0	0.0	0.0	0.0	0.0	0.0	0.0	0.0	0.0	0.0	TI
AL	0.0	0.001	0.0	0.001	0.0	0.0	0.0	0.0	0.0	0.0	0.0	AL
CR	0.0	0.001	0.0	0.000	0.0	0.0	0.001	0.0	0.0	0.0	0.0	CR
FE	0.203	0.212	0.205	0.208	0.296	0.302	0.299	0.301	0.299	0.301	0.297	FE
MG	1.809	1.759	1.812	1.773	1.727	1.696	1.718	1.727	1.721	1.711	1.731	MG
CA	0.0	0.001	0.0	0.001	0.0	0.0	0.0	0.000	0.0	0.0	0.0	CA
MN	0.003	0.002	0.002	0.002	0.006	0.007	0.006	0.007	0.005	0.007	0.005	MN
NI	0.005	0.004	0.004	0.003	0.003	0.002	0.001	0.001	0.001	0.001	0.0	NI
XMG	0.899	0.893	0.898	0.895	0.854	0.849	0.852	0.852	0.852	0.850	0.854	XMG
KD	8.925	8.313	8.852	8.546	5.829	5.607	5.754	5.747	5.747	5.686	5.827	KD

XMG=MG/MG+FE KD=XMG/XFE

MICROPROBE ANALYSES OF OLIVINE

S.NO	100.22	100.30	100.31	105.10	105.12	105.20	105.31	105.32	105.41	105.42	107.10	
SIO2	39.07	38.64	39.32	39.67	39.95	39.47	39.68	39.51	39.75	39.91	40.12	SIO2
TIO2	0.0	0.0	0.0	0.0	0.0	C.0	0.0	0.0	0.0	0.0	C.0	TIO2
AL2O3	0.0	0.0	0.0	0.0	0.0	0.0	0.0	0.0	0.0	0.0	C.0	AL2O3
CR2O3	0.0	0.05	0.C	0.05	0.0	C.0	0.0	0.0	0.0	0.14	0.0	CR2O3
FEO	14.74	13.68	14.61	12.71	12.64	12.96	12.99	13.01	12.74	12.85	10.46	FEO
MGO	45.92	45.42	45.74	47.36	47.38	47.07	47.08	47.00	47.34	47.64	48.48	MGO
CAO	0.0	0.0	0.0	0.0	0.0	C.0	0.0	0.0	0.0	0.C	C.0	CAO
MNO	0.31	0.18	0.31	0.13	0.14	C.20	0.2C	0.16	0.18	0.18	0.18	MNO
NIO	0.07	0.09	0.07	0.06	0.15	0.0	0.06	0.21	0.13	0.22	C.21	NIO
TOTAL	100.11	98.06	100.05	99.98	100.26	99.70	100.01	99.89	100.14	100.94	99.45	TOTAL

CATION PROPORTIONS ON THE BASIS OF 4 OXYGENS

SI	0.982	C.986	0.987	0.987	0.991	0.986	0.988	0.986	0.988	0.985	0.993	SI
TI	0.0	C.0	0.0	0.0	0.0	0.0	0.0	C.0	C.C	0.0	C.0	TI
AL	0.0	0.0	0.0	0.0	0.0	0.0	C.0	C.0	0.0	0.0	C.0	AI
CR	0.0	0.001	0.0	0.001	0.0	0.0	0.0	0.0	0.0	0.003	C.0	CR
FE	0.310	0.292	0.307	0.264	0.262	0.271	0.271	C.272	0.265	0.265	0.217	FE
MG	1.719	1.728	1.711	1.756	1.751	1.753	1.747	1.748	1.753	1.752	1.789	MG
CA	0.C	C.0	0.0	0.0	0.0	0.0	0.0	0.0	0.0	0.0	C.0	CA
MN	0.007	C.004	0.007	C.C03	0.003	0.004	0.C04	0.003	C.004	0.004	C.004	MN
NI	0.001	C.C02	0.001	C.CC1	0.003	0.0	0.001	C.004	C.003	0.004	0.004	NI
XMG	0.847	0.855	0.848	0.869	0.870	0.866	0.866	0.866	C.869	0.869	0.892	XMG
KD	5.552	5.917	5.579	6.640	6.680	6.472	6.459	6.438	6.622	6.607	8.259	KD

XMG=MG/MG+FE KD=XMG/XFE

MICROPROBE ANALYSES OF OLIVINE

S.NO	107.11	107.12	107.31	107.41	107.43	110.11	110.12	110.41	110.42	112.11	112.11	
SIO2	40.37	40.79	40.65	40.25	40.70	40.16	39.91	40.01	40.10	39.61	41.66	SIO2
TIO2	0.0	0.0	0.0	0.0	0.0	0.0	0.0	0.0	0.0	0.0	0.0	TIO2
AL2O3	0.0	0.0	0.0	0.0	0.0	0.0	0.0	0.0	0.0	0.0	0.0	AL2O3
CR2O3	0.0	0.0	0.0	0.0	0.0	0.0	0.06	0.0	0.05	0.0	0.0	CR2O3
FEO	10.89	10.89	10.97	10.94	10.97	9.97	10.31	10.28	10.20	10.19	10.41	FEO
MGO	47.92	47.53	48.30	47.23	47.71	49.04	49.20	49.37	49.28	48.69	47.21	MGO
CAO	0.02	0.02	0.01	0.01	0.01	0.0	0.0	0.0	0.0	0.0	0.02	CAO
MNO	0.21	0.23	0.22	0.21	0.22	0.23	0.34	0.21	0.24	0.15	0.19	MNO
NIO	0.28	0.33	0.25	0.29	0.27	0.22	0.39	0.37	0.39	0.21	0.17	NIO
TOTAL	99.69	99.79	100.40	98.93	99.88	99.62	100.21	100.24	100.26	98.85	99.66	TOTAL

CATION PROPORTIONS ON THE BASIS OF 4 OXYGENS

SI	0.999	1.007	0.998	1.003	1.004	0.991	0.983	0.984	0.986	0.987	1.024	SI
TI	0.0	0.0	0.0	0.0	0.0	0.0	0.0	0.0	0.0	0.0	0.0	TI
AL	0.0	0.0	0.0	0.0	0.0	0.0	0.0	0.0	0.0	0.0	0.0	AI
CR	0.0	0.0	0.0	0.0	0.0	0.0	0.001	0.0	0.001	0.0	0.0	CR
FE	0.225	0.225	0.225	0.228	0.226	0.206	0.212	0.211	0.210	0.212	0.214	FE
MG	1.767	1.749	1.768	1.755	1.755	1.803	1.806	1.809	1.805	1.807	1.730	MG
CA	0.001	0.001	0.000	0.000	0.000	0.0	0.0	0.0	0.0	0.0	0.001	CA
MN	0.004	0.005	0.005	0.004	0.005	0.005	0.007	0.004	0.005	0.003	0.004	MN
NI	0.006	0.007	0.005	0.006	0.005	0.004	0.008	0.007	0.008	0.004	0.003	NI
XMG	0.887	0.886	0.887	0.885	0.886	0.898	0.895	0.895	0.896	0.895	0.890	XMG
KD	7.841	7.778	7.846	7.693	7.750	8.765	8.504	8.558	8.609	8.515	8.081	KD

XMG=MG/MG+FE KD=XMG/XFE

MICROPROBE ANALYSES OF OLIVINE

S.NO	112.12	112.13	112.20	114.10	114.20	130.11	130.12	130.20	135.11	135.12	135.20	
SIO2	39.87	40.07	40.15	39.99	40.02	39.97	39.81	39.62	39.58	39.82	39.73	SIO2
TIO2	0.0	0.0	0.0	0.0	0.0	0.0	0.0	0.0	0.0	0.0	0.0	TIO2
AL2O3	0.0	0.0	0.0	0.0	0.0	0.0	0.0	0.0	0.0	0.0	0.0	AL2O3
CR2O3	0.0	0.05	0.0	0.04	0.05	0.08	0.07	0.05	0.08	0.0	0.0	CR2O3
FEO	10.04	10.05	9.83	10.03	10.56	10.39	10.27	10.61	10.68	10.31	10.32	FEO
MGO	48.78	49.02	48.62	48.70	48.70	48.79	48.80	48.65	48.76	48.55	48.35	MGO
CAO	0.0	0.0	0.0	0.0	0.0	0.0	0.0	0.0	0.0	0.0	0.0	CAO
MNO	0.17	0.23	0.18	0.25	0.22	0.34	0.26	0.21	0.25	0.16	0.25	MNO
NIO	0.11	0.30	0.22	0.19	0.26	0.23	0.29	0.25	0.39	0.25	0.33	NIO
TOTAL	98.97	99.72	99.00	99.20	99.81	99.80	99.50	99.39	99.74	99.09	98.98	TOTAL

CATION PROPORTIONS ON THE BASIS OF 4 OXYGENS

SI	0.990	0.989	0.996	0.991	0.989	0.987	0.986	0.984	0.981	0.990	0.989	SI
TI	0.0	0.0	0.0	0.0	0.0	0.0	0.0	0.0	0.0	0.0	0.0	TI
AL	0.0	0.0	0.0	0.0	0.0	0.0	0.0	0.0	0.0	0.0	0.0	AL
CR	0.0	0.001	0.0	0.001	0.001	0.002	0.001	0.001	0.002	0.0	0.0	CR
FE	0.209	0.207	0.204	0.208	0.218	0.215	0.213	0.220	0.221	0.214	0.215	FE
MG	1.805	1.803	1.797	1.799	1.793	1.796	1.802	1.801	1.801	1.798	1.794	MG
CA	0.0	0.0	0.0	0.0	0.0	0.0	0.0	0.0	0.0	0.0	0.0	CA
MN	0.004	0.005	0.004	0.005	0.005	0.007	0.005	0.004	0.005	0.003	0.005	MN
NI	0.002	0.006	0.004	0.004	0.005	0.005	0.006	0.005	0.008	0.005	0.007	NI
XMG	0.896	0.897	0.898	0.896	0.892	0.893	0.894	0.891	0.891	0.894	0.893	XMG
KD	8.658	8.692	8.814	8.652	8.218	8.368	8.468	8.171	8.136	8.391	8.349	KD

XMG=MG/MG+FE KD=XMG/XFE

MICROPROBE ANALYSES OF OLIVINE

S.NO	135.22	139.10	139.20	139.30	141.11	141.12	141.20	144.11	144.12	144.21	145.10	
SIO2	39.76	39.15	39.63	39.47	39.70	39.50	39.45	40.01	39.75	40.60	39.69	SIO2
TIO2	0.0	0.0	0.0	0.0	0.0	0.0	0.0	0.0	0.0	0.0	0.0	TIO2
AL2O3	0.0	0.0	0.0	0.0	0.0	0.0	0.0	0.02	0.37	0.0	0.0	AL2O3
CR2O3	0.06	0.0	0.0	0.0	0.0	0.0	0.0	0.07	0.21	0.06	0.0	CR2O3
FEO	10.21	10.85	10.69	10.72	10.72	10.63	10.62	10.60	10.94	10.89	10.64	FEO
MGO	48.55	48.18	48.23	48.42	48.51	48.48	48.23	48.04	47.83	47.65	48.75	MGO
CAO	0.0	0.0	0.0	0.0	0.0	0.0	0.0	0.01	0.0	0.0	0.0	CAO
MNO	0.13	0.24	0.14	0.13	0.17	0.23	0.25	0.17	0.19	0.17	0.22	MNO
NIO	0.26	0.14	0.20	0.19	0.29	0.27	0.26	0.24	0.23	0.25	0.28	NIO
TOTAL	98.97	98.56	98.89	98.93	99.39	99.11	98.81	99.16	99.52	99.62	99.58	TOTAL

CATION PROPORTIONS ON THE BASIS OF 4 OXYGENS

SI	0.989	0.982	0.989	0.985	0.986	0.984	0.986	0.994	0.986	1.004	0.984	SI
TI	0.0	0.0	0.0	0.0	0.0	0.0	0.0	0.0	0.0	0.0	0.0	TI
AL	0.0	0.0	0.0	0.0	0.0	0.0	0.0	0.001	0.011	0.0	0.0	AI
CR	0.001	0.0	0.0	0.0	0.0	0.0	0.0	0.001	0.004	0.001	0.0	CR
FE	0.212	0.228	0.223	0.224	0.223	0.221	0.222	0.220	0.227	0.225	0.221	FE
MG	1.800	1.801	1.793	1.800	1.796	1.800	1.796	1.779	1.769	1.756	1.801	MG
CA	0.0	0.0	0.0	0.0	0.0	0.0	0.0	0.000	0.0	0.0	0.0	CA
MN	0.003	0.005	0.003	0.003	0.004	0.005	0.005	0.004	0.004	0.004	0.005	MN
NI	0.005	0.003	0.004	0.004	0.006	0.005	0.005	0.005	0.005	0.005	0.006	NI
XMG	0.894	0.888	0.889	0.889	0.890	0.890	0.890	0.890	0.886	0.886	0.891	XMG
KD	8.474	7.913	8.040	8.049	8.064	8.127	8.093	8.076	7.791	7.797	8.165	KD

XMG=MG/MG+FE KD=XMG/XFE

MICROPROBE ANALYSES OF OLIVINE

S.NO	145.11	145.12	145.20	145.21	145.31	145.32	145.41	147.10	147.11	147.20	147.21	
SIO2	41.41	40.87	39.51	41.20	40.03	39.77	40.84	39.32	41.52	39.88	41.69	SIO2
TIO2	0.0	0.0	0.C	0.0	0.0	0.0	0.0	0.0	0.0	0.0	C.0	TIC2
AL2O3	0.0	0.0	0.C	0.0	0.0	0.0	0.0	0.C	0.0	0.0	0.0	AL2O3
CR2O3	0.0	0.0	0.10	0.0	0.0	0.06	0.0	0.05	0.0	0.11	C.0	CR2O3
FEO	10.80	10.71	10.44	10.86	10.38	9.78	10.51	10.02	10.53	9.92	10.64	FEC
MGO	47.94	48.67	48.51	48.31	48.89	49.16	47.94	48.41	47.67	48.85	47.08	MGC
CAO	0.0	0.0	0.0	0.0	0.0	C.0	0.0	0.0	0.0	0.0	C.0	CAC
MNO	0.25	0.22	0.14	0.20	0.26	0.21	0.18	0.29	0.24	0.23	0.23	MNC
NIO	0.22	0.22	0.29	0.25	0.35	0.19	0.22	0.24	0.08	0.30	0.08	NIC
TOTAL	100.62	100.69	98.99	100.82	99.91	99.17	99.69	98.33	100.09	99.29	99.72	TOTAL

CATIOS PROPORTIONS ON THE BASIS OF 4 OXYGENS

SI	1.012	0.999	0.985	1.006	0.988	0.986	1.007	0.985	1.018	0.988	1.025	SI
TI	0.0	C.0	0.0	0.0	0.0	0.0	0.0	0.0	0.0	0.0	0.0	TI
AL	0.0	C.0	0.0	C.0	0.0	0.0	0.0	0.0	0.0	0.0	C.C	AI
CR	0.0	C.0	0.002	0.0	0.0	0.001	0.0	0.001	0.0	0.002	C.0	CR
FE	0.221	C.219	0.218	C.222	0.214	0.203	0.217	0.210	0.216	0.206	0.219	FE
MG	1.746	1.774	1.802	1.758	1.798	1.816	1.761	1.807	1.742	1.804	1.725	MG
CA	0.0	C.0	0.0	0.0	0.0	0.0	0.0	0.0	0.0	0.0	C.0	CA
MN	0.005	C.005	0.003	C.C04	0.005	0.004	C.004	C.006	C.C05	0.005	0.005	MN
NI	0.004	0.004	0.006	C.005	0.007	0.004	0.004	C.005	0.002	0.006	C.CC2	NI
XMG	0.888	0.890	0.892	0.888	0.894	0.900	0.890	0.896	C.890	0.898	0.887	XMG
KD	7.910	8.098	8.280	7.927	8.393	8.957	8.128	8.609	8.067	8.775	7.885	KD

XMG=MG/MG+FE KD=XMG/XFE

MICROPROBE ANALYSES OF OLIVINE

S.NO	147.22	150.10	150.12	210.11	210.20	227.10	227.20	227.30	233.10	233.20	254.10	
SIO2	41.95	39.81	39.52	39.29	39.40	39.53	39.62	39.69	39.15	39.23	39.00	SIO2
TIO2	0.0	0.0	0.0	0.0	0.0	0.0	0.0	0.0	0.0	0.0	0.0	TIO2
AL2O3	0.0	0.0	0.0	0.0	0.0	0.0	0.0	0.0	0.0	0.0	0.0	AL2O3
CR2O3	0.0	0.0	0.0	0.05	0.0	0.11	0.0	0.0	0.05	0.0	0.0	CR2O3
FEO	9.82	11.31	11.37	13.37	13.52	13.16	13.14	13.55	14.58	14.13	15.27	FEO
MGO	48.47	47.85	47.87	46.44	46.46	46.54	46.70	47.01	45.56	45.87	44.87	MGO
CAO	0.0	0.0	0.0	0.0	0.0	0.0	0.0	0.0	0.0	0.0	0.0	CAO
MNO	0.23	0.20	0.25	0.19	0.31	0.21	0.21	0.27	0.25	0.34	0.23	MNO
NIO	0.03	0.11	0.16	0.05	0.07	0.0	0.0	0.0	0.09	0.07	0.0	NIO
TOTAL	100.50	99.28	99.17	99.39	99.76	99.55	99.67	100.52	99.68	99.64	99.37	TOTAL

CATION PROPORTIONS ON THE BASIS OF 4 OXYGENS

SI	1.020	0.991	0.987	0.987	0.987	0.990	0.990	0.986	0.987	0.987	0.988	SI
TI	0.0	0.0	0.0	0.0	0.0	0.0	0.0	0.0	0.0	0.0	0.0	TI
AL	0.0	0.0	0.0	0.0	0.0	0.0	0.0	0.0	0.0	0.0	0.0	AL
CR	0.0	0.0	0.0	0.001	0.0	0.002	0.0	0.0	0.001	0.0	0.0	CR
FE	0.200	0.236	0.237	0.281	0.283	0.276	0.275	0.282	0.307	0.297	0.324	FE
MG	1.756	1.776	1.781	1.739	1.735	1.737	1.740	1.741	1.711	1.720	1.695	MG
CA	0.0	0.0	0.0	0.0	0.0	0.0	0.0	0.0	0.0	0.0	0.0	CA
MN	0.005	0.004	0.005	0.004	0.007	0.004	0.004	0.006	0.005	0.007	0.005	MN
NI	0.001	0.002	0.003	0.001	0.001	0.0	0.0	0.0	0.002	0.001	0.0	NI
XMG	0.898	0.883	0.882	0.861	0.860	0.863	0.864	0.861	0.848	0.853	0.840	XMG
KD	8.796	7.539	7.503	6.190	6.124	6.302	6.333	6.182	5.568	5.785	5.236	KD

XMG=MG/MG+FE KD=XMG/XFE

MICROPROBE ANALYSES OF OLIVINE

S.NO	254.20	402.10	402.20	501.10	912.11	924.10	924.21	924.22	924.30	927.10	927.12	
SIO2	39.02	38.85	38.72	39.41	38.11	38.07	38.14	38.11	37.78	38.33	38.54	SIO2
TIO2	0.0	0.0	0.0	0.0	0.0	0.0	0.0	0.0	0.0	0.0	0.0	TIO2
AL2O3	0.0	0.0	0.0	0.0	0.0	0.0	0.0	0.0	0.0	0.0	0.0	AL2O3
CR2O3	0.06	0.0	0.06	0.0	0.0	0.0	0.0	0.06	0.0	0.0	0.89	CR2O3
FEO	15.45	13.98	13.95	12.04	21.06	20.76	21.14	21.04	20.57	19.17	18.03	FEO
MGO	44.88	45.64	45.65	47.02	39.98	39.95	39.38	39.60	39.48	41.20	41.70	MGO
CAO	0.0	0.0	0.0	0.0	0.0	0.0	0.0	0.0	0.0	0.0	0.0	CAO
MNO	0.33	0.25	0.27	0.35	0.32	0.37	0.30	0.36	0.43	0.32	0.35	MNO
NIO	0.0	0.09	0.17	0.07	0.24	0.41	0.27	0.33	0.20	0.24	0.18	NIO
TOTAL	99.74	98.81	98.82	98.89	99.71	99.56	99.23	99.50	98.46	99.26	99.69	TOTAL

CATION PROPORTIONS ON THE BASIS OF 4 OXYGENS

SI	0.987	0.985	0.983	0.989	0.991	0.991	0.996	0.993	0.993	0.992	0.989	SI
TI	0.0	0.0	0.0	0.0	0.0	0.0	0.0	0.0	0.0	0.0	0.0	TI
AL	0.0	0.0	0.0	0.0	0.0	0.0	0.0	0.0	0.0	0.0	0.0	AL
CR	0.001	0.0	0.001	0.0	0.0	0.0	0.0	0.001	0.0	0.0	0.018	CR
FE	0.327	0.297	0.296	0.253	0.458	0.452	0.462	0.459	0.452	0.415	0.387	FE
MG	1.691	1.725	1.727	1.759	1.549	1.550	1.533	1.538	1.547	1.589	1.596	MG
CA	0.0	0.0	0.0	0.0	0.0	0.0	0.0	0.0	0.0	0.0	0.0	CA
MN	0.007	0.005	0.006	0.007	0.007	0.008	0.007	0.008	0.010	0.007	0.008	MN
NI	0.0	0.002	0.003	0.001	0.005	0.009	0.006	0.007	0.004	0.005	0.004	NI
XMG	0.838	0.853	0.854	0.874	0.772	0.774	0.768	0.770	0.774	0.793	0.805	XMG
KD	5.176	5.818	5.831	6.959	3.383	3.429	3.320	3.354	3.420	3.830	4.121	KD

XMG=MG/MG+FE KD=XMG/XFE

MICROPROBE ANALYSES OF OLIVINE

S.NO	927.2C	934.10	934.20	934.22	934.30	937.11	937.12	
SIO2	38.42	37.94	38.43	37.93	38.03	38.80	38.75	SIC2
TIO2	0.0	0.0	0.0	0.0	0.0	0.0	0.0	TIC2
AL2O3	0.0	0.0	0.0	0.0	0.0	0.0	0.0	AL2O3
CR2O3	0.05	0.0	0.09	0.10	0.0	0.0	0.0	CR2O3
FEO	18.90	19.41	19.28	19.27	19.17	18.02	18.78	FEC
MGO	41.66	40.30	41.13	40.73	41.03	42.82	41.62	MGC
CAO	0.0	0.0	0.C	0.0	0.0	0.0	0.C	CAC
MNO	0.29	0.35	0.42	0.34	0.31	0.32	0.20	MNC
NIO	0.12	0.24	0.38	0.11	0.32	0.14	0.16	NIO
TOTAL	99.44	98.24	99.73	98.48	98.86	100.10	99.51	TOTAL

CATION PROPORTIONS ON THE BASIS OF 4 OXYGENS

SI	0.991	C.994	0.991	0.991	0.989	0.989	0.997	SI
TI	0.0	0.0	0.0	C.C	0.0	0.0	0.0	TI
AL	0.0	0.0	0.0	0.0	0.0	0.0	0.0	AI
CR	0.001	C.0	0.002	0.002	0.0	0.0	0.0	CR
FE	0.408	C.425	0.416	0.421	0.417	0.384	0.4C4	FE
MG	1.601	1.574	1.581	1.585	1.591	1.627	1.595	MG
CA	0.0	C.0	0.0	C.C	0.0	0.0	C.0	CA
MN	0.006	C.C08	0.009	C.C08	0.007	0.007	0.004	MN
NI	0.002	C.C05	0.008	0.C02	0.007	0.003	0.003	NI
XMG	0.797	0.787	0.792	0.790	0.792	0.809	0.798	XMG
KD	3.928	3.7C0	3.802	3.767	3.814	4.234	3.949	KD

XMG=MG/MG+FE KD=XMG/XFE

MICROPROBE ANALYSES OF PYROXENE

S.NO	60.10	63.10	64.10	64.20	67.12	67.20	72.10	72.20	73.10	73.20	85.10	
SIO2	57.23	56.10	57.63	57.87	57.41	57.45	57.17	56.68	56.39	56.72	56.76	SIC2
TIO2	0.0	C.0	0.0	C.0	0.0	0.0	0.09	0.0	0.0	0.0	C.0	TIC2
AL203	0.36	1.05	0.91	0.32	0.76	0.25	0.97	1.43	1.77	1.26	1.12	AL203
CR203	0.10	0.07	0.05	0.0	0.0	0.0	0.14	0.0	0.08	0.17	0.12	CR203
FEO	8.72	6.84	7.01	6.73	6.18	6.43	9.38	9.33	9.65	9.56	9.97	FEC
MGO	33.45	34.17	34.49	35.13	34.99	34.90	33.02	32.86	32.49	32.75	32.15	MGO
CAO	0.13	0.14	0.08	0.09	0.21	0.13	0.09	0.16	0.10	0.21	0.10	CAC
MNO	0.21	0.21	0.15	0.26	0.24	0.12	0.33	0.20	0.26	0.37	C.30	MNC
NIO	0.0	0.04	0.04	C.07	0.15	0.0	0.0	0.0	C.0	0.0	0.0	NIC
K2O	0.0	0.0	0.0	0.0	0.0	0.0	0.0	0.0	0.0	0.0	C.0	K2C
NA2O	0.0	0.0	0.0	0.0	0.0	0.0	C.0	0.0	0.0	0.07	C.0	NA2O
TOTAL	100.20	98.62	100.36	100.47	99.94	99.28	101.19	100.66	100.74	101.11	100.52	TOTAL

CATION PROPORTIONS ON THE BASIS OF 24 OXYGENS

SI	7.954	7.867	7.929	7.952	7.917	7.971	7.895	7.863	7.831	7.856	7.908	SI
AL4	0.046	C.133	0.071	0.048	0.083	0.029	0.105	0.137	C.169	0.144	0.092	AL4
	8.000	8.000	8.000	8.000	8.000	8.000	8.000	8.000	8.000	8.000	8.000	
AL6	0.013	C.041	0.077	0.004	0.041	0.012	0.053	C.097	0.121	0.062	0.092	AI6
TI	0.0	C.C	0.0	C.C	0.0	0.0	0.009	C.0	0.C	0.0	C.0	TI
CR	0.011	C.008	0.005	0.0	0.0	0.0	0.015	0.0	0.009	0.019	C.013	CR
FE	1.014	C.802	0.807	0.773	0.713	0.746	1.083	1.062	1.121	1.107	1.162	FE
MG	6.929	7.141	7.072	7.194	7.191	7.217	6.796	6.794	6.724	6.760	6.676	MG
CA	0.019	C.021	0.012	C.013	0.031	0.019	0.013	C.024	0.015	0.031	0.015	CA
MN	0.025	0.025	0.017	C.C30	0.028	0.014	0.039	0.024	0.031	0.043	C.035	MN
NI	0.C	C.C05	0.004	C.C08	C.017	C.0	0.0	C.0	C.0	0.0	C.0	NI
K	0.C	C.C	0.0	C.0	0.0	0.C	C.0	0.0	0.0	0.0	C.C	K
NA	0.C	C.0	0.0	C.0	0.0	0.0	0.0	0.0	C.0	0.019	C.0	NA
	8.011	8.042	7.994	8.022	8.021	8.008	8.009	8.020	8.020	8.041	7.993	
XMG	0.872	0.899	0.898	0.903	0.910	0.906	0.863	0.863	C.857	0.859	0.852	XMG
KD	6.836	8.902	8.768	9.302	10.089	9.672	6.273	6.276	6.000	6.105	5.746	KD

XMG=MG/MG+FE KD=XMG/XFE

MICROPROBE ANALYSES OF PYROXENE

S.NO	85.12	85.13	90.10	90.12	105.10	110.10	110.31	110.32	139.10	139.30	145.10	
SIO2	57.07	57.04	56.20	55.59	57.79	58.90	57.05	58.53	57.50	57.31	57.89	SIO2
TIO2	0.0	0.0	0.0	0.09	0.0	0.0	0.0	0.0	0.0	0.09	0.0	TIO2
AL2O3	0.71	0.57	1.07	1.23	1.22	0.43	0.0	0.25	1.15	0.98	0.89	AL2O3
CR2O3	0.12	0.14	0.0	0.05	0.11	0.22	0.0	0.07	0.09	0.12	0.13	CR2O3
FEO	9.94	9.66	9.56	9.97	8.68	6.82	6.48	6.71	7.37	7.28	7.14	FEO
MGO	32.50	32.33	32.25	31.99	33.24	34.64	35.19	34.91	33.45	33.60	33.92	MGO
CAO	0.11	0.08	0.17	0.08	0.15	0.18	0.10	0.11	0.04	0.11	0.15	CAO
MNO	0.40	0.27	0.38	0.29	0.31	0.23	0.22	0.12	0.26	0.16	0.29	MNO
NIO	0.0	0.0	0.0	0.0	0.06	0.13	0.04	0.0	0.0	0.0	0.0	NIO
K2O	0.0	0.0	0.0	0.0	0.0	0.0	0.0	0.0	0.0	0.0	0.0	K2O
NA2O	0.0	0.0	0.0	0.0	0.11	0.0	0.0	0.0	0.10	0.0	0.13	NA2O
TOTAL	100.85	100.09	99.63	99.29	101.67	101.55	99.08	100.70	99.96	99.65	100.54	TOTAL

CATION PROPORTIONS ON THE BASIS OF 24 OXYGENS

SI	7.929	7.967	7.894	7.853	7.914	8.003	7.947	8.007	7.953	7.948	7.959	SI
AL4	0.071	0.033	0.106	0.147	0.086	0.0	0.053	0.0	0.047	0.052	0.041	AL4
	8.000	8.000	8.000	8.000	8.000	8.003	8.000	8.007	8.000	8.000	8.000	
AL6	0.045	0.061	0.072	0.058	0.111	0.069	-0.053	0.040	0.141	0.109	0.103	AL6
TI	0.0	0.0	0.0	0.010	0.0	0.0	0.0	0.0	0.0	0.009	0.0	TI
CR	0.013	0.015	0.0	0.006	0.012	0.024	0.0	0.008	0.010	0.013	0.014	CR
FE	1.155	1.128	1.123	1.178	0.994	0.775	0.755	0.768	0.853	0.844	0.821	FE
MG	6.729	6.730	6.751	6.735	6.784	7.014	7.306	7.117	6.895	6.945	6.950	MG
CA	0.016	0.012	0.026	0.012	0.022	0.026	0.015	0.016	0.006	0.016	0.022	CA
MN	0.047	0.032	0.045	0.035	0.036	0.026	0.026	0.014	0.030	0.019	0.034	MN
NI	0.0	0.0	0.0	0.0	0.007	0.014	0.004	0.0	0.0	0.0	0.0	NI
K	0.0	0.0	0.0	0.0	0.0	0.0	0.0	0.0	0.0	0.0	0.0	K
NA	0.0	0.0	0.0	0.0	0.029	0.0	0.0	0.0	0.027	0.0	0.035	NA
	8.006	7.978	8.017	8.032	7.996	7.949	8.053	7.963	7.962	7.956	7.979	
XMG	0.854	0.856	0.857	0.851	0.872	0.901	0.906	0.903	0.890	0.892	0.894	XMG
KD	5.826	5.964	6.011	5.718	6.824	9.051	9.677	9.271	8.088	8.225	8.466	KD

XMG=MG/MG+FE KD=XMG/XFE

MICROPROBE ANALYSES OF PYROXENE

S.NO	145.30	163.10	210.10	210.20	227.19	227.29	227.39	233.19.	254.10	402.20	501.20	
SIO2	58.20	56.58	56.32	56.27	56.45	54.91	56.10	56.35	55.87	55.42	56.21	SIO2
TIO2	0.11	0.0	0.12	0.06	0.0	0.11	0.0	0.10	0.10	0.09	0.0	TIO2
AL2O3	0.46	0.62	1.06	1.05	0.51	1.35	0.98	0.92	0.89	1.46	0.96	AL2O3
CR2O3	0.09	0.12	0.14	0.22	0.22	1.40	0.13	0.11	0.13	0.13	0.10	CR2O3
FEO	7.08	8.73	8.69	8.61	8.55	9.15	8.64	9.19	9.77	9.05	7.28	FEO
MGO	34.42	33.20	33.11	33.07	33.00	32.47	33.11	32.90	32.13	32.32	33.66	MGO
CAO	0.11	0.20	0.21	0.16	0.21	0.15	0.07	0.11	0.11	0.19	0.15	CAO
MNO	0.31	0.29	0.39	0.30	0.26	0.30	0.33	0.30	0.26	0.31	0.44	MNO
NIO	0.0	0.0	0.0	0.0	0.0	0.0	0.0	0.0	0.0	0.0	0.0	NIO
K2O	0.0	0.0	0.0	0.0	0.0	0.0	0.0	0.0	0.0	0.0	0.0	K2O
NA2O	0.09	0.07	0.09	0.0	0.0	0.05	0.0	0.0	0.09	0.12	0.0	NA2O
TOTAL	100.87	99.81	100.13	99.74	99.20	99.89	99.36	99.98	99.37	99.09	98.80	TOTAL

CATION PROPORTIONS ON THE BASIS OF 24 OXYGENS

SI	7.974	7.908	7.853	7.867	7.930	7.727	7.873	7.877	7.882	7.823	7.888	SI
AL4	0.026	0.092	0.147	0.133	0.070	0.273	0.127	0.123	0.118	0.177	0.112	AI4
	8.000	8.000	8.000	8.000	8.000	8.000	8.000	8.000	8.000	8.000	8.000	
AL6	0.048	0.011	0.028	0.040	0.015	-0.049	0.035	0.028	0.030	0.066	0.047	AI6
TI	0.011	0.0	0.013	0.006	0.0	0.012	0.0	0.011	0.011	0.010	0.0	TI
CR	0.010	0.013	0.015	0.024	0.024	0.156	0.014	0.012	0.014	0.015	0.011	CR
FE	0.811	1.021	1.013	1.007	1.005	1.077	1.014	1.074	1.153	1.068	0.854	FE
MG	7.028	6.916	6.881	6.891	6.909	6.810	6.925	6.854	6.756	6.799	7.040	MG
CA	0.016	0.030	0.031	0.024	0.032	0.023	0.011	0.016	0.017	0.029	0.023	CA
MN	0.036	0.034	0.046	0.036	0.031	0.036	0.039	0.036	0.033	0.037	0.052	MN
NI	0.0	0.0	0.0	0.0	0.0	0.0	0.0	0.0	0.0	0.0	0.0	NI
K	0.0	0.0	0.0	0.0	0.0	0.0	0.0	0.0	0.0	0.0	0.0	K
NA	0.024	0.019	0.024	0.0	0.0	0.014	0.0	0.0	0.025	0.033	0.0	NA
	7.985	8.043	8.051	8.028	8.015	8.078	8.039	8.031	8.038	8.056	8.027	
XMG	0.897	0.871	0.872	0.873	0.873	0.863	0.872	0.864	0.854	0.864	0.892	XMG
KD	8.663	6.777	6.790	6.844	6.878	6.324	6.829	6.380	5.860	6.364	8.239	KD

XMG=MG/MG+FE KD=XMG/XFE

MICROPROBE ANALYSES OF PYROXENE

S.NO	901.30	901.11	901.12	912.10	912.11	924.10	924.12	924.20	924.30	927.10	934.10	
SIO2	56.39	51.66	51.59	52.39	52.78	53.39	51.92	53.68	53.26	53.64	53.69	SIO2
TIO2	0.0	0.30	0.28	0.21	0.24	0.21	0.25	0.27	0.16	0.21	0.14	TIO2
AL2O3	1.00	2.93	2.77	3.75	4.66	3.33	2.56	3.77	4.39	4.46	3.53	AL2O3
CR2O3	0.10	0.68	0.84	1.23	0.39	0.33	0.86	0.75	0.68	0.68	0.68	CR2O3
FEO	7.44	5.72	5.78	11.16	12.05	12.30	4.95	10.10	10.69	10.54	10.43	FEO
MGO	33.30	17.03	16.08	28.20	27.82	27.81	16.58	28.82	28.12	28.20	28.73	MGO
CAO	0.09	19.58	20.50	1.53	1.37	1.07	21.01	1.84	2.28	1.90	0.89	CAO
MNO	0.32	0.08	0.14	0.21	0.20	0.22	0.17	0.21	0.24	0.26	0.16	MNO
NIO	0.0	0.0	0.0	0.17	0.06	0.0	0.0	0.11	0.0	0.13	0.0	NIO
K2O	0.0	0.0	0.0	0.0	0.0	0.0	0.0	0.0	0.0	0.0	0.0	K2O
NA2O	0.0	0.16	0.09	0.0	0.09	0.0	0.08	0.10	0.07	0.07	0.0	NA2O
TOTAL	98.64	98.14	98.07	98.85	99.66	98.66	98.38	99.65	99.89	100.09	98.25	TOTAL

CATION PROPORTIONS ON THE BASIS OF 24 OXYGENS

SI	7.920	7.695	7.716	7.552	7.543	7.699	7.723	7.621	7.568	7.592	7.704	SI
AL4	0.080	0.305	0.284	0.448	0.457	0.301	0.277	0.379	0.432	0.408	0.296	AL4
	8.000	8.000	8.000	8.000	8.000	8.000	8.000	8.000	8.000	8.000	8.000	
AL6	0.085	0.209	0.204	0.189	0.328	0.265	0.172	0.252	0.304	0.337	0.301	AL6
TI	0.0	0.034	0.031	0.023	0.026	0.023	0.028	0.029	0.017	0.022	0.015	TI
CR	0.011	0.080	0.099	0.140	0.044	0.038	0.101	0.084	0.076	0.076	0.077	CR
FE	0.874	0.713	0.723	1.345	1.440	1.483	0.616	1.199	1.270	1.248	1.252	FE
MG	6.970	3.780	3.584	6.058	5.925	5.976	3.676	6.098	5.955	5.949	6.143	MG
CA	0.014	3.125	3.285	0.236	0.210	0.165	3.349	0.280	0.347	0.288	0.137	CA
MN	0.038	0.010	0.016	0.026	0.024	0.027	0.021	0.025	0.029	0.031	0.019	MN
NI	0.0	0.0	0.0	0.020	0.007	0.0	0.0	0.013	0.0	0.015	0.0	NI
K	0.0	0.0	0.0	0.0	0.0	0.0	0.0	0.0	0.0	0.0	0.0	K
NA	0.0	0.046	0.026	0.0	0.025	0.0	0.023	0.028	0.019	0.019	0.0	NA
	7.992	7.997	7.972	8.037	8.029	7.977	7.986	8.007	8.018	7.985	7.944	
XMG	0.889	0.841	0.832	0.818	0.804	0.801	0.857	0.836	0.824	0.827	0.831	XMG
KD	7.976	5.305	4.958	4.503	4.114	4.029	5.969	5.085	4.688	4.768	4.909	KD

XMG=MG/MG+FE KD=XMG/XFE

MICROPROBE ANALYSES OF PYROXENE

SAMPLE NO	934.20	937.10	
SIO2	50.97	52.87	SIO2
TIO2	0.33	0.15	TIO2
AL2O3	4.01	2.09	AL2O3
CR2O3	1.26	0.83	CR2O3
FEO	5.38	5.12	FEO
MGO	16.65	17.50	MGO
CAO	19.34	20.34	CAO
MNO	0.17	0.18	MNO
NIO	0.15	0.05	NIO
K2O	0.0	0.0	K2O
NA2O	0.34	0.23	NA2O
TOTAL	98.56	99.36	TOTAL

CATION PROPORTIONS ON THE BASIS OF 24 OXYGENS

SI	7.569	7.774	SI
AL4	0.431	0.226	AL4
	8.000	8.000	
AL6	0.271	0.136	AL6
TI	0.037	0.017	TI
CR	0.148	0.096	CR
FE	0.668	0.630	FE
MG	3.685	3.835	MG
CA	3.077	3.205	CA
MN	0.021	0.022	MN
NI	0.018	0.006	NI
K	0.0	0.0	K
NA	0.086	0.066	NA
	8.012	8.013	
XMG	0.847	0.859	XMG
KD	5.515	6.091	KD

XMG=MG/MG+FE KD=XMG/XFE

MICROPROBE ANALYSES OF AMPHIBOLE

S.NO	72.10	107.10	139.10	141.20	145.40	147.30	147.30	924.20	927.10	927.20	
SIO2	50.76	51.54	55.53	53.83	52.61	52.36	52.32	41.95	43.45	43.27	SIO2
TIO2	0.77	0.73	0.0	0.45	0.47	0.45	0.47	2.08	0.46	0.70	TIO2
AL2O3	8.42	7.67	3.24	4.74	6.07	5.27	5.44	13.78	13.94	11.65	AL2O3
CR2O3	0.44	0.36	0.46	0.42	0.50	0.40	0.47	0.67	0.66	1.25	CR2O3
FEO	3.51	2.50	2.46	2.52	2.75	2.59	2.58	9.29	7.85	7.13	FEO
MGO	20.00	20.40	22.24	21.21	21.08	21.34	21.11	14.68	15.66	17.31	MGO
CAO	12.59	12.72	12.68	12.81	12.54	12.35	12.32	10.95	11.11	11.08	CAO
MNO	0.10	0.14	0.12	0.05	0.11	0.05	0.08	0.12	0.16	0.12	MNO
NIO	0.04	0.06	0.15	0.0	0.0	0.0	0.08	0.0	0.0	0.04	NIO
K2O	0.22	0.19	0.05	0.0	0.07	0.0	0.11	0.13	0.18	0.17	K2O
NA2O	0.85	0.79	0.35	0.31	0.62	0.68	0.64	2.74	2.56	2.91	NA2O
TOTAL	97.70	97.10	97.28	96.34	96.82	95.49	95.62	96.39	96.03	95.63	TOTAL

CATION PROPORTIONS ON THE BASIS OF 23 OXYGENS

SI	7.058	7.169	7.661	7.503	7.327	7.384	7.375	6.169	6.342	6.364	SI
AL4	0.942	0.831	0.339	0.497	0.673	0.616	0.625	1.831	1.658	1.636	AL4
	8.000	8.000	8.000	8.000	8.000	8.000	8.000	8.000	8.000	8.000	
AL6	0.439	0.427	0.188	0.282	0.324	0.260	0.279	0.557	0.741	0.384	AL6
TI	0.081	0.076	0.0	0.047	0.049	0.048	0.050	0.230	0.050	0.077	TI
CR	0.048	0.040	0.050	0.046	0.055	0.045	0.052	0.078	0.076	0.145	CR
FE	0.408	0.291	0.284	0.294	0.320	0.305	0.304	1.142	0.958	0.877	FE
MG	4.145	4.229	4.573	4.406	4.375	4.485	4.435	3.217	3.407	3.794	MG
CA	1.876	1.896	1.874	1.913	1.871	1.866	1.861	1.725	1.738	1.746	CA
MN	0.012	0.016	0.014	0.006	0.013	0.006	0.010	0.015	0.020	0.015	MN
NI	0.004	0.007	0.017	0.0	0.0	0.0	0.009	0.0	0.0	0.005	NI
K	0.039	0.034	0.009	0.0	0.012	0.0	0.020	0.024	0.034	0.032	K
NA	0.229	0.213	0.094	0.084	0.167	0.186	0.175	0.781	0.725	0.830	NA
	7.281	7.229	7.102	7.079	7.188	7.201	7.194	7.771	7.749	7.906	
XMG	0.910	0.936	0.942	0.937	0.932	0.936	0.936	0.738	0.780	0.812	XMG
KD	10.154	14.541	16.110	14.998	13.660	14.683	14.581	2.816	3.555	4.326	KD

XMG=MG/MG+FE KD=XMG/XFE

MICROPROBE ANALYSES OF AMPHIBOLE

S.NO	927.21	934.10	934.20	
SIO2	46.71	42.06	43.30	SIO2
TIO2	0.57	1.36	0.38	TIO2
AL2O3	9.45	13.91	13.23	AL2O3
CR2O3	0.99	0.77	0.36	CR2O3
FEO	7.56	8.11	7.90	FEO
MGO	19.84	15.09	16.14	MGO
CAO	9.22	11.23	11.27	CAO
MNO	0.11	0.13	0.06	MNO
NIO	0.0	0.0	0.0	NIO
K2O	0.15	0.17	0.16	K2O
NA2O	2.16	2.77	2.35	NA2O
TOTAL	96.78	95.60	95.17	TOTAL

CATION PROPORTIONS ON THE BASIS OF 23 OXYGENS

SI	6.705	6.206	6.377	SI
AL4	1.295	1.794	1.623	AL4
	8.000	8.000	8.000	
AL6	0.304	0.625	0.674	AL6
TI	0.062	0.151	0.042	TI
CR	0.112	0.090	0.042	CR
FE	0.910	1.001	0.973	FE
MG	4.244	3.318	3.542	MG
CA	1.418	1.775	1.778	CA
MN	0.013	0.016	0.007	MN
NI	0.0	0.0	0.0	NI
K	0.027	0.032	0.034	K
NA	0.601	0.792	0.671	NA
	7.692	7.801	7.764	
XMG	0.823	0.768	0.785	XMG
KD	4.664	3.316	3.641	KD

XMG=MG/MG+FE KD=XMG/XFE

MICROPROBE ANALYSES OF SPINEL

S.NO	60.10	63.10	63.20	64.10	67.20	72.10	72.20	73.10	73.20	85.20	90.10	
SIO2	0.0	0.0	0.0	0.0	0.0	0.0	0.0	0.0	0.0	0.0	0.0	SIC2
TIO2	0.17	0.0	0.06	0.0	0.0	0.0	0.0	0.0	0.0	0.0	0.0	TIC2
AL2O3	41.78	57.42	59.11	58.87	59.20	49.81	58.17	59.99	60.56	51.22	58.54	AL2O3
CR2O3	25.30	9.25	8.24	9.26	9.34	16.51	8.69	7.75	6.86	15.36	7.49	CR2O3
V2O3	0.13	0.13	0.11	0.16	0.31	0.18	0.13	0.0	0.15	0.57	0.08	V2O3
FE2O3	0.34	0.91	0.36	0.25	0.17	0.83	0.71	0.23	0.45	0.11	0.83	FE2O3
FEO	19.54	10.96	10.59	11.29	10.18	16.59	14.40	15.59	14.71	20.30	14.81	FEC
MGO	12.92	19.23	19.71	19.47	20.22	14.98	17.41	17.09	17.63	12.80	17.04	MGO
CAO	0.0	0.0	0.0	0.0	2.12	0.0	0.0	0.0	0.0	0.0	0.0	CAO
MNO	0.30	0.0	0.11	0.17	0.20	0.25	0.13	0.10	0.12	0.23	0.16	MNC
NIO	0.0	0.15	0.19	0.18	0.55	0.0	0.0	0.0	0.0	0.0	0.0	NIC
TOTAL	99.48	98.07	98.48	99.65	102.30	99.15	99.64	100.75	100.48	100.59	98.96	TOTAL

CATION PROPORTIONS ON THE BASIS OF 32 OXYGENS

SI	0.0	0.0	0.0	0.0	0.0	0.0	0.0	0.0	0.0	0.0	0.0	SI
TI	0.029	0.0	0.009	0.0	0.0	0.0	0.0	0.0	0.0	0.0	0.0	TI
AL	11.283	14.284	14.536	14.392	14.147	12.940	14.415	14.684	14.778	13.249	14.591	AI
CR	4.582	1.543	1.359	1.518	1.497	2.676	1.444	1.272	1.123	2.664	1.252	CR
V	0.024	0.022	0.018	0.027	0.050	0.032	0.022	0.0	0.025	0.100	0.014	V
FE3	0.059	0.144	0.056	0.040	0.026	0.137	0.113	0.036	0.070	0.018	0.133	FE3
FE2	3.551	1.938	1.848	1.956	1.727	3.057	2.532	2.708	2.547	3.725	2.619	FE2
MG	4.411	6.047	6.127	6.017	6.108	4.919	5.454	5.268	5.439	4.185	5.369	MG
CA	0.0	0.0	0.0	0.0	0.460	0.0	0.0	0.0	0.0	0.0	0.0	CA
MN	0.058	0.0	0.019	0.030	0.034	0.047	0.023	0.018	0.021	0.043	0.029	MN
NI	0.0	0.025	0.032	0.030	0.090	0.0	0.0	0.0	0.0	0.0	0.0	NI
XMG	0.554	0.757	0.768	0.755	0.780	0.617	0.683	0.661	0.681	0.529	0.672	XMG
YCR	0.288	0.097	0.085	0.095	0.096	0.180	0.090	0.080	0.070	0.167	0.078	YCR

XMG=MG/MG+FE YCR=CR/CR+AL+FE3

MICROPROBE ANALYSES OF SPINEL

S.NO	90.20	100.30	100.40	105.20	107.20	107.21	110.11	110.12	110.21	110.22	114.10	
SIO2	0.0	0.55	0.0	0.0	0.0	0.0	0.0	0.0	0.0	0.0	0.0	SIC2
TIO2	0.0	0.0	0.0	0.0	0.24	0.15	0.0	0.0	0.13	0.0	0.0	TIO2
AL2O3	57.50	59.16	58.35	58.03	14.28	15.66	54.29	63.82	28.63	39.05	62.26	AL2O3
CR2O3	8.66	9.02	10.77	12.10	53.63	52.12	16.27	7.57	41.56	31.68	6.27	CR2O3
V2O3	0.15	0.0	0.23	0.0	1.26	0.0	0.12	0.0	0.21	0.22	0.0	V2C3
FE2O3	0.09	0.44	0.97	0.98	0.07	0.04	0.46	2.03	0.39	0.82	0.22	FE2O3
FEO	16.43	15.56	14.67	13.86	24.15	24.67	14.08	9.57	20.02	16.90	10.65	FEO
MGO	15.90	16.50	16.47	17.14	6.34	6.13	17.30	19.30	10.62	13.38	20.03	MGO
CAO	0.0	0.18	0.0	0.0	0.0	0.0	0.05	0.0	0.0	0.0	0.0	CAO
MNO	0.23	0.21	0.05	0.09	0.67	0.0	0.21	0.11	0.36	0.29	0.14	MNO
NIO	0.05	0.0	0.06	0.0	0.0	0.05	0.12	0.11	0.0	0.04	0.18	NIO
TOTAL	99.23	101.62	101.57	102.20	100.64	98.81	102.90	102.50	101.92	102.57	99.75	TOTAL

CATION PROPORTIONS ON THE BASIS OF 32 OXYGENS

SI	0.0	0.114	0.0	0.0	0.0	0.0	0.0	0.0	0.0	0.0	0.0	SI
TI	0.0	0.0	0.0	0.0	0.048	0.030	0.0	0.0	0.023	0.0	0.0	TI
AL	14.446	14.410	14.273	14.098	4.452	4.941	13.312	14.948	8.080	10.346	14.979	AI
CR	1.496	1.473	1.767	1.971	11.211	11.027	2.675	1.189	7.865	5.664	1.012	CR
V	0.026	0.0	0.036	0.0	0.267	0.0	0.020	0.0	0.040	0.040	0.0	V
FE3	0.014	0.068	0.151	0.151	0.014	0.007	0.072	0.303	0.070	0.138	0.034	FE3
FE2	2.928	2.689	2.595	2.389	5.340	5.521	2.449	1.589	4.008	3.176	1.817	FE2
MG	5.050	5.080	5.093	5.264	2.499	2.445	5.363	5.714	3.789	4.481	6.092	MG
CA	0.0	0.040	0.0	0.0	0.0	0.0	0.011	0.0	0.0	0.0	0.0	CA
MN	0.042	0.037	0.009	0.016	0.150	0.0	0.037	0.019	0.073	0.055	0.024	MN
NI	0.009	0.0	0.010	0.0	0.0	0.011	0.020	0.018	0.0	0.007	0.030	NI
XMG	0.633	0.654	0.667	0.688	0.319	0.307	0.686	0.782	0.486	0.585	0.770	XMG
YCR	0.094	0.092	0.109	0.122	0.715	0.690	0.167	0.072	0.491	0.351	0.063	YCR

XMG=MG/MG+FE YCR=CR/CR+AL+FE3

MICROPROBE ANALYSES OF SPINEL

S.NO	114.20	130.10	130.12	135.20	139.20	139.30	141.10	141.20	144.10	144.21	145.31	
SIO2	0.0	0.0	0.0	0.0	0.0	0.0	0.0	0.0	0.0	0.0	0.0	SIO2
TIO2	0.0	0.0	0.0	0.0	0.05	0.0	0.27	0.20	0.28	0.26	0.29	TIO2
AL2O3	51.92	26.21	32.20	49.30	58.38	60.60	14.97	23.58	14.15	18.96	14.96	AL2O3
CR2O3	16.57	41.44	35.22	19.54	9.90	7.47	52.70	44.49	53.96	48.05	52.21	CR2O3
V2O3	0.0	0.18	0.31	0.0	0.13	0.15	0.43	0.29	1.73	1.90	0.83	V2O3
FE2O3	0.28	0.24	0.33	0.20	0.16	0.31	0.39	0.09	0.38	0.81	0.56	FE2O3
FEO	13.35	21.58	19.18	18.20	11.63	11.21	23.45	22.46	23.62	23.46	22.69	FEO
MGO	17.51	9.31	11.40	16.46	19.23	19.74	6.84	8.40	6.75	7.28	7.17	MGO
CAO	0.0	0.0	0.0	0.0	0.0	0.0	0.0	0.0	0.0	0.0	0.0	CAO
MNO	0.23	0.27	0.57	0.07	0.16	0.23	0.46	0.43	0.48	0.49	0.62	MNO
NIO	0.16	0.0	0.0	0.0	0.17	0.21	0.0	0.0	0.0	0.0	0.0	NIO
TOTAL	100.02	99.23	99.21	99.77	99.80	99.92	99.51	99.93	101.35	101.21	99.33	TOTAL

CATION PROPORTIONS ON THE BASIS OF 32 OXYGENS

SI	0.0	0.0	0.0	0.0	0.0	0.0	0.0	0.0	0.0	0.0	0.0	SI
TI	0.0	0.0	0.0	0.0	0.008	0.0	0.054	0.038	0.055	0.050	0.058	TI
AL	13.114	7.717	9.136	12.649	14.298	14.682	4.686	7.011	4.370	5.723	4.679	AI
CR	2.807	8.182	6.701	3.362	1.626	1.214	11.062	8.870	11.174	9.726	10.950	CR
V	0.0	0.036	0.060	0.0	0.022	0.025	0.092	0.059	0.363	0.390	0.177	V
FE3	0.045	0.046	0.060	0.033	0.024	0.048	0.078	0.018	0.076	0.156	0.111	FE3
FE2	2.392	4.507	3.860	2.584	2.020	1.926	5.206	4.738	5.175	5.024	5.035	FE2
MG	5.591	3.465	4.089	5.338	5.953	6.046	2.707	3.157	2.635	2.778	2.835	MG
CA	0.0	0.0	0.0	0.0	0.0	0.0	0.0	0.0	0.0	0.0	0.0	CA
MN	0.042	0.057	0.116	0.013	0.028	0.040	0.103	0.092	0.107	0.106	0.139	MN
NI	0.028	0.0	0.0	0.0	0.028	0.035	0.0	0.0	0.0	0.0	0.0	NI
XMG	0.700	0.435	0.514	0.674	0.747	0.758	0.342	0.400	0.337	0.356	0.360	XMG
YCR	0.176	0.513	0.422	0.210	0.102	0.076	0.699	0.558	0.715	0.623	0.696	YCR

XMG=MG/MG+FE YCR=CR/CR+AL+FE3

MICROPROBE ANALYSES OF SPINEL

S.NO	145.32	145.41	145.42	145.43	147.11	147.12	147.13	147.21	145.31	145.32	145.41	
SIO2	0.0	0.0	0.0	0.0	0.0	0.0	0.0	0.0	0.0	0.0	0.0	SIO2
TIO2	0.26	0.20	0.21	0.08	0.23	0.0	0.09	0.31	0.20	0.26	0.32	TIO2
AL2O3	13.94	15.11	15.05	19.45	15.40	37.36	38.32	13.42	15.27	13.79	14.72	AL2O3
CR2O3	53.72	52.22	52.70	48.22	52.26	31.02	30.47	55.19	52.67	53.57	53.84	CR2O3
V2O3	1.36	1.08	1.01	1.05	1.21	1.06	0.90	1.76	0.0	0.0	0.0	V2O3
FE2O3	0.13	0.08	0.09	0.02	0.04	0.05	0.75	0.14	0.20	0.42	0.00	FE2O3
FEO	23.00	23.05	23.14	22.50	23.16	18.06	17.47	22.87	23.61	23.43	23.79	FEO
MGO	6.89	6.91	6.97	7.83	6.90	12.81	12.48	6.94	6.81	6.62	6.75	MGO
CAO	0.0	0.0	0.0	0.0	0.0	0.0	0.0	0.08	0.0	0.0	0.0	CAO
MNO	0.49	0.78	0.59	0.36	0.56	0.21	0.25	0.63	0.0	0.0	0.0	MNO
NIO	0.0	0.0	0.0	0.0	0.0	0.0	0.18	0.04	0.10	0.05	0.06	NIO
TOTAL	99.73	99.43	99.76	99.51	99.76	100.56	100.91	101.37	98.86	98.14	99.48	TOTAL

CATION PROPORTIONS ON THE BASIS OF 32 OXYGENS

SI	0.0	0.0	0.0	0.0	0.0	0.0	0.0	0.0	0.0	0.0	0.0	SI
TI	0.052	0.040	0.042	0.016	0.046	0.0	0.016	0.061	0.040	0.053	0.064	TI
AL	4.369	4.726	4.693	5.928	4.794	10.173	10.361	4.149	4.802	4.399	4.614	AL
CR	11.269	10.957	11.020	9.855	10.910	5.664	5.525	11.441	11.107	11.458	11.316	CR
V	0.277	0.230	0.214	0.218	0.256	0.196	0.165	0.370	0.0	0.0	0.0	V
FE3	0.027	0.015	0.016	0.004	0.009	0.008	0.130	0.027	0.040	0.085	0.000	FE3
FE2	5.113	5.117	5.118	4.865	5.115	3.488	3.350	5.014	5.267	5.302	5.289	FE2
MG	2.730	2.733	2.748	3.017	2.715	4.409	4.266	2.712	2.707	2.669	2.675	MG
CA	0.0	0.0	0.0	0.0	0.0	0.0	0.0	0.022	0.0	0.0	0.0	CA
MN	0.110	0.175	0.132	0.079	0.125	0.041	0.049	0.140	0.0	0.0	0.0	MN
NI	0.0	0.0	0.0	0.0	0.0	0.0	0.033	0.008	0.021	0.011	0.013	NI
XMG	0.348	0.348	0.349	0.383	0.347	0.558	0.560	0.351	0.339	0.335	0.336	XMG
YCR	0.720	0.698	0.701	0.624	0.694	0.357	0.345	0.733	0.696	0.719	0.710	YCR

XMG=MG/MG+FE YCR=CR/CR+AL+FE3

MICROPROBE ANALYSES OF SPINEL

S.NO	145.42	145.43	147.11	147.12	147.21	150.20	163.10	163.20	210.20	227.30	227.32	
SIO2	0.0	0.0	0.0	0.0	0.0	C.C	0.0	0.0	0.0	0.0	C.0	SIO2
TIO2	0.27	0.15	0.31	0.13	0.22	C.15	0.0	0.0	0.0	0.0	C.09	TIO2
AL2O3	14.38	19.93	14.52	18.18	15.03	26.27	56.31	57.90	42.82	15.78	48.40	AL2O3
CR2O3	53.65	47.41	54.19	50.32	53.45	41.48	9.08	7.67	23.03	50.34	18.85	CH2O3
V2O3	0.0	0.0	0.C	0.0	0.0	0.22	0.17	0.34	0.14	0.30	0.17	V2O3
FE2O3	0.01	0.86	0.35	0.67	0.42	0.10	0.08	0.14	1.24	0.41	0.38	FE2O3
FEO	23.86	21.34	23.44	22.61	23.57	22.86	17.80	16.55	18.55	24.92	15.36	FEC
MGO	6.53	8.70	7.05	8.02	7.00	8.59	14.59	15.47	12.95	5.71	15.62	MGO
CAO	0.0	0.0	0.0	0.0	0.0	0.0	0.0	0.0	0.0	0.0	0.0	CAO
MNO	0.0	0.0	0.0	0.0	0.0	0.28	0.21	0.13	0.20	0.50	C.29	MNO
NIO	0.10	0.05	0.11	0.0	0.02	C.0	0.07	0.05	0.06	0.0	0.0	NIC
TOTAL	98.80	98.44	99.97	99.93	99.71	99.95	98.31	98.25	98.99	97.96	99.16	TOTAL

CATION PROPORTIONS ON THE BASIS OF 32 OXYGENS

SI	0.0	C.C	0.0	0.0	0.0	0.0	0.0	0.0	0.0	0.0	C.0	SI
TI	0.054	0.029	0.062	0.025	0.044	0.028	0.0	0.0	0.0	0.0	C.015	TI
AL	4.550	6.067	4.527	5.547	4.689	7.718	14.402	14.650	11.569	5.037	12.585	AI
CR	11.383	9.710	11.330	10.296	11.182	8.172	1.557	1.301	4.172	10.775	3.287	CR
V	0.0	C.0	0.0	0.0	0.0	0.044	0.030	0.059	0.026	0.065	C.030	V
FE3	0.002	C.168	0.070	0.131	0.083	0.019	0.013	0.022	0.215	0.083	0.064	FE3
FE2	5.356	4.624	5.185	4.894	5.216	4.764	3.229	2.971	3.555	5.643	2.833	FE2
MG	2.612	3.359	2.779	3.094	2.761	3.190	4.717	4.948	4.423	2.304	5.134	MG
CA	0.0	C.0	0.0	0.0	0.0	0.0	0.0	C.0	0.0	0.0	0.0	CA
MN	0.0	C.0	0.0	0.0	0.0	0.059	C.039	C.024	0.039	0.115	C.054	MN
NI	0.022	C.010	0.023	0.0	0.004	0.0	C.012	0.009	0.011	0.0	C.0	NI
XMG	0.328	0.421	0.349	0.387	0.346	0.401	0.594	0.625	C.554	0.290	0.644	XMG
YCR	0.714	0.608	0.711	0.645	0.701	0.514	0.097	0.081	C.261	0.678	0.206	YCR

XMG=MG/MG+FE YCR=CR/CR+AL+FE3

MICROPROBE ANALYSES OF SPINEL

S.NO	233.21	233.22	254.20	401.10	501.10	501.30	600.10	600.20	600.30	912.10	924.10	
SIO2	0.0	0.0	0.0	0.0	0.0	0.0	0.0	0.11	0.0	0.0	0.0	SIO2
TIO2	0.25	0.0	0.13	0.0	0.0	0.0	0.37	0.28	0.33	0.51	0.26	TIO2
AL2O3	16.06	49.11	55.59	59.20	59.54	57.95	26.09	15.14	25.26	32.58	36.84	AL2O3
CR2O3	49.04	17.58	12.02	6.30	10.30	10.52	39.88	46.09	38.13	21.21	19.51	CR2O3
V2O3	0.29	0.0	0.11	0.0	0.09	0.06	0.84	0.99	0.78	0.47	1.09	V2O3
FE2O3	1.10	0.61	0.22	0.96	0.40	0.71	0.86	3.47	1.76	10.63	7.90	FE2O3
FEO	25.48	16.38	17.26	12.47	13.60	13.23	23.30	27.35	25.44	27.33	26.61	FEO
MGO	5.34	15.05	15.21	16.86	18.75	17.38	6.73	3.74	6.27	5.66	6.81	MGO
CAO	0.0	0.10	0.0	0.0	0.0	0.0	0.0	0.06	0.0	0.07	0.05	CAO
MNO	0.72	0.32	0.24	0.20	0.22	0.20	0.39	0.73	0.32	0.20	0.35	MNO
NIO	0.0	0.0	0.0	0.15	0.06	0.0	0.0	0.0	0.0	0.07	0.44	NIO
TOTAL	98.28	99.15	100.78	96.15	102.96	100.05	98.46	97.97	98.29	98.93	99.86	TOTAL

CATION PROPORTIONS ON THE BASIS OF 32 OXYGENS

SI	0.0	0.0	0.0	0.0	0.0	0.0	0.0	0.030	0.0	0.0	0.0	SI
TI	0.051	0.0	0.021	0.0	0.0	0.0	0.071	0.058	0.064	0.096	0.047	TI
AL	5.117	12.788	13.940	14.979	14.251	14.292	7.823	4.911	7.673	9.603	10.528	AL
CR	10.478	3.070	2.021	1.069	1.653	1.740	8.019	10.024	7.767	4.192	3.739	CR
V	0.063	0.0	0.019	0.0	0.015	0.010	0.171	0.218	0.161	0.094	0.212	V
FE3	0.224	0.101	0.035	0.156	0.061	0.112	0.164	0.719	0.341	2.000	1.441	FE3
FE2	5.759	3.025	3.071	2.239	2.309	2.315	4.957	6.294	5.483	5.714	5.394	FE2
MG	2.151	4.954	4.822	5.393	5.673	5.419	2.551	1.533	2.408	2.184	2.460	MG
CA	0.0	0.024	0.0	0.0	0.0	0.0	0.0	0.018	0.0	0.019	0.013	CA
MN	0.165	0.060	0.043	0.036	0.038	0.035	0.084	0.170	0.070	0.042	0.072	MN
NI	0.0	0.0	0.0	0.026	0.010	0.0	0.0	0.0	0.0	0.014	0.086	NI
XMG	0.272	0.621	0.611	0.707	0.711	0.701	0.340	0.196	0.306	0.276	0.313	XMG
YCR	0.662	0.192	0.126	0.066	0.104	0.108	0.501	0.640	0.492	0.265	0.238	YCR

XMG=MG/MG+FE YCR=CR/CR+AL+FE3

MICROPROBE ANALYSES OF SPINEL

S.NO	924.31	927.10	927.20	934.30	
SIO2	0.0	0.0	0.0	0.0	SIO2
TIO2	0.40	0.34	0.27	0.30	TIO2
AL2O3	24.21	24.95	30.41	26.35	AL2O3
CR2O3	28.91	30.41	22.49	26.51	CR2O3
V2O3	2.11	1.93	2.67	2.13	V2O3
FE2O3	10.62	9.94	11.69	11.66	FE2O3
FEO	28.79	28.09	26.83	27.95	FEO
MGO	3.77	4.68	5.89	4.71	MGO
CAO	0.04	0.0	0.05	0.0	CAO
MNO	0.30	0.28	0.41	0.61	MNO
NIO	0.0	0.10	0.09	0.24	NIO
TOTAL	99.15	100.72	100.79	100.46	TOTAL

CATION PROPORTIONS ON THE BASIS OF 32 OXYGENS

SI	0.0	0.0	0.0	0.0	SI
TI	0.079	0.065	0.050	0.058	TI
AL	7.473	7.529	8.897	7.933	AI
CR	5.984	6.153	4.412	5.352	CR
V	0.443	0.396	0.531	0.436	V
FE3	2.092	1.915	2.183	2.240	FE3
FE2	6.304	6.013	5.568	5.970	FE2
MG	1.471	1.785	2.178	1.792	MG
CA	0.011	0.0	0.013	0.0	CA
MN	0.067	0.061	0.086	0.132	MN
NI	0.0	0.021	0.018	0.049	NI
XMG	0.189	0.229	0.281	0.231	XMG
YCR	0.385	0.395	0.285	0.345	YCR

XMG=MG/MG+FE YCR=CR/CR+AL+FE3

Appendix B

WHOLE ROCK ANALYSES

Analyses of major elements and trace elements were carried out on a Philips 1410 automated X-ray fluorescence unit at the Department of Geology, University of Ottawa. The determinations were made on fused disk ($Li_2B_4O_7$, $LiCO_3$ and the sample) using a Cr tube and the technique of alpha coefficients described by DeJongh (1975). Precision and accuracy of the analyses obtained from replicate analyses and runs on USGS standards (DTS-1, PCC-1, BCR-1), are given in Table 3 and Table 4, respectively. Analyses are listed in Table 5. Average composition of the T-3 ultramafic body and miscellaneous analyses referred in the text are given in Table 6. Description and location of analysed samples from DDH 64599 and DDH 64816 are listed in Table 7, whereas those from various locations in the Thompson Nickel Belt and from DDH 64830 (Cuthbert Lake dike) are given in Table 8.

TABLE 3

Precision of Whole Rock Analyses

	Range	2s
SiO2	40-65	±1.0
Al2O3	3-16	±0.3
Fe2O3(t)	6-13	±0.2
MgO	4-10	±0.2
	24-35	±0.9
CaO	4-12	±0.2
Na2O	<1.0	±0.15
	1-2	±0.34
K2O	<0.12	±0.01
TiO2	0.1-0.9	±0.01
MnO	0.1-0.2	±0.01
ppm		
Ba	20-35	±4
Cr	1400-3500	±100
	100-200	±26
Zr	20-40	±14
Sr	15-130	±9
Y	<10	±10
Zn	25-80	±8
Ni	1000-2700	±150
	<200	±50

2s, confidence limit given as 2 times standard deviation.

TABLE 4

Accuracy of Whole Rock Analyses

	PCC-1			DTS-1			BCR-1		
n	9			10			14		
	mean	2s	R.V	mean	2s	R.V	mean	2s	R.V
SiO2	42.14	0.53	42.10	40.61	0.77	40.61	54.65	0.63	54.53
Al2O3	0.68	0.02	0.73	0.23	0.03	0.25	13.68	0.18	13.72
Fe2O3	8.30	0.12	8.28	8.62	0.06	8.70	13.51	0.23	13.41
MgO	43.68	0.99	43.50	49.74	0.84	49.80	3.44	0.18	3.48
CaO	0.54	0.01	0.55	0.12	0.01	0.14	6.95	0.08	6.97
Na2O	0.14	0.28	0.01	0.05	0.06	0.01	3.30	0.23	3.30
K2O	0.00	0.00	0.00	0.00	0.00	0.00	1.72	0.02	1.70
TiO2	0.00	0.00	0.00	0.00	0.00	0.00	2.25	0.02	2.26
P2O5	0.00	0.00	0.01	0.00	0.00	0.00	0.36	0.05	0.36
MnO	0.12	0.01	0.12	0.12	0.00	0.12	0.18	0.10	0.18
S	0.01	0.01	0.01	0.00	0.00	0.00	0.03	0.02	0.04
ppm									
Ba	7	3	nr	6	3	2.4	694	15	680
Cr	3033	30	3000	4443	79	4400	29	15	16
Zr	7	8	nr	6	5	nr	171	9	185
Sr	2	5	0.4	2	5	0.4	384	13	330
Rb	2	2	0.1	1	2	0.1	48	7	47
Y	2	6	nr	0	0	nr	41	1	37
Zn	41	4	36	44	6	45	119	10	120
Ni	2466	33	2500	2428	15	2400	0	0	13

n, number of sample; 2s, confidence limit given as 2 times standard deviation; R.V, recommended value (Abbey,1977); nr, not reported; Fe2O3 is total iron.

TABLE 5 WHOLE ROCK ANALYSES

S.NO	2	9	25	26	35	41	52	55	56	59	64	68	S.NO
SIO2	48.93	46.46	45.93	50.45	48.46	40.14	40.65	48.85	41.15	43.30	54.72	47.77	SIO2
AL2O3	6.01	8.87	8.56	5.66	3.12	2.22	1.92	7.18	1.91	2.68	2.22	2.44	AL2O3
FEO	10.61	10.50	9.36	7.47	8.13	9.14	11.10	8.38	10.30	11.15	6.87	7.72	FEO
MGO	14.22	22.41	24.57	27.57	33.97	37.68	35.88	23.42	40.46	40.16	34.37	36.48	MGO
CAO	15.26	7.97	1.10	1.80	1.67	1.33	0.81	5.66	0.41	0.12	0.44	3.00	CAO
NA2O	1.06	0.61	0.09	0.20	0.14	0.08	0.05	0.45	0.06	0.02	0.09	0.22	NA2O
K2O	1.17	0.50	4.38	2.09	0.11	0.06	0.14	0.31	0.03	0.01	0.05	0.06	K2O
TIO2	0.68	0.49	0.37	0.23	0.10	0.09	0.08	0.28	0.09	0.10	0.07	0.12	TIO2
P2O5	0.0	0.0	0.0	0.0	0.0	0.0	0.0	0.02	0.0	0.0	0.0	0.0	P2O5
MNO	0.26	0.19	0.12	0.12	0.13	0.10	0.15	0.15	0.15	0.14	0.13	0.12	MNO
S	0.0	0.04	0.0	0.05	0.16	0.13	0.01	0.03	0.12	0.06	0.12	0.04	S
TOTAL	98.20	98.04	94.48	95.64	95.99	90.97	90.79	94.73	94.68	97.74	99.08	97.97	TOTAL
PPM													
BA	106	16	499	520	30	32	13	132	30	27	30	29	BA
CR	2146	2050	2067	3592	2796	1438	2298	2972	3588	3044	1138	863	CR
ZR	42	34	25	15	16	12	19	34	14	16	17	12	ZR
SR	27	8	17	24	14	14	26	29	7	11	7	24	SR
RB	35	1	176	86	5	6	1	3	2	0	0	1	RB
Y	13	1	16	5	0	0	0	0	0	0	0	3	Y
ZN	105	82	88	32	76	51	70	50	88	72	47	31	ZN
NI	372	1039	757	1363	2851	2227	3733	205	2296	2260	2386	1731	NI

TABLE 5 WHOLE ROCK ANALISES

S.NO	70	73	76	77	79	82	86	90	95	98	104	105	S.NO
SIO2	41.65	49.28	40.26	49.67	51.27	51.59	51.66	51.73	45.46	48.23	42.70	45.14	SIO2
AL2O3	2.50	6.90	1.62	7.09	6.07	6.42	5.23	4.76	5.48	5.41	3.04	3.37	AL2O3
FEO	8.82	8.79	10.42	8.65	9.70	8.52	9.40	9.86	9.25	9.90	11.35	9.83	FEO
MGO	40.37	27.36	40.92	23.98	26.78	26.40	27.94	28.86	26.97	30.82	40.29	40.25	MGO
CAO	2.29	4.13	0.43	6.03	4.13	4.61	3.44	3.04	3.49	3.66	2.08	1.87	CAO
NA2O	0.20	0.30	0.05	0.69	0.42	0.44	0.39	0.19	0.22	0.32	0.20	0.20	NA2O
K2O	0.05	0.09	0.04	0.06	0.28	0.51	0.15	0.06	0.06	0.06	0.03	0.03	K2O
TIO2	0.14	0.38	0.07	0.33	0.27	0.28	0.21	0.22	0.24	0.25	0.17	0.14	TIO2
P2O5	0.0	0.03	0.0	0.0	0.04	0.0	0.0	0.02	0.02	0.0	0.01	0.0	P2O5
MNO	0.12	0.19	0.15	0.15	0.19	0.18	0.18	0.19	0.19	0.19	0.13	0.14	MNO
S	0.02	0.02	0.09	0.07	0.04	0.05	0.12	0.11	0.16	0.03	0.08	0.09	S
TOTAL	96.16	97.47	94.05	97.52	99.19	99.00	98.72	99.04	91.54	98.87	100.08	101.06	TOTAL
PPM													
BA	6	30	28	303	93	99	33	35	25	30	27	30	BA
CR	1992	3442	3400	2784	3488	3530	3359	3290	3522	4423	1599	1652	CR
ZR	4	58	10	23	62	30	24	19	29	21	27	36	ZR
SR	9	32	12	29	21	32	16	20	29	19	14	22	SR
RB	0	0	5	28	8	24	1	1	0	0	0	0	RB
Y	11	5	0	18	0	6	0	0	3	19	0	0	Y
ZN	46	77	91	47	75	73	88	74	77	96	60	69	ZN
NI	3645	265	2148	68	385	128	314	220	258	258	2072	2679	NI

TABLE 5 WHOLE ROCK ANALYSES

S.NO	107	111	113	119	120	127	132	133	137	139	144	147	S.NO
SIO2	43.07	47.90	44.52	42.71	42.54	43.87	42.16	42.42	43.14	45.72	41.07	41.36	SIO2
AL203	3.30	3.68	3.38	2.99	2.98	3.44	2.97	3.11	2.76	2.97	1.36	1.39	AL203
FEO	8.91	6.86	7.96	8.40	8.92	7.75	9.06	9.10	9.65	9.36	10.21	10.03	FEO
MGO	41.14	35.78	40.57	41.70	42.48	39.53	41.15	41.57	41.07	39.92	44.12	45.71	MGO
CAO	2.38	4.31	2.82	1.73	1.18	3.28	2.75	2.83	1.56	1.19	1.16	0.62	CAO
NA2O	0.26	0.47	0.30	0.21	0.04	0.23	0.26	0.0	0.06	0.0	0.0	0.12	NA2O
K2O	0.04	0.07	0.04	0.02	0.01	0.06	0.04	0.04	0.01	0.01	0.01	0.01	K2O
TIO2	0.15	0.21	0.13	0.14	0.14	0.12	0.14	0.14	0.13	0.14	0.06	0.06	TIO2
P2O5	0.07	0.0	0.01	0.0	0.0	0.0	0.01	0.0	0.0	0.0	0.0	0.0	P2O5
MNO	0.15	0.13	0.14	0.13	0.14	0.12	0.13	0.14	0.12	0.14	0.17	0.17	MNO
S	0.08	0.08	0.08	0.11	0.09	0.08	0.06	0.06	0.18	0.25	0.14	0.10	S
TOTAL	99.49	99.49	99.95	98.14	98.52	98.48	98.73	99.41	98.68	99.70	98.30	99.57	TOTAL
PPM													
BA	27	23	6	27	5	28	27	2	24	6	27	29	BA
CR	1458	1455	1632	1592	1679	1568	1447	1570	1871	1745	2684	3351	CR
ZR	22	22	20	21	16	17	22	22	17	23	16	9	ZR
SR	15	26	19	16	8	25	16	8	13	4	20	9	SR
RB	1	0	0	3	0	0	0	0	1	0	1	2	RB
Y	0	9	1	0	2	3	0	0	0	0	0	0	Y
ZN	58	30	53	52	55	48	44	49	52	49	74	90	ZN
NI	2471	2650	2771	3008	2848	2852	2335	2574	2759	3730	2981	2671	NI

TABLE 5 WHOLE ROCK ANALYSES

S.NO	152	156	158	168	174	176	178	179	201	202	203	206	S.NO
SIO2	41.01	39.77	42.58	51.26	50.09	48.87	49.83	49.69	47.41	51.22	43.22	46.83	SIO2
AL203	1.96	2.83	2.18	7.55	7.91	7.12	8.78	9.97	14.54	16.06	3.55	5.83	AL203
FEO	9.18	7.25	6.98	7.30	8.65	8.97	8.03	7.36	10.30	9.94	10.55	9.84	FEO
MGO	43.83	36.70	35.68	26.44	23.61	24.74	19.97	16.00	9.56	7.53	39.68	32.34	MGO
CAO	1.50	2.18	2.49	5.85	5.40	5.69	6.37	7.29	10.74	10.84	2.24	3.95	CAO
NA2O	0.18	0.29	0.11	0.61	0.84	0.50	0.67	1.56	1.96	2.66	0.22	0.50	NA2O
K2O	0.04	0.03	0.01	0.28	1.74	0.31	2.48	1.41	1.56	0.34	0.05	0.43	K2O
TIO2	0.11	0.11	0.08	0.33	0.36	0.27	0.39	0.41	0.90	0.96	0.15	0.27	TIO2
P2O5	0.0	0.0	0.0	0.03	0.02	0.0	0.01	0.0	0.05	0.07	0.0	0.03	P2O5
MNO	0.13	0.09	0.12	0.16	0.16	0.18	0.16	0.16	0.17	0.17	0.16	0.16	MNO
S	0.04	0.03	0.11	0.05	0.03	0.07	0.0	0.01	0.01	0.0	0.04	0.07	S
TOTAL	97.98	89.28	90.34	99.86	98.81	96.72	96.69	93.86	97.20	99.79	99.86	100.25	TOTAL
PPM													
BA	25	9	26	27	194	134	263	246	77	103	20	112	BA
CR	1622	1925	1753	2919	3109	3192	2580	1737	572	274	4875	4223	CR
ZR	16	10	15	37	38	21	39	36	63	59	21	38	ZR
SR	10	6	14	58	22	24	27	120	234	148	16	26	SR
RB	0	0	0	6	63	9	94	44	63	3	0	11	BB
Y	1	14	0	8	10	13	11	16	28	29	0	0	Y
ZN	54	42	25	71	76	67	90	79	65	66	141	80	ZN
NI	2702	2548	2331	253	225	116	231	82	169	141	2296	571	NI

TABLE 5 WHOLE ROCK ANALYSES

S.NO	208	211	218	224	232	237	242	248	253	255	256	401	S.NO
SIO2	45.08	44.83	44.42	45.71	43.09	44.44	47.30	48.76	45.41	52.80	46.11	37.46	SIO2
AL2O3	5.38	5.07	5.20	4.54	4.37	5.13	4.63	4.83	5.11	4.14	7.38	3.10	AL2O3
FEO	10.02	9.56	9.43	9.99	11.69	10.71	9.70	9.60	9.38	10.05	10.44	16.42	FEO
MGO	33.48	34.41	34.20	34.46	34.87	34.75	31.98	31.29	29.80	29.92	25.05	37.82	MGO
CAO	3.50	2.93	3.52	3.59	2.83	2.95	3.22	3.05	4.80	0.26	2.33	0.59	CAO
NA2O	0.46	0.49	0.41	0.69	0.56	0.44	0.42	0.35	0.51	0.19	0.49	0.05	NA2O
K2O	0.62	0.67	0.57	0.15	0.40	0.65	0.41	0.37	0.09	1.11	2.93	0.03	K2O
TIO2	0.23	0.21	0.20	0.23	0.15	0.22	0.20	0.21	0.26	0.13	0.30	0.11	TIO2
P2O5	0.01	0.01	0.0	0.02	0.0	0.01	0.0	0.0	0.03	0.0	0.02	0.0	P2O5
MNO	0.16	0.15	0.15	0.16	0.17	0.16	0.17	0.18	0.16	0.21	0.13	0.11	MNO
S	0.24	0.08	0.09	0.18	0.16	0.07	0.05	0.08	0.10	0.03	0.18	0.28	S
TOTAL	99.18	98.41	98.19	99.72	98.29	99.53	98.08	96.72	95.65	98.84	95.36	95.97	TOTAL
PPM													
BA	114	159	109	44	81	132	142	110	30	134	366	7	BA
CR	4344	4120	4100	4396	3976	4381	4126	4081	4051	4216	2749	3753	CR
ZR	29	27	27	28	30	27	28	32	34	26	35	14	ZR
SR	39	34	41	36	30	24	26	23	25	5	35	10	SR
RB	19	22	17	2	13	17	14	8	0	44	112	3	RB
Y	5	0	1	0	10	7	0	0	3	0	11	0	Y
ZN	81	85	100	76	94	92	93	80	95	96	27	1126	ZN
NI	690	530	575	710	1185	567	338	311	357	255	1730	7553	NI

TABLE 5 WHOLE ROCK ANALYSES

S.NO	711	712	721	611	622	623	1	22	181	901	903	905	S.NO
SIO2	50.39	50.16	62.27	44.11	51.17	51.28	64.73	59.15	64.62	50.17	47.66	48.05	SIO2
AL2O3	13.41	13.52	14.30	2.84	12.85	12.89	15.77	16.00	15.06	15.16	12.34	14.27	AL2O3
FEO	10.11	10.38	6.83	10.73	10.22	9.89	4.15	5.67	6.17	10.41	11.26	10.52	FEO
MGO	10.42	9.61	4.47	29.26	11.81	12.25	2.00	1.71	1.58	8.48	9.13	8.62	MGO
CAO	11.33	13.83	6.29	2.87	9.93	8.85	3.49	1.43	1.10	12.05	12.57	11.43	CAO
NA2O	2.26	0.99	3.18	0.0	1.57	1.50	3.96	2.00	2.65	2.18	1.70	1.75	NA2O
K2O	0.13	0.11	0.37	0.02	0.28	0.72	2.70	2.29	2.92	0.11	0.20	0.66	K2O
TIO2	0.86	0.86	0.74	0.19	0.62	0.62	0.50	0.65	0.63	0.80	1.09	0.96	TIO2
P2O5	0.0	0.0	0.0	0.0	0.0	0.0	0.06	0.0	0.03	0.05	0.07	0.06	P2O5
MNO	0.18	0.18	0.11	0.15	0.17	0.18	0.06	0.13	0.05	0.19	0.19	0.18	MNO
S	0.0	0.02	0.04	0.20	0.01	0.08	0.01	0.08	0.07	0.01	0.20	0.05	S
TOTAL	99.09	99.66	98.60	90.37	98.63	98.26	97.43	89.11	94.88	99.61	96.41	96.55	TOTAL
PPM													
BA	43	26	113	13	84	187	733	309	745	31	47	297	BA
CR	591	649	143	3623	883	952	54	107	116	172	558	349	CR
ZR	49	59	97	16	57	55	176	153	137	40	60	55	ZR
SR	85	142	47	9	81	90	393	156	180	102	102	139	SR
RB	0	0	0	0	0	12	94	100	96	2	6	14	RB
Y	14	11	17	0	8	9	18	26	18	19	16	29	Y
ZN	61	55	73	28	40	76	63	71	74	54	59	56	ZN
NI	209	251	17	2087	121	245	13	11	42	80	265	181	NI

TABLE 5 WHOLE ROCK ANALYSES

S.NO	906	996	908	909	912	913	915	916	919	923	927	930	S.NO
SIO2	49.06	48.89	63.22	44.67	45.06	45.04	48.23	46.94	45.22	45.61	44.23	43.71	SIO2
AL2O3	14.22	16.11	16.87	7.49	7.15	9.24	12.33	9.56	9.46	8.12	6.14	6.20	AL2O3
FEO	11.00	12.18	4.32	10.98	12.49	9.40	9.54	10.62	10.24	11.62	12.09	11.99	FEO
MGO	8.61	7.64	2.55	22.88	23.81	21.01	17.61	18.56	20.02	23.77	26.25	26.24	MGO
CAO	12.82	9.63	3.56	8.13	8.73	9.30	9.75	9.05	8.38	7.53	6.89	6.81	CAO
NA2O	2.12	2.06	4.29	0.84	0.47	0.87	1.61	1.33	0.98	1.00	0.77	0.77	NA2O
K2O	0.20	0.95	2.97	0.06	0.01	0.06	0.11	0.09	0.12	0.06	0.05	0.06	K2O
TIO2	1.01	1.27	0.87	0.46	0.64	0.27	0.45	1.97	0.97	0.32	0.36	0.35	TIO2
P2O5	0.0	0.01	0.56	0.0	0.0	0.0	0.0	0.03	0.02	0.01	0.01	0.01	P2O5
MNO	0.21	0.20	0.05	0.17	0.19	0.17	0.17	0.17	0.16	0.18	0.18	0.18	MNO
S	0.0	0.03	0.13	0.03	0.02	0.01	0.02	0.03	0.03	0.03	0.02	0.02	S
TOTAL	99.25	98.97	99.39	95.71	98.57	95.37	99.82	98.35	95.60	98.25	96.99	96.34	TOTAL
PPM													
BA	41	160	2869	27	8	21	27	27	95	24	26	28	BA
CR	361	95	8	2656	2784	2167	1743	2136	2282	2837	3151	3192	CR
ZR	69	73	255	28	20	25	34	40	34	31	25	25	ZR
SR	95	123	1031	39	36	35	76	66	49	59	36	34	SR
RB	0	1	28	2	2	0	0	3	0	2	2	0	RB
Y	21	17	14	10	5	2	19	17	7	5	11	0	Y
ZN	58	68	50	57	66	44	54	57	60	66	70	76	ZN
NI	498	118	37	1076	1053	969	777	801	938	1135	1292	1488	NI

TABLE 5 WHOLE ROCK ANALYSES

S.NO	934	938	941	944	946	948	951	953	954	955	956	S.NO
SIO2	44.66	43.89	43.52	44.79	44.91	43.65	45.86	46.46	45.80	69.08	46.61	SIO2
AL2O3	5.28	7.44	4.98	4.55	8.58	6.82	8.33	9.27	9.09	12.74	14.83	AL2O3
FEO	12.72	11.06	12.10	9.20	10.32	10.75	10.24	10.66	10.68	0.25	13.82	FEO
MGO	27.70	24.30	25.71	23.91	21.28	24.28	21.75	20.53	21.09	0.35	6.46	MGO
CAO	6.26	6.92	7.03	9.01	9.34	7.93	8.92	8.35	7.95	0.38	9.16	CAO
NA2O	0.75	0.92	0.73	0.68	0.88	0.69	0.82	1.38	0.90	2.20	2.91	NA2O
K2O	0.05	0.06	0.05	0.05	0.04	0.03	0.04	0.07	0.11	7.88	0.48	K2O
TIO2	0.44	0.33	0.29	0.28	0.24	0.31	0.31	0.55	0.54	0.03	0.98	TIO2
P2O5	0.02	0.02	0.02	0.01	0.0	0.0	0.01	0.02	0.0	0.0	0.05	P2O5
MNO	0.20	0.17	0.17	0.14	0.16	0.17	0.17	0.17	0.18	0.0	0.23	MNO
S	0.02	0.02	0.03	0.02	0.01	0.02	0.02	0.04	0.0	0.01	0.26	S
TOTAL	98.10	95.13	94.63	92.64	95.76	94.65	96.47	97.50	96.34	92.92	95.79	TOTAL
PPM												
BA	19	29	21	19	42	27	27	13	16	1780	111	BA
CR	3545	2930	3497	2932	2451	3112	2468	2363	2333	8	46	CR
ZR	24	27	26	22	19	19	21	31	32	15	51	ZR
SR	22	55	29	15	61	38	44	41	23	220	107	SR
RB	0	5	4	0	5	0	0	0	0	176	7	RB
Y	0	3	4	4	0	0	3	16	2	7	43	Y
ZN	70	66	75	38	53	70	49	50	62	0	103	ZN
NI	1406	1185	1301	1117	1020	1194	945	944	926	29	95	NI

TABLE 6

Miscellaneous analyses referred to in the text

	T1	T2	M	P1	P2	K1	K2	K3
SiO2	45.71	46.00	44.20	43.20	43.95	40.00	41.40	41.10
Al2O3	3.86	5.01	2.05	4.01	3.88	3.70	6.90	8.74
FeO(t)	8.81	9.71	8.29	8.20	8.18	8.20	12.40	12.80
MgO	35.43	32.79	42.21	39.54	39.00	35.10	25.60	22.10
CaO	2.57	3.01	1.92	2.67	2.60	3.28	5.90	8.76
Na2O	0.23	0.44	0.27	0.61	0.60	0.07	0.06	0.11
K2O	0.26	0.65	0.06	0.22	0.22	0.10	0.07	0.01
TiO2	0.17	0.21	0.13	0.58	0.57	0.14	0.33	0.42
P2O5	0.01	0.01	0.03	-	-	-	-	-
MnO	0.15	0.16	0.13	0.13	0.13	0.15	0.24	0.20
NiO	0.24	0.10	0.28	-	-	0.03	0.02	0.01
Cr2O3	0.35	0.60	0.44	0.42	0.41	0.26	0.45	0.48

T1, average composition of the ultramafic body calculated along DDH 64599; T2, average composition of the ultramafic body calculated along DDH 64816; M, composition of uppermost mantle (Maaloe & Aoki 1977); P1 and P2, pyrolites (Ringwood 1966 and Green & Ringwood 1970); K1, cumulate peridotite; K2, STPK; K3, flow top breccia; K1, K2, K3 are after Arndt et al 1977.

	A		C (ppm)
SiO2	45-52	Al	12300
Al2O3	3.59-4.94	Ca	13500
FeO(t)	8.6-9.7	Ti	720
MgO	38	Cr	3460
CaO	2.96-4.07	Mn	2590
Na2O	0.32-0.43	Fe	219000
K2O	0.02-0.03	Ni	12100
TiO2	0.18-0.24	Zn	460
P2O5	0.02	Zr	7
MnO	0.15		

A, estimated Archean mantle composition (Sun & Nesbitt 1977); C, ordinary chondrites (Kay & Hubbard 1978).

TABLE 7

Description and location of samples analysed

DDH 64599

no	d	t	no	d	t	no	d	t
1	50	gns	79	2324	4	132	2469	5b
2	172	ampte	82	2335	4	133	2471	5b
9	1260	spert	85	2353	4	134	2472	5b
25	2190	1	86	2358	4	135	2475	5b
26	2193	1	90	2377	4	137	2478	5b
35	2200	2	95	2402	5a	139	2483	5b
41	2210	2	98	2410	5a	141	2490	5c
52	2227	2	99	2411	5a	144	2496	5c
55	2238	2	100	2415	5a	145	2500	5c
56	2242	2	103	2418	5a	147	2504	5c
59	2260	2	104	2419	5a	150	2513	5c
60	2262	3	105	2421	5a	152	2518	5c
63	2269	3	107	2435	5a	156	2528	6
64	2272	3	110	2438	5b	158	2539	6
65	2273	3	111	2439	5b	160	2543	6
67	2279	3	112	2440	5b	163	2548	7
68	2284	3	113	2442	5b	168	2560	7
70	2287	3	114	2443	5b	174	2580	7
72	2289	4	119	2540	5b	177	2591	7
73	2291	4	120	2451	5b	178	2605	8
76	2306	4	127	2459	5b	179	2612	8
77	2314	4	130	2467	5b	181	2633	scht

DDH 64816

no	d	t	no	d	t	no	d	t
201	5652	ampte	218	6149	11c	242	6298	11e
202	5701	gabb	224	6187	11c	248	6332	11e
203	5993	9	227	6205	11c	253	6371	11e
206	6032	10	232	6228	11d	254	6381	11e
208	6072	11a	233	6233	11d	255	6391	12
210	6091	11a	237	6260	11e	256	6411	12
211	6110	11b						

no, sample number; d, distance along DDH (feet); t, rock type or zone number referred in the text and Figure 8; gns, basement gneiss; ampt, amphibolite; gabb, gabbro; spert, serpentinized peridotite; scht, garnet-sillimanite-biotite schist.

TABLE 8

Description and location of samples analysed

Thompson Nickel Belt

no	d	t
401	Thompson Mine, 2400 Lv., 330 stop	serp
402	Thompson Mine, 2400 Lv., 330 stop	opxt
501	Thompson Mine, 2400 Lv., 315 stop	olopxt
600	Mystery Lake Mine	olopxt
611	Mystery Lake Mine	olopxt
622	Mystery Lake	Mgbas
623	Mystery Lake	Mgbas
711	Lower Ospwagan Lake	bas
712	Lower Ospwagan Lake	bas
721	Lower Ospwagan Lake	bas

Cuthbert Lake dike-DDH 64830

no	d	t	no	d	t	no	d	t
901	396	gabb	915	586	pxp	941	720	olpx
903	410	pxp	916	591	pxp	944	739	olpx
905	426	gabb	919	610	olpx	946	765	per
906	440	mmin	923	627	olpx	948	780	per
996	440	mmin	924	632	olpx	951	803	per
908	550	ggn	927	648	olpx	953	820	pxt
909	557	olpx	930	665	olpx	954	827	mmaj
912	573	olpx	934	685	olpx	955	835	ggn
913	580	olpx	937	695	olpx	956	865	gabb
			938	706	olpx			

serp, serpentinite; olopxt, olivine orthopyroxenite; Mgbas, magnesian basalt; bas, basalt; gabb, gabbro; pxp, pyroxene picrite; olpx, olivine pyroxenite; per, peridotite; mmin, minor dike margin; ggn, granulite gneiss; pxt, pyroxenite; mmaj, major dike margin; opxt, orthopyroxenite; see Table 7 for other symbols.